VOLUME XXXIX

GEMS & GEMOLOGY

WINTER 2003

Featuring:

CVD Synthetic Diamonds

Pezzottaite, A New Gem

Red Beryl Update

THE QUARTERLY JOURNAL OF THE GEMOLOGICAL INSTITUTE OF AMERICA

GEMS & GEMOLOGY

Winter 2003 VOLUME 39, NO. 4

pg. 269

pg. 299

EDITORIAL

FEATURE ARTICLES

REGULAR FEATURES

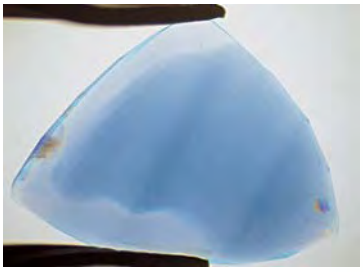

pg. 319

pg. 332

GEMS & GEMOLOGY

SUBSCRIPTIONS

Subscriptions to addresses in the U.S. are priced as follows: **$74.95** for one year (4 issues), **$194.95** for three years (12 issues). Subscriptions sent elsewhere are **$85.00** for one year, **$225.00** for three years. Canadian subscribers should add GST.

Special rates are available for GIA Alumni Association members and current GIA students. One year: **$64.95** to addresses in the U.S., **$75.00** elsewhere; three years: **$179.95** to addresses in the U.S.; **$210.00** elsewhere. Please have your student or Alumni number ready when ordering.

Single copies of this issue may be purchased for **$19.00** in the U.S., **$22.00** elsewhere. Discounts are given for bulk orders of 10 or more of any one issue. A limited number of back issues are also available for purchase. Please address all inquiries regarding subscriptions and single copy or back issue purchases to the Circulation Coordinator (see above) or visit www.gia.edu.

To obtain a Japanese translation of *Gems & Gemology*, contact GIA Japan, Okachimachi Cy Bldg., 5-15-14 Ueno, Taitoku, Tokyo 110, Japan. Our Canadian goods and service registration number is 126142892RT.

MANUSCRIPT SUBMISSIONS

Gems & Gemology welcomes the submission of articles on all aspects of the field. Please see the Guidelines for Authors in the Fall 2003 issue, or contact the Managing Editor for a copy. Letters on articles published in *Gems & Gemology* are also welcome.

COPYRIGHT AND REPRINT PERMISSIONS

Gems & Gemology is published quarterly by the Gemological Institute of America, a nonprofit educational organization for the jewelry industry, 5345 Armada Drive, Carlsbad, CA 92008.

Postmaster: Return undeliverable copies of *Gems & Gemology* to 5345 Armada Drive, Carlsbad, CA 92008.

ABOUT THE COVER

Within the beryl group, two of the rarest gem materials are red beryl and the new mineral pezzottaite, both of which are featured in this issue. The article by Shigley et al. presents an update on the only known commercial occurrence of gem-quality red beryl in the world: the Ruby Violet (or Red Beryl) mine in Utah's Wah Wah Mountains. Shown here is a unique suite of red beryl jewelry designed and manufactured by Van Cleef & Arpels. From left to right: the ring contains a 3.36 ct red beryl; the bracelet contains a 3.27 ct red beryl; the red beryl in the pendant is 4.25 ct; and the red beryl in the earrings, 0.95 and 0.92 ct.

Red beryls courtesy of Van Cleef & Arpels and Nese Aiumu, South American Imports, Seattle, Washington. Diamonds (D-E color, VVS clarity) supplied by Van Cleef & Arpels. Photo © GIA and Harold & Erica Van Pelt.

Color separations for Gems & Gemology *are by PacificPreMedia, Carlsbad, California.*
Printing is by Fry Communications Inc., Mechanicsburg, Pennsylvania.

ISSN 0016-626X

Tomorrow's Challenge:
CVD Synthetic Diamonds

Most gemologists know that General Electric Co. created the first industrial-quality synthetic diamonds in 1955. What many gemologists don't know is that the production of polycrystalline thin films of synthetic diamond actually predates this, beginning in 1952. For decades, chemical vapor deposition (CVD) polycrystalline synthetic diamond has been grown over substrates and used in a variety of industrial products.

The lead article in this issue of *Gems & Gemology* describes the creation of single-crystal synthetic diamonds grown by Apollo Diamond Inc. using a CVD process. At first glance, this doesn't seem so alarming. After all, gem-quality synthetic diamonds grown by the classic "belt" and BARS (high pressure/high temperature) techniques have been around for decades, and have been available commercially (although in very small quantities and sizes and, for the most part, in yellow colors) since the mid-1980's. Put simply, however, CVD-grown synthetic diamond generally is a purer product than commercial synthetic diamonds created by high pressure/high temperature techniques, and the CVD synthetics typically fall on the D-to-Z scale or are "brownies." In addition, in most cases sophisticated analytical equipment must be used to conclusively identify the material. After Apollo Diamond begins commercial production of CVD synthetic diamond in 2004, it will be vital for every practicing gemologist to understand the challenges that the material may pose to identification.

The producer has stated that, initially, 5,000–10,000 carats of faceted CVD synthetic diamond will be available. Most of these goods will be quarters and thirds, but by the end of 2004, stones as large as a full carat may be on the market. While larger sizes typically will be identified in a qualified laboratory, the fact that most diamonds under a carat are not sold with grading reports is cause for concern. The producers are unequivocal about their insistence on proper disclosure, and all indications to GIA certainly support that premise. But could these goods later be "salted" into parcels of natural diamonds by unscrupulous hands, fully intending to deceive their customers? Undoubtedly.

Let us all remember that there is nothing inherently wrong with laboratory-grown products, provided they are properly disclosed at each stage of the distribution pipeline. Ultimately, though, the case for synthetic diamonds will not be played out in the trade *per se*, but rather in the marketplace and in the mind of the consumer. We all know that consumer confidence is the key to the success of the diamond industry. Anything that shakes that confidence will shake the market and, inevitably, the industry itself.

The good news about synthetic diamonds is that, for the last two decades, we have stayed well ahead of the learning curve for identifying them, and I see no reason why this can't continue. For much of this time, experts have debated whether diamonds grown synthetically would become commercially available in sizes, quantities, and prices that could fuel consumer demand for the product. The jury may still be out on these issues. However, it is inevitable, given the technology available today, that the right level of investment and the right long-term commitment to the product will result in commercially viable gem synthetic diamonds. Indeed, the time for readiness appears to be now.

So what have we learned about synthetic diamonds over the past half century? We know that, while technology will provide the innovation necessary to create new and interesting products, this same technology will help fuel the identification of these products as well. Gemological research laboratories are making every effort to keep up with this technology, challenging as it may be, and to do everything they can to protect the public by properly identifying and disclosing gem-quality synthetic diamonds.

William E. Boyajian, President
Gemological Institute of America

GEM-QUALITY SYNTHETIC DIAMONDS GROWN BY A CHEMICAL VAPOR DEPOSITION (CVD) METHOD

Wuyi Wang, Thomas Moses, Robert C. Linares, James E. Shigley,
Matthew Hall, and James E. Butler

Brown-to-gray and near-colorless single-crystal type IIa synthetic diamonds grown using a chemical vapor deposition (CVD) technique by Apollo Diamond Inc. have gemological properties that are distinct from those of both natural diamonds and HPHT-grown synthetic gem diamonds. The tabular crystals typically range up to 1 ct or more and a few millimeters thick, and consist of an overgrowth on a natural or synthetic diamond substrate. Faceted CVD synthetic diamond usually cannot be separated from natural diamond with standard gemological techniques; although when portions of the substrate are still present, an experienced gemologist may be able to recognize differences in luminescence or color between the overgrowth and substrate. In all cases, however, the CVD synthetic diamonds examined to date could be identified in a gemological laboratory by the combination of a strong orangy red fluorescence seen with the De Beers DiamondView deep-ultraviolet imaging system, a characteristic anomalous birefringence (strain) pattern, and distinctive features in their infrared absorption spectra (e.g., at 3123 cm^{-1}) and photoluminescence spectra (strong 575 and 637 nm emissions, a doublet at 596 and 597 nm, and a line at 737 nm).

Apollo Diamond Inc. of Boston, Massachusetts, has succeeded in growing facetable, single-crystal type IIa synthetic diamonds using a patented chemical vapor deposition (CVD) technique (Linares and Doering, 1999, 2003). For characterization of this material, the company has provided a number of brown-to-gray and near-colorless gem-quality crystals and faceted samples, which represent what is intended to become a commercial product for use in high-technology applications as well as for jewelry purposes (figure 1). Because of the growth conditions and mechanisms used, the gemological properties of these CVD-produced synthetic diamonds differ from those of both natural diamonds and synthetic diamonds grown at high pressures and temperatures. For the same reasons, the brown coloration of CVD synthetic diamonds may not react in the same way, or as efficiently, as most natural type IIa brown diamonds, which can be decolorized at high pressure and high temperature (see box A). Preliminary notes on GIA's examination of some of these Apollo samples were published by Wang et al. (2003) and appeared in the August 8, 2003 issue of the *GIA Insider* (GIA's electronic newsletter: http://www.gia.edu/newsroom/issue/2798/1842/insider_newsletter_details.cfm#3). Spectroscopic analysis of an Apollo CVD synthetic diamond also was performed recently by other researchers (Deljanin et al., 2003). The purpose of the present article is to provide a more complete description of this material and its identifying features.

See end of article for About the Authors and Acknowledgments.
GEMS & GEMOLOGY, Vol. 39, No. 4, pp. 268–283.

Figure 1. This jewelry is set with CVD synthetic diamonds from Apollo Diamond Inc. The pendant contains an HPHT-annealed 0.2 ct CVD synthetic diamond with a color equivalent to "K" on the GIA diamond grading scale (sample no. 57687). The 0.31 ct sample (no. 56924) in the ring on the left is equivalent to Fancy Dark brown in color. The Fancy Light brown 0.45 ct CVD synthetic diamond (no. 57688) in the ring on the right was HPHT annealed, but no change in color was observed (see box A). Composite of photos by Elizabeth Schrader.

BACKGROUND

Synthetic diamonds have been produced by the high pressure/high temperature (HPHT) technique since 1955, with the growth of crystals of a size and quality suitable for jewelry first announced in 1970 (Crowningshield, 1971; Burns and Davies, 1992). HPHT-grown synthetic diamonds have distinctive physical features, such as a cuboctahedral crystal form and a related arrangement of internal growth sectors, as a result of growth at high pressures and temperatures from a molten metal or metal alloy flux/catalyst. The crystals produced in this manner typically weigh 1–3 ct; when faceted for jewelry use, they occasionally exceed 1 ct. The vast majority of crystals are yellow, although limited numbers of blue and colorless synthetic diamonds have also been produced (other colors, such as pink or red, are the result of post-growth treatment of material that is yellow as grown). Shigley et al. (1995) summarized the distinctive gemological properties of both colored and colorless HPHT-grown synthetic diamonds.

A diamond crystal, which is composed solely of carbon atoms, has a structure in which each carbon atom is symmetrically surrounded by four other carbon atoms. Because of this structure, diamond has unique physical and chemical properties that make it highly desirable for a wide range of applications (see, e.g., Field, 1992; Davies, 1994; Spear and Dismukes, 1994; Wilks and Wilks, 1994). Specifically, diamond:

- Is the hardest known natural material
- Is the best thermal conductor of any material near room temperature
- Has the lowest coefficient of thermal expansion
- Is resistant to heat, acids, and radiation
- Is a good electrical insulator, but can be doped to act as a semiconductor
- Is transparent to visible and almost all infrared radiation

Given these many notable properties, it is hardly surprising that diamond not only is the most important gem material, but it also has extensive industrial applications in thermal management, cutting tools, wear-resistant coatings, optical components, and possibly semiconductor electronic devices. An increasing proportion of these applications use synthetic diamond. The resulting demand has, in turn, supported active research and development programs on synthetic diamond growth worldwide.

Most of the techniques currently used to produce gem-quality synthetic diamond employ high pressures and temperatures—similar to those under which diamonds form in nature—to transform elemental carbon into diamond. Recently, however, the growth of gem-quality synthetic diamond by one of several new chemical vapor deposition (CVD) techniques, which do not require high pressure, is drawing increased attention worldwide (Hunter and Paparella, 2003). In contrast to the conventional HPHT synthesis process, CVD techniques involve gas-phase chemical reactions that deposit layers of a synthetic diamond film on a solid substrate (Butler and Woodin, 1993; Davis, 1993; Spear and Dismukes, 1994—see figure 2). If a natural diamond or a synthetic diamond is used as the substrate, single-crystal CVD diamond can be produced; however, if another material (such as silicon) is used, com-

BOX A: PRELIMINARY NOTE ON CHANGING THE COLOR OF CVD-GROWN SYNTHETIC DIAMONDS BY HPHT ANNEALING

The as-grown CVD synthetic diamond samples examined for this study were type IIa, and for the most part their color varied from light to dark brown. It is now well-known in the jewelry industry that the brown coloration of natural type IIa diamond can be changed to near-colorless or colorless by annealing at high pressures and temperatures. Therefore, we conducted a preliminary study to determine whether HPHT treatment could lighten the brown color of some of our samples, and also to determine any gemological and spectroscopic variations related to HPHT annealing.

Three samples were selected for HPHT treatment at pressure and temperature conditions initially in the graphite-stable region (similar to those commonly used in HPHT treatment; see, e.g., De Beers Industrial Diamonds et al., 2001) using a belt-type press. After annealing, only one sample showed a clear improvement in color.

In one instance (sample no. 57608), the color changed from Fancy Dark brown to Fancy black (figure A-1). In the second sample (no. 57688), the Fancy Light brown color did not show any perceptible change after treatment. When this second sample was annealed again at a temperature and pressure in the "diamond-stable region," there was still no improvement in its color (figure A-2). The third sample was cut into two pieces, with the as-grown portion (no. 58768) retained as a control while the other portion was HPHT annealed. The color changed from brown to light gray (figure A-3) after HPHT annealing. Significant color improvement after HPHT annealing was also observed in sample no. 57687 (see table 1 and figure 1) by one author (RCL); unfortunately this sample was not color graded or analyzed before HPHT annealing.

Although our HPHT-treatment experiments were limited, they do indicate that, unlike natural type IIa diamonds reported to date, different CVD synthetic diamonds will react differently to HPHT treatment, with no improvement in some cases. This can perhaps be explained by the fact that the cause of color in natural brown diamonds is different from that in these CVD-grown synthetic diamonds.

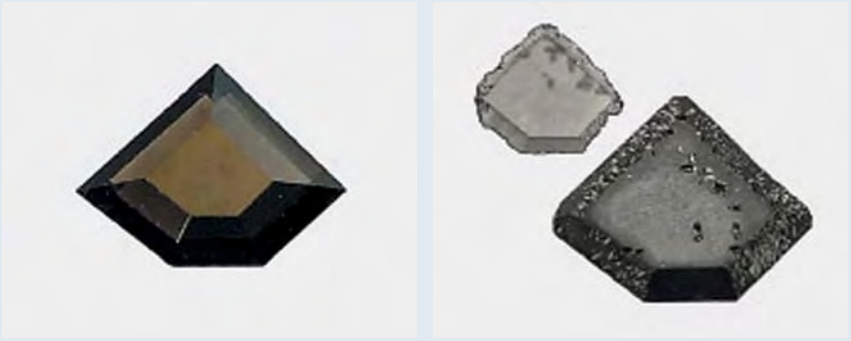

Figure A-1. The color of this 1.11 ct faceted CVD-grown synthetic diamond (no. 57608) changed from Fancy Dark brown as-grown (left) to Fancy black (right) after HPHT annealing in the graphite-stable region. The sample broke into two pieces after treatment, and now exhibits dissolution features along its edges. Photos by Elizabeth Schrader.

monly polycrystalline CVD diamond is created.

The first successful, reproducible growth of synthetic diamond as a thin film was achieved by W. G. Eversole in 1952 using a CVD technique (Angus, 1994, p. 21; it is interesting to note that this event predated General Electric's 1955 announcement that its researchers had created single-crystal synthetic diamonds). Goodwin and Butler (1997) reviewed the important features of the growth environment and critical aspects of the growth process. As illustrated in figure 2, the CVD method involves bringing together the needed gaseous reagents—typically a small amount of methane (CH_4) in hydrogen (H_2)—in a chamber with a substrate. A reaction among these components is initiated at high temperatures and low pressures (between 10 milliTorr [0.0000013 atm] and 1 atm). The reactants, products, and reactive species are transported throughout the chamber by diffusion and convection. Over the substrate surface, various reactions (adsorption, diffusion, and desorption) occur among the chemical species, leading to the deposition of synthetic diamond and, ultimately, the growth of a continuous layer of synthetic diamond. A number of variations of the CVD growth technique have been developed (see, e.g., Spear and Dismukes, 1994), and it is now possible to grow a colorless, high-purity, single-crystal layer of material to a thickness of a

Figure A-2. As grown, this 0.45 ct CVD synthetic diamond (no. 57688) was light brown (left). After HPHT annealing, first at the graphite-stable region and then at the diamond-stable region, the sample showed virtually no change in color (right). Photos by Wuyi Wang.

The brown color of type IIa natural diamonds is generally thought to result from the diamonds' having been subjected over geologic time to high stresses deep in the earth's mantle, resulting in plastic deformation (see, e.g., Wilks and Wilks, 1994). This deformation produces an atomic-level defect (i.e., an internal extended defect) by moving carbon atoms slightly away from their normal positions in the diamond lattice. HPHT treatment can remove brown coloration related to this defect in natural type IIa diamonds, and this is the basis of the diamond decolorization process announced in 1999 by scientists at General Electric Co. (see, e.g., Fisher and Spits, 2000).

In contrast, the brown color in the type IIa CVD-grown samples from Apollo Diamond Inc. results from precipitation of non-diamond carbon and/or internal extended defects such as dislocations. It appears that these defects in CVD synthetic diamonds do not react to HPHT annealing in the same way as plastic deformation in natural diamonds, and thus they do not always produce similar decolorization. This may help explain the diversified results we observed.

It should be noted that the HPHT annealing strongly affected some other defects in the CVD-grown diamonds. The H-related absorptions in the mid- and near-infrared regions described in the present article disappeared entirely after treatment. However, little variation was detected in the Si-related emission lines. In addition, the hardness of the CVD diamond seems to have been enhanced by the treatment, as gauged by the cutter during re-polishing (M. Witriol, pers. comm., 2003). Further experimental work is needed to explore the potential for HPHT treatment of CVD-grown synthetic diamonds to remove their brown color, and to identify these HPHT-treated CVD synthetic diamonds.

Figure A-3. A CVD synthetic diamond crystal was sawn in two, and the 0.18 ct as-grown portion on the left (no. 58768) was retained as a control sample while the 0.36 ct portion on the right was HPHT annealed. The brown as-grown sample became light gray after HPHT annealing. Photo by Wuyi Wang.

few millimeters on a diamond substrate.

Recent successes in the coating of relatively large surface areas (up to 100 cm^2 or more) with a continuous layer of diamond have created a whole new range of potential applications for polycrystalline CVD synthetic diamond products in other industries (see, e.g., Ravi, 1994). More than a decade ago, Fritsch et al. (1989) discussed some possible uses of this technique to coat gemstones with polycrystalline CVD synthetic diamond. So far, however, the application of CVD growth in the jewelry industry has remained negligible due to the problem of coating a polished gem with a synthetic diamond layer of sufficient thickness and the difficulty of growing single diamond crystals of a sufficient size and thickness to be faceted. This situation has now changed.

In the first quarter of 2004, Apollo Diamond Inc. will start commercial production of CVD synthetic diamonds for jewelry use. Brown to near-colorless type IIa crystals up to 1 ct or more are anticipated, with some experimental production of colorless type IIa and blue type IIb synthetic diamonds scheduled to start in 2005. A total annual production of 5,000–10,000 carats of faceted synthetic diamonds is planned initially, with expanded production in the future. Faceted samples will be mainly 0.25–0.33 ct, but they could reach 1 ct in mid-2004. Apollo Diamond Inc. is negotiating with a wide range of

jewelry industry distributors to develop possible marketing relationships, and the products will be sold with proper disclosure.

MATERIALS AND METHODS

A total of 13 CVD-grown synthetic diamonds were provided by one of the authors (RCL) for this study (see table 1). These samples are representative of the material currently produced by Apollo. Eight of the samples were crystals, and five were faceted. (Two of the crystals were subsequently faceted, and these faceted samples also were examined.) The largest crystal weighed 0.87 ct, and the largest faceted sample weighed 1.11 ct. Substrates and poor-quality exterior portions of some as-grown crystals were removed using a laser before examination in this study.

The visual features of the studied samples were observed with a gemological microscope. Reactions to ultraviolet radiation were checked in a darkened room with conventional four-watt long-wave (366 nm) and short-wave (254 nm) lamps, and also with the De Beers DiamondView deep-ultraviolet (<230 nm) imaging system (Welbourn et al., 1996). The faceted samples were examined by experienced diamond graders and given color and clarity descriptions equivalent to those used in the GIA diamond grading system.

Many of the studied samples were characterized by various spectrometric methods (again, see table 1). Certain data on some samples could not be obtained due to time constraints. Infrared absorption spectra were recorded on all samples in the mid-infrared range (6000–400 cm^{-1}) and nine samples (four crystals and five faceted) in the near-infrared range (11,000–4000 cm^{-1}) at room temperature with a Thermo-Nicolet Nexus 670 Fourier-transform infrared (FTIR) spectrometer, with a resolution of 1 cm^{-1} for the mid-infrared range and 4 cm^{-1} for the near-infrared range. A total of 1,024 scans per spectrum were collected to improve the signal-to-noise ratio. A KBr beam splitter was used

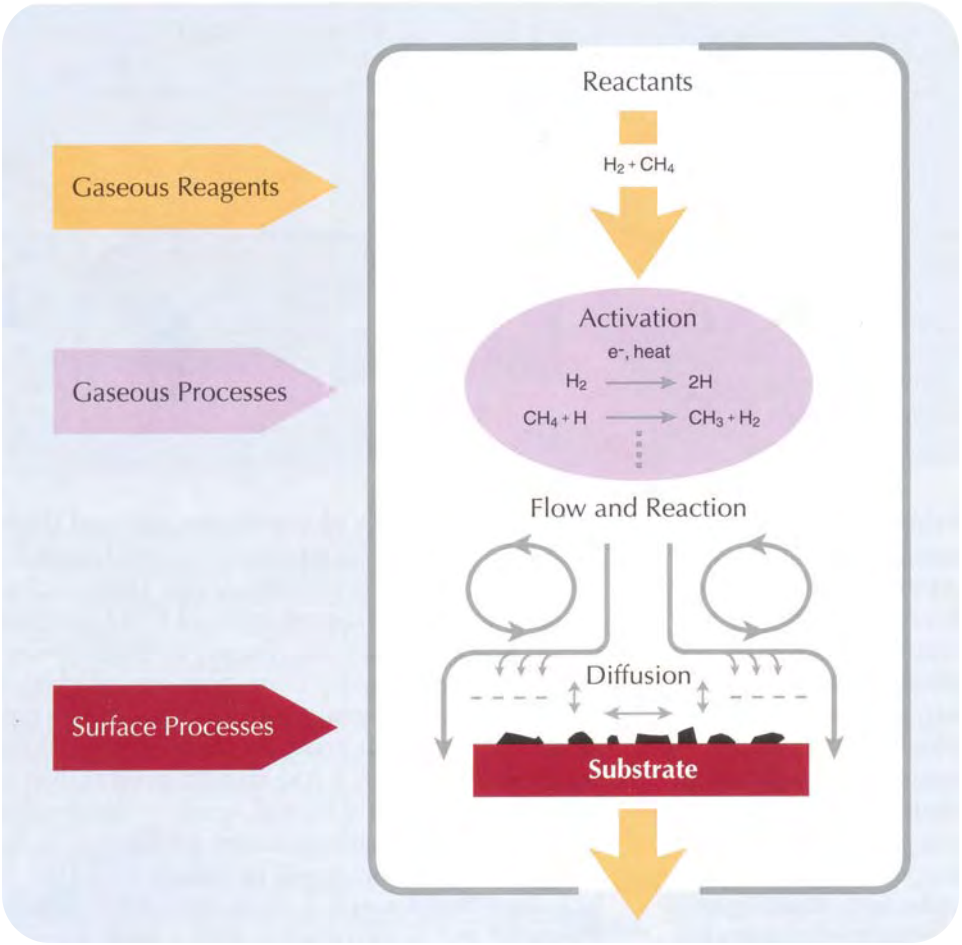

Figure 2. This schematic diagram shows the complex chemical reactions and transport processes that occur during the CVD growth of diamond layers on a substrate (modified after Butler and Woodin, 1993).

for the mid-infrared range, and a quartz beam splitter for the near-infrared range. A 6× beam condenser focused the incident beam on the sample. For comparison purposes and for calculation of absorption coefficients, each infrared spectrum was normalized according to its absorption in the two-phonon region (2664–1500 cm^{-1}).

A Thermo-Spectronic Unicam UV500 spectrophotometer was used to record absorption spectra on eleven samples (eight crystals and three faceted) over the range 250–850 nm with a sampling interval of 0.1 nm. For these analyses, the samples were held in a cryogenic cell cooled by liquid nitrogen. Photoluminescence spectra were recorded on all samples with a Raman Renishaw 1000 microspectrometer using two different lasers. The range 520–900 nm was recorded using an Argon-ion laser providing excitation at 514.5 nm operating at an initial power of 40 mW, while a He-Ne laser (632.8 nm) was used to record the range 650–850 nm in order to obtain better emission intensity and spectral resolution for some specific point defects. The samples were again held in a cryogenic cell cooled by liquid nitrogen. For all photoluminescence spectra, five scans were accumulated to achieve a better signal-to-noise ratio. Raman spectroscopy also was employed to identify some inclusions at room temperature.

RESULTS AND DISCUSSION

The characteristics of the CVD-grown synthetic diamond crystals and faceted samples are reported in table 1 and discussed below.

Crystals. CVD-grown diamond crystals from Apollo Diamond Inc. are very different in appearance from natural diamonds, as well as from traditional HPHT-grown synthetic diamonds; this is due to the dramatic differences in their formation environments and growth mechanisms (figure 3). Five of the eight crystals showed evidence of a substrate. In four of these, the substrate was type Ib HPHT synthetic diamond; in the fifth, it was CVD synthetic diamond. On the remaining three crystals, this substrate appeared to have been entirely removed. Without the substrate, the crystals were transparent with a light brown or gray to near-colorless appearance.

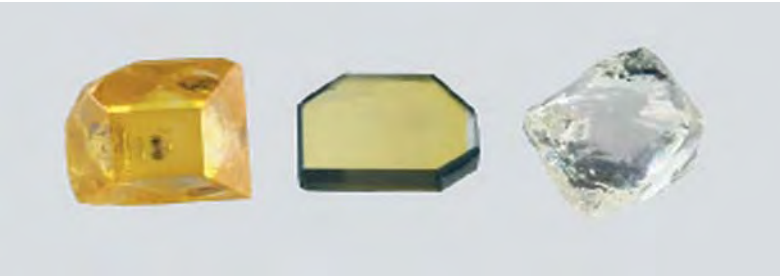

Figure 3. Due to the dramatic differences in their formation environments and growth mechanisms, CVD synthetic diamond crystals differ in appearance from natural diamonds, as well as from traditional HPHT-grown synthetic diamonds. HPHT synthetic diamonds (left) usually show well-developed {111} and {100} faces, and the flat surfaces have characteristic growth features. CVD-grown diamond crystals (center, no. 48922) usually have a tabular form, and {111} and {110} are poorly developed. Natural diamond crystals (right) may occur in any of several shapes that are very different from those of either CVD or HPHT synthetic diamonds. The octahedron is a very common form. Many natural diamonds display resorption features on their surfaces. Photo by Elizabeth Schrader.

The crystal form of a CVD synthetic diamond is dependent on the conditions under which it is grown. As is typical of the material Apollo Diamond has grown to date, our crystals exhibited a tabular shape with two near-parallel surfaces (which correspond to cubic {100} crystal faces; see figure 4). In addition, small but distinct octahedral {111} and dodecahedral {110} faces were present on

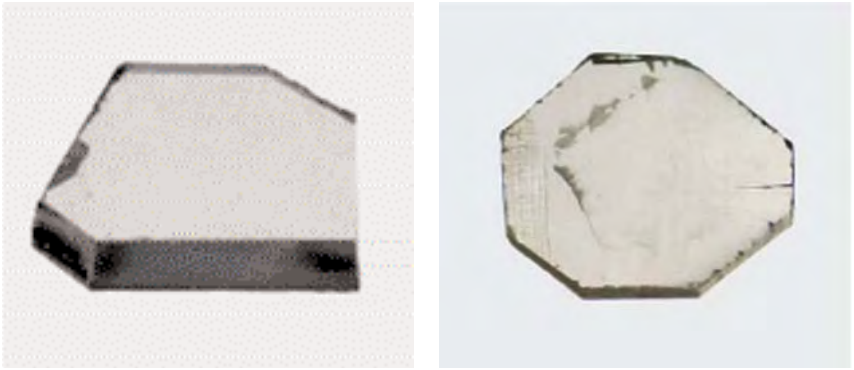

Figure 4. These CVD-grown synthetic diamond crystals illustrate the typical tabular shape of this material. The crystal on the left (no. 48921a) weighs 0.34 ct, while the one on the right (no. 56923) weighs 0.57 ct. The large, flat upper faces on both are the growth surfaces where new diamond material crystallized by chemical vapor deposition at high temperatures but low pressures. Photos by Elizabeth Schrader.

TABLE 1. Characteristics of Apollo Diamond Inc. CVD-grown synthetic diamonds, listed by GIA sample number.[a]

Property	48922	56923	57595	57597	58060	58768[b]	48921a
Weight (ct)	0.50	0.57	0.57	0.37	0.40	0.18	0.34
Description	Crystal	Crystal	Crystal	Crystal	Crystal	Crystal	Crystal
Shape	Tabular	Tabular	Tabular	Tabular	Tabular	Tabular	Tabular
Dimensions (mm)	5.6 × 4.5 × 1.5	8.5 × 8.2 × 0.6	7.1 × 7.1 × 0.8	6.1 × 6.4 × 0.6	5.0 × 4.5 × 1.4	3.6 × 2.9 × 1.1	4.9 × 3.7 × 1.3
Substrate	Type Ib HPHT synthetic diamond	None	Type Ib HPHT synthetic diamond	Type Ib HPHT synthetic diamond	Type Ib HPHT synthetic diamond	None	None
Color	Light brown	Light brown	Light brown	Very light brown	Light gray	Brown	Light brown
Clarity	nd	nd	nd	nd	nd	nd	nd
Fluorescence:							
Long-wave UV	Inert	Inert	Inert	Inert	Inert	Inert	Very weak orange
Short-wave UV	Very weak orange-yellow (chalky)	Very weak (color uncertain)	Strong, chalky green-yellow due to type Ib synthetic diamond substrate	Strong, chalky green-yellow due to type Ib synthetic diamond substrate, only at a small corner	Tiny region of chalky green-yellow due to type Ib synthetic diamond substrate, only at a small corner	Inert	Weak orange
DiamondView luminescence	Orangy red	Orangy red	Pink to orange (+greenish yellow from substrate)	Orangy red	Orangy red	Orangy red	nd
Infrared spectra (cm^{-1})	1344 3123 nd	1344	1344 3123 8753, 7354, 6856, 6425, 5564 group of features	3123 8753, 7354, 6856, 6425, 5564 group of features	1344 3123 8753, 7354, 6856, 6425, 5564 group of features	3123 8753, 7354, 6856, 6425, 5564 group of features	nd 3123 nd
UV-Vis-NIR spectra (nm)	Increasing absorption below 500	Increasing absorption below 500 Broad feature centered at 520	Broad 270 band Increasing absorption below 500 Broad feature centered at 520 268, 271	Broad 270 band Increasing absorption below 500 Broad feature centered at 520 268, 271	Broad 270 band Increasing absorption below 500 268, 271	Broad 270 band Increasing absorption below 500	Increasing absorption below 500 Broad feature centered at 520 271
	591, 596	591	591, 596	591, 596	591, 596	591, 596	591, 596
Photoluminescence spectra (nm)	575 637 596–597 doublet 737 543, 546, 589	575 637 596–597 doublet 737 534, 543, 563, 589, 591, 592	575 637 596–597 doublet 737 543, 563, 591, 592, 604	575 637 596–597 doublet 737 543, 563, 588, 591, 592, 604	575 637 596–597 doublet 737 543	575 637 596–597 doublet 737[d] 543, 559	575 637 596–597 doublet 737 543, 545, 546

[a] *nd = not determined.*
[b] *HPHT annealed for this study. Properties for pretreated material only are listed.*
[c] *HPHT annealed by Apollo Diamond Inc. Examined after treatment only.*
[d] *Very weak in intensity, detected only by using 632.8 nm laser excitation.*

one of the eight crystals. In several cases, these faces around the edges of the examined crystals had been removed from the samples.

Figure 5 illustrates a CVD diamond grown on a substrate of type Ib HPHT synthetic diamond. Because of the trace amounts of isolated nitrogen impurity in the substrate, this crystal appeared slightly yellow (although the CVD-grown portion is light brown as viewed from the side). A sharp boundary between the two portions of the crystal was visible to the unaided eye. When the sample was observed from the side with a strong ultraviolet radiation source (De Beers DiamondView), the two layers could be clearly distinguished due to their different luminescence (figure 6). Although the substrate in this sample was eye visible, in some instances it is very thin (less than 100 μm) and thus hardly detectable even with an optical microscope. However, even when a sample with such a thin substrate was observed with a DiamondView, it showed the strong green-yellow fluorescence and growth-sector pattern characteristic of HPHT synthetic diamonds (figure 7).

Figure 8 shows the growth of CVD synthetic diamond on a CVD synthetic diamond substrate. Initially, high-quality synthetic diamond was

48921b	49806a	49806b	45441	56924	57608[b]	57687[c]	57688[b]
0.14	0.87	0.28	0.23	0.31	1.11	~0.2	0.45
Faceted from 48921a	Crystal	Faceted from 49806a	Faceted	Faceted	Faceted	Faceted	Faceted
Cut-corner rectangular modified brilliant	Tabular	Square modified brilliant	Pear-shaped brilliant	Cut-corner square modified brilliant	Kite modified brilliant	Round brilliant	Portrait cut
4.0 × 1.8 × 3.6	nd	3.6 × 3.5 × 2.5	nd	4.1 × 3.8 × 2.5	6.7 × 6.8 × 2.2	nd	7.6 × 3.9 × 1.2
None	Type IIa CVD synthetic diamond	None	None	None	Type Ib HPHT synthetic diamond	None	None
Fancy Light pinkish brown	Near-colorless	Fancy brownish yellow	Fancy brown	Fancy Dark brown	Fancy Dark brown	K (faint brown)	Fancy Light brown
VS_2	nd	VS_1	nd	SI_2	SI_1	SI_2	SI_1
Very weak orange	Very weak orange-yellow	Very weak orange-yellow	nd	Inert	Inert	Very weak orange	Very weak yellow
Weak orange	Moderate orange-yellow	Moderate orange-yellow	nd	Moderate chalky orange-yellow	Tiny region of chalky green-yellow due to type Ib synthetic diamond substrate, only at a small corner	Moderate yellowish green	Very weak orange
Orangy red	Orangy red	Orangy red	nd	Orangy red	Orangy red	nd	Orangy red
nd	1344 3123 nd	nd	1344 3123 8753, 7354, 6856, 6425, 5564 group of features	1344 3123 8753, 7354, 6856, 6425, 5564 group of features	1344 3123 8753, 7354, 6856, 6425, 5564 group of features	3029	3123 8753, 7354, 6856, 6425, 5564 group of features
nd	Increasing absorption below 500 Broad feature centered at 520 591, 596 737	nd	nd	Broad 270 band Increasing absorption below 500 Broad feature centered at 520 268, 271 419, 447, 625, 637 591, 596 737	Broad 270 band Increasing absorption below 500 268, 271 301, 305, 447, 625, 637, 653 591, 596 737	nd	Broad 270 band Increasing absorption below 500 271 591, 596 737
575 637 596–597 doublet 737 543, 545, 546	575 637 596–597 doublet 737 543, 563, 589, 591, 592	nd	575 637 596–597 doublet 737 543	575 637 596–597 doublet 737 543, 563, 591, 592	575 637 737 543	575 637 596 737 532, 533, 535, 543, 544, 546, 764, 765, 792	575 637 596–597 doublet 737 543, 546, 563

deposited on the substrate. After this initial precipitation, the growth process tended to deposit a grayish black phase—best described as "non-diamond carbon"—around the edges of the crystal, which is removed during faceting. However, with this sub-

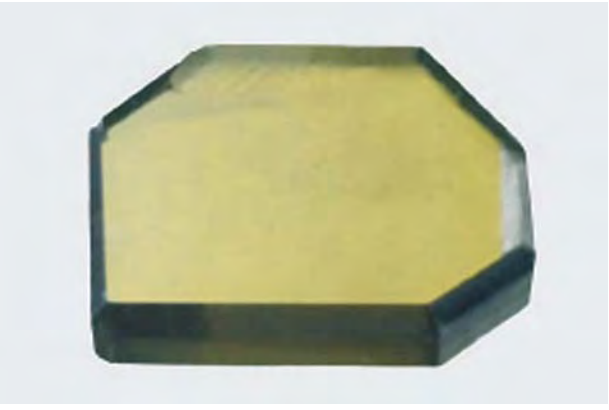

Figure 5. Depending on the intended application, synthetic diamond can be grown on various substrate materials by the CVD process. This 0.50 ct light brown CVD synthetic diamond (no. 48922) was produced on a substrate of yellow HPHT synthetic diamond. Photo by Elizabeth Schrader.

Figure 6. The two layers in the sample shown in figure 5 exhibit different reactions to UV radiation when observed with the De Beers DiamondView imaging system (CVD-grown diamond on the left and HPHT synthetic diamond substrate on the right). Photo by Wuyi Wang.

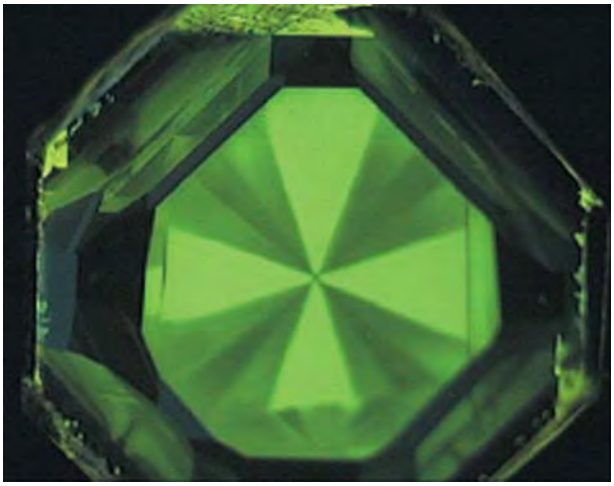

Figure 7. Although what remains of the HPHT synthetic diamond substrate on this 0.57 ct CVD crystal (no. 57595) is so thin it is almost undetectable with an optical microscope, the DiamondView reveals the strong green-yellow fluorescence and growth-sector pattern typical of HPHT synthetic diamond. Photo by Wuyi Wang.

strate the synthetic diamond overgrowth is relatively thick (here, 2.5 mm). The substrate and the overgrowth appear to be continuous—no physical boundary between them could be seen with an optical microscope up to 100× magnification.

Faceted Gems. All of the faceted samples were cut to optimize the yield from the tabular crystals (see, e.g., figure 9). In general, they displayed an evenly distributed brown coloration, which varied from faint to Fancy Dark brown; one was near-colorless. The near-colorless crystal (no. 49806a) became Fancy brownish yellow (no. 49806b) after faceting. It is likely that this change in color was due to the heat of the faceting process, much the same way natural rough or a partially polished diamond will change color in the course of faceting. Unlike some natural and HPHT-grown synthetic colored diamonds, no graining or color zoning was seen in the CVD samples when they were examined with magnification through the table facet. However, when observed through the girdle (which is perpendicular to the growth direction of the tabular crystals), at least one sample displayed more than five faint brown planes oriented parallel to {100} (figure 10). These represent short disruptions or changes in deposition, such as a fluctuation in temperature.

We believe that these brown planes reflect the deposition of relatively more non-diamond carbon and/or the presence of internal extended defects such as dislocations. This is different from the banded coloration seen in natural brown diamonds, which is due to plastic deformation of the diamond

Figure 8. In this 0.87 ct sample (no. 49806a), shown here from two different views, near-colorless CVD synthetic diamond has been grown over a CVD substrate, resulting in a much thicker crystal than would have been produced with an HPHT synthetic diamond substrate. Note the precipitation of graphite and non-diamond carbon around the crystal that gives rise to the dark gray to black rim. Photos by Elizabeth Schrader.

Figure 9. As these samples illustrate (left, no. 48921b at 0.14 ct; right, no. 49806b at 0.28 ct), the CVD-grown diamonds were faceted to get the best yield from the tabular crystals. The sample on the right, which was equivalent to Fancy brownish yellow, was cut from a near-colorless crystal (see table 1). It is likely that the color changed during faceting, as has been known to occur with natural diamonds. Photos by Elizabeth Schrader.

while in the earth. In the CVD material, the brown planes seem to be narrow, and they exhibit a sharper boundary, than the slip bands typically seen in natural brown diamonds (e.g., Fritsch, 1998). The overall brown color of the material, like the brown planes mentioned above, could be attributed to the presence of non-diamond carbon and/or internal extended defects such as dislocations.

Relative to the GIA diamond grading system, the samples ranged in clarity from VS_1 to SI_2. We observed only a few small inclusions—they were opaque and irregularly shaped, possibly due to deposition of non-diamond carbon (figure 11). In addition, tiny pinpoints were common in many samples, and these were principally responsible for each sample's resulting clarity grade (figure 12). Since no metal flux/catalyst is used in the CVD growth process, the metallic inclusions that commonly occur in HPHT-

Figure 10. When viewed perpendicular to the growth direction and the table facet {100}, this CVD-grown diamond (here, no. 57688) exhibited brown graining parallel to {100}. Photomicrograph by Wuyi Wang; magnified 30×.

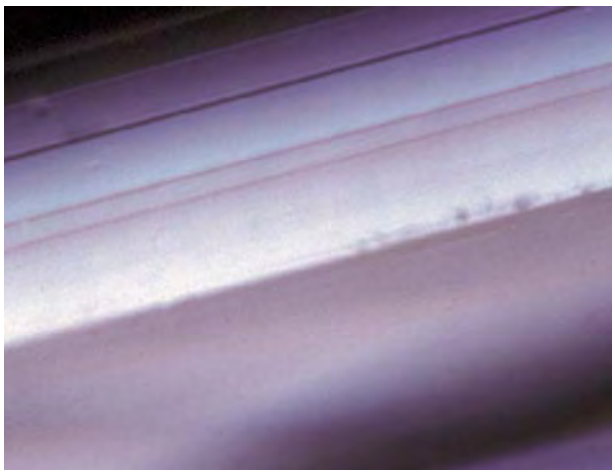

Figure 11. On occasion, CVD-grown synthetic diamonds (here, no. 49806b) display small, opaque, irregular inclusions that are thought to be particles of non-diamond carbon on the basis of Raman spectroscopy. Opaque inclusions in natural or HPHT synthetic diamonds might look similar in appearance, so these non-diamond carbon inclusions may be of little diagnostic value for identification purposes. Photomicrograph by Wuyi Wang; magnified 15×.

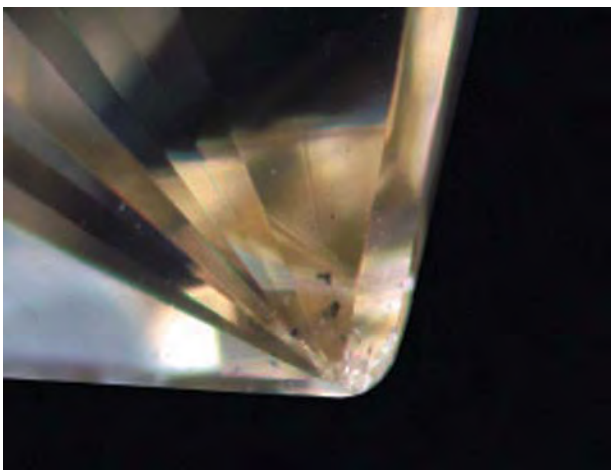

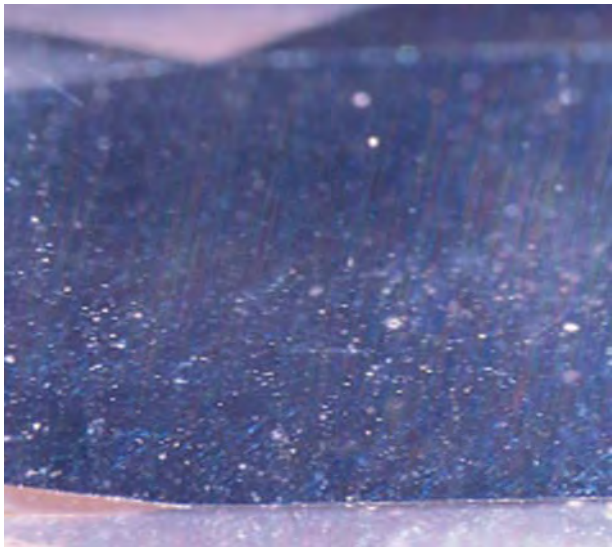

Figure 12. Pinpoint inclusions of uncertain identity were seen in some of the CVD-grown diamonds (here, no. 57688). Photomicrograph by Christopher P. Smith; magnified 30×.

grown synthetic diamonds are absent in the Apollo material. In rare cases, small fractures were seen.

Anomalous birefringence, a typical feature of diamond, is formed due to residual internal strain. All the CVD-grown synthetic diamonds examined in this study displayed cross-hatched bands of low-order interference colors (when viewed through the table facet perpendicular to the {100} face), probably due to an uneven rate of deposition in growth. Although the table-facet orientation in a natural diamond varies according to the shape of the rough, the strain pattern is typically a much more well-defined cross-hatch pattern with higher-order interference colors, especially in type IIa diamonds. We also saw small, localized strain areas with relatively higher interference colors surrounding tiny defect centers as well as small inclusions or fractures in some of our samples (see, e.g., figure 13). Observation of such strain patterns could be considered as a strong indication of CVD-grown synthetic diamond.

Luminescence. As detailed in table 1, the reaction to ultraviolet radiation emitted by a standard gemological UV lamp varied among all the samples we examined. Eight were inert to long-wave UV, and the balance of those tested fluoresced a very weak orange, orange-yellow, or yellow. However, all except one (no. 58768) of the as-grown CVD samples tested showed some reaction to short-wave UV, ranging from very weak to moderate in orange to orange-yellow. In those samples where some HPHT-synthetic diamond substrate remained, the substrate fluoresced more strongly, with a chalky green-yellow color (figure 14). In general, no phosphoresce was observed.

A characteristic feature seen in nine of the 10 CVD-grown diamonds tested is a strong orangy red fluorescence when they were exposed to high-energy UV radiation in the DiamondView imaging system (figure 15). In our experience, this fluorescence is related to the emission from N-V centers (mainly 575 nm) and is very rare in natural type IIa diamonds. Note that, depending on its size, a remnant of HPHT synthetic diamond substrate in a faceted CVD diamond could have a strong impact on the DiamondView fluorescence image. In sample no. 57595, for example, the HPHT synthetic diamond substrate covers the whole {100} face, so it could entirely shield the emission from the CVD-grown diamond if the UV radiation hit the {100} face direct-

Figure 13. This crystal (no. 57595), measuring 7.1 mm across, displays the characteristic strain pattern of a CVD-grown diamond when viewed perpendicular to a cubic crystal face {100}. Photo by Wuyi Wang; crossed polarizers.

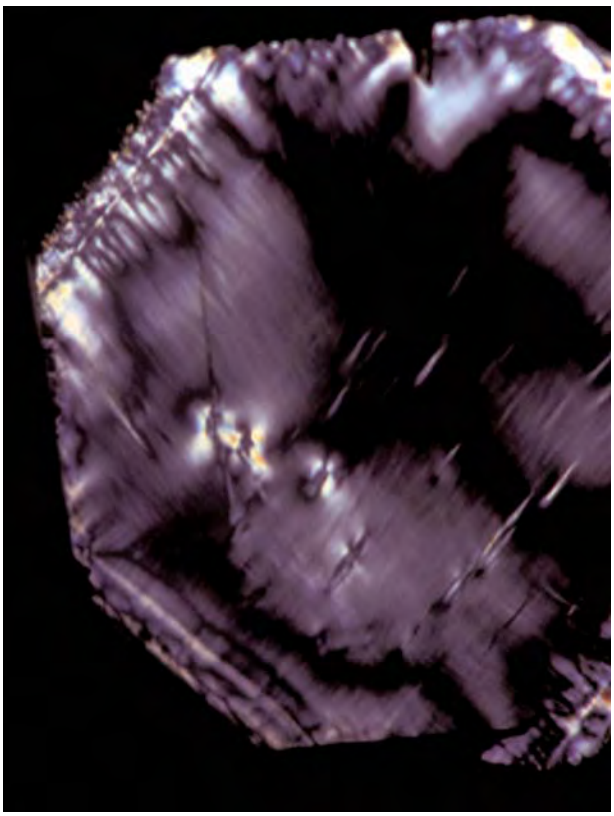

ly. When the CVD side was faced to the UV radiation, pink to orange fluorescence was observed.

Spectroscopy. *Infrared.* The infrared absorption spectra shown in figure 16 are representative of the as-grown CVD synthetic diamonds examined. Most samples displayed little absorption around the one-phonon region (<1332 cm^{-1}; again, see table 1). Eight samples displayed a very weak absorption peak at 1344 cm^{-1}, demonstrating the presence of trace amounts of isolated nitrogen impurity (typical of type Ib diamond).

Analysis of those diamonds that did not have an HPHT synthetic diamond substrate, or of selected regions where the substrates had been removed, showed that the strongest absorption at 1344 cm^{-1} corresponded to an absorption coefficient of 0.14 cm^{-1} (no. 56924), and the second highest was 0.06 cm^{-1}. No absorption at 1344 cm^{-1} was detected in four samples. These observations indicate that the nitrogen concentration differs from sample to sample, and thus the purity of CVD synthetic diamond depends on the specific conditions under which it was grown. Using the calibration of Lawson et al. (1998), we see that the highest concentration of isolated nitrogen in the studied CVD diamonds should be less than 5 ppm.

Based on a working definition of diamond types (Wilks and Wilks, 1994, pp. 75–77), all the CVD samples we examined were type IIa. Traces of hydrogen also were detected in 11 samples, as a sharp absorption peak at 3123 cm^{-1} with full width at the half maximum (FWHM) varying from 3.58 to 1.81 cm^{-1} (figure 17; also see Zaitzev, 2001, p. 32) and an absorption coefficient ranging from 0.08 to 0.01 cm^{-1}. In all the as-grown CVD synthetic diamonds examined, only one sample (no. 56923), which was light brown, did not show this H-related

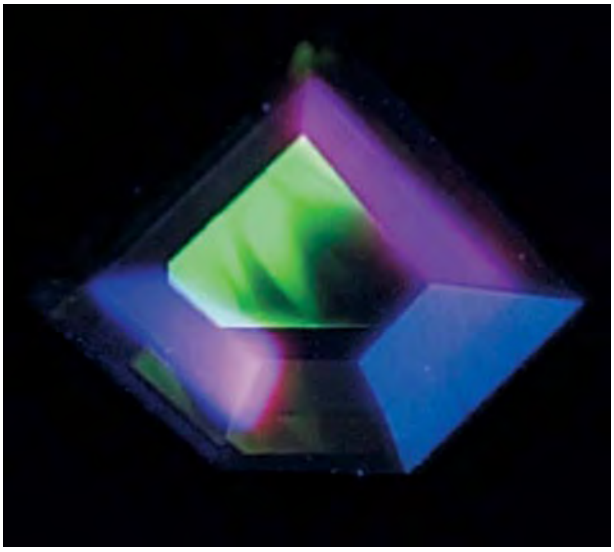

Figure 14. The CVD synthetic diamond portion of this 1.11 ct faceted sample (no. 57608) is inert to short-wave UV radiation, but the small area of HPHT-synthetic diamond substrate that remained after cutting fluoresces a strong green-yellow color. Photo by Elizabeth Schrader.

absorption. The fact that the strongest 3123 cm^{-1} absorption was observed in Fancy Dark brown sample no. 56924 does not necessarily mean the coloration is due to hydrogen, since the color may be due to non-diamond carbon and/or internal extended defects while coincidentally more hydrogen was captured during growth. Hydrogen is a common impurity in natural diamond; however, the position of the fundamental C-H stretching vibration is almost always at 3107 cm^{-1}.

In the near-infrared region (again, see figure 16), one or more distinct absorptions of unknown origin were observed at 8753, 7354, 6856, 6425, and 5564 cm^{-1} in all eight as-grown CVD synthetic diamonds analyzed, with the one at 7354 cm^{-1} commonly

Figure 15. The CVD-grown diamonds examined during this study displayed a strong orangy red fluorescence when they were exposed to UV radiation in the De Beers DiamondView imaging system. The sample on the left is no. 48921b (0.14 ct); on the right is sample no. 49806b (0.28 ct). Photos by Wuyi Wang.

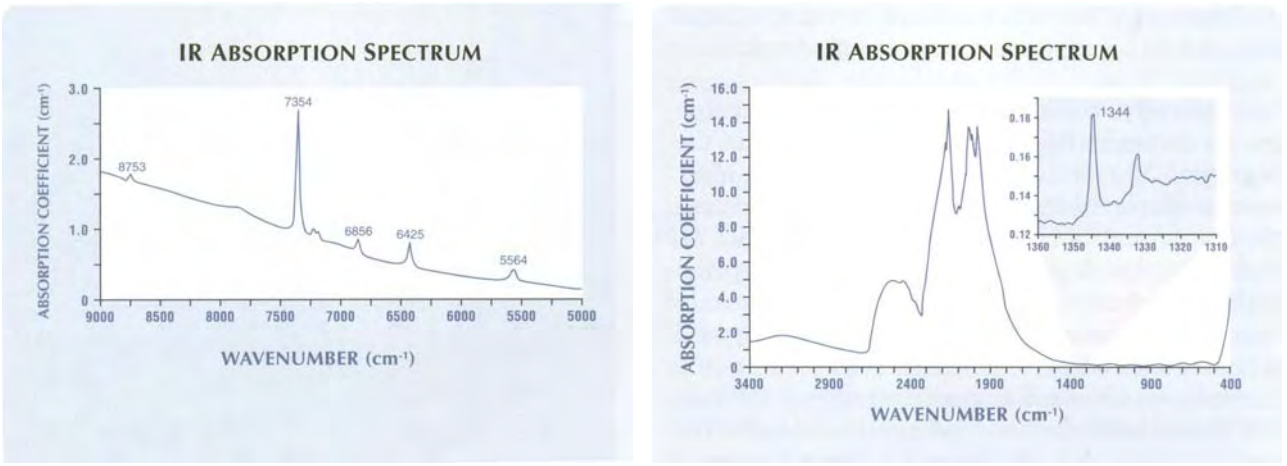

Figure 16. These infrared absorption spectra (left, sample no. 57608; right, no. 49806a) are typical of those recorded from the as-grown CVD synthetic diamonds. All samples examined were type IIa, but a few contained trace amounts of an isolated nitrogen impurity (at concentrations of less than 5 ppm, with most less than 1.0 ppm). Absorption bands at 8753, 7354, 6856, 6425, and 5564 cm^{-1} were observed in all tested as-grown CVD synthetic diamonds.

showing the strongest intensity. In two samples (nos. 57595 and 57597), the peak at 6856 cm^{-1} was the strongest absorption in the near-infrared region. These absorptions in the NIR range have been attributed to hydrogen impurities in as-grown CVD diamond (Fuchs et al., 1995a,b).

UV-Vis-NIR. Most of the samples tested displayed a smooth, gradual increase in absorption from about 500 nm toward the blue end of the spectrum. In general, the stronger brown coloration corresponded to an increase in this absorption.

A few of the samples also showed distinct absorption lines (again, see table 1). For example, the spectrum of a dark brown CVD synthetic diamond (see figure 18, sample no. 57608) exhibited a broad band around 270 nm and two sharp absorption lines at 268 and 271 nm, all of which are related to traces of isolated nitrogen (Zaitsev, 2001, pp. 342–344). Weak but sharp lines at 447, 591, 596, 625, 637, 653, and 737 nm were also detected in this sample. In addition, a broad band around 520 nm occurred in two other samples. Among the tested samples, the FWHM of the 271 nm absorption peak varied from 0.60 to 0.85 nm.

Weak absorptions at 591 nm and/or 596 nm were detected in 11 samples. These two peaks were relatively broad, with a FWHM around 3 nm. The FWHM of absorptions at 447 nm and 625 nm is generally less than 1.0 nm. Also as described in Zaitsev (2001, pp. 197–203), the 637 nm peak is caused by the nitrogen-vacancy (N-V center). Causes of the other peaks remain unknown, but some of them could be related to traces of hydrogen in the lattice. A weak absorption line at 737 nm, due to traces of silicon (Zaitzev, 2001, pp. 174–181), was observed in four samples.

Photoluminescence (PL). Despite a large variation in coloration, all the as-grown CVD synthetic dia-

Figure 17. This expanded portion of the infrared spectrum from sample no. 56924 shows a weak absorption at 3123 cm^{-1} due to hydrogen as an impurity in the crystal lattice. This sample had the strongest absorption at 3123 cm^{-1} of all those tested.

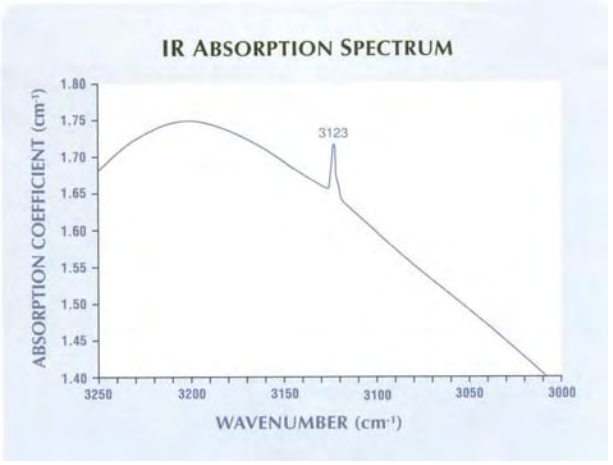

monds in this study showed similar PL spectra (again, see table 1 and also figure 19). When a green 514.5 nm laser was employed, the CVD samples displayed strong N-V emission lines at 575 and 637 nm. The relative intensities of these two lines varied, but in general the 575 nm was more intense. All but one of the samples also showed a doublet at 596 and 597 nm, the cause of which is uncertain. Although these two peaks may not be observable at room temperature, they are very sharp, with a FWHM of 0.30–0.38 nm and 0.28–0.37 nm, respectively.

All samples tested also had a moderately strong 737 nm emission line—actually, a doublet peak at 736.5 and 736.9 nm—due to the incorporation of trace amounts of silicon during growth. The FWHM of this peak varied from 0.91 to 1.04 nm. This peak could be very useful for identification of CVD-grown diamonds because it usually does not occur in natural diamonds or HPHT-grown synthetic diamonds (see, e.g., Zaitzev, 2001).

The He-Ne red laser at 632.8 nm is extremely efficient in exciting the silicon peak in diamond. For instance, in sample no. 58768, the concentration of Si is so low that no 737 nm emission could be detected when using the 514.5 nm laser. Weak but distinct 737 nm emission was confirmed in this sample by using the 632.8 nm laser. In addition to these strong emission lines, relatively weak lines at 543, 546, 559, 563, 588, 589, 591, 592, and 604 nm were also observed in some of the samples. In one case (no. 57597), the emission at 563 nm was as strong as the first-order diamond Raman peak. Assignment of these emission lines generally has not yet been determined.

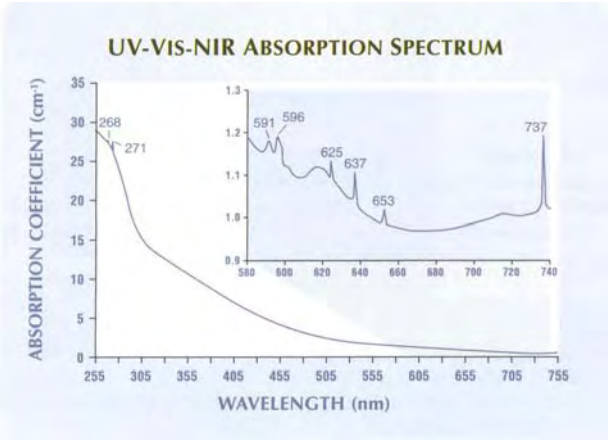

Figure 18. As was representative of the CVD synthetic diamonds examined, this UV-Vis-NIR absorption spectrum (from sample no. 57608) exhibited a broad band around 270 nm and two sharp absorption lines at 268 and 271 nm, all of which are related to trace isolated nitrogen. Weak but sharp lines at 625, 637, 653, and 737 nm were detected. Also evident were two relatively broad absorptions at 591 and 596 nm. The absorption at 737 nm is due to a trace amount of silicon. Note that a region of the sample without any HPHT synthetic diamond substrate was selected for spectroscopic analysis using a metal mask.

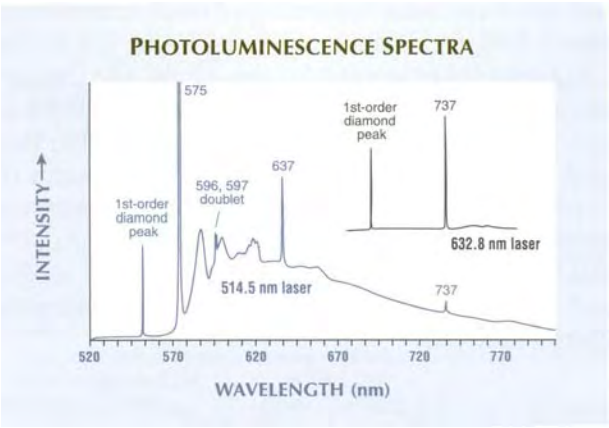

Figure 19. These representative photoluminescence spectra (here, from sample 48921a) display strong emissions from the N-V center at 575 and 637 nm, and also the sharp 596/597 nm doublet. The 737 nm emission is particularly sensitive to excitation by the 632.8 nm red laser.

IDENTIFICATION

When they become available in the marketplace, CVD synthetic diamonds are likely to be difficult for a jeweler/gemologist to identify, since there are few diagnostic features that can be determined with standard gemological equipment. A brown coloration, the shallow depth of a cut stone, and the characteristic strain pattern of this CVD-grown material may provide clues in some cases. In the laboratory, the strong orangy red luminescence seen with the DiamondView is generally the best visual clue to a CVD sample's identity. However, conclusive identification requires the use of advanced spectroscopic methods. All the Apollo samples examined are type IIa diamonds, although some showed an infrared absorption feature at 1344 cm^{-1} due to trace amounts of isolated nitrogen. The two PL peaks related to the N-V center at 575 and

637 nm have been reported in HPHT-treated diamonds (see, e.g., Fisher and Spits, 2000), but in the CVD samples examined for this study, the intensities of both peaks were much stronger. A doublet at 596–597 nm, which has never been reported in natural diamond, was recorded in the PL spectra of almost all the samples tested. Finally, the infrared absorption due to hydrogen (mainly at 3123 cm^{-1}) and the spectroscopic features due to silicon (at 737 nm) appear to be unique to these CVD-grown synthetic diamonds.

CONCLUSION

Gem-quality synthetic diamonds grown by Apollo Diamond Inc. represent some of the first examples of single-crystal material produced by the CVD process that is intended for the jewelry trade. Although production is limited at present, plans call for larger-scale manufacturing of crystals weighing up to 3 ct in the near future. Faceted pieces of this material do not exhibit most of the characteristic features shown by HPHT-grown synthetic diamonds (such as pronounced color and fluorescence zoning, or metal inclusions), although they do have a distinctive strain pattern. Strong orangy red luminescence as seen in the DiamondView provides another good indication. However, these CVD-grown synthetic diamonds can be positively identified only by spectroscopy, with instrumentation that typically is available only in advanced gemological laboratories.

Given the range of potential technological applications, further improvements in CVD growth processes are likely. Various additional kinds of CVD synthetic diamonds could become available in the future. These include high-purity colorless crystals and crystals that are blue due to the incorporation of boron. Also possible is the crystallization of CVD material on a natural gem diamond, either on a rough crystal that is then faceted, or perhaps as an overgrowth on portions of a faceted diamond, depending on its crystallographic orientation. These products may or may not exhibit the features described in this article. It is also important to note that the diagnostic absorption or emission features observed in the spectra of the CVD synthetic diamonds examined so far could be below the instrument detection limit with improved purity of this material. Gemological laboratories and others involved with gem identification must continue to develop techniques to recognize these new kinds of gem materials as they become available.

ABOUT THE AUTHORS

Dr. Wang is a research scientist, Mr. Moses is vice president of Identification and Research, and Mr. Hall is supervisor of analytical equipment at the GIA Gem Laboratory, New York; Dr. Linares is chairman, Apollo Diamond Inc., Boston, Massachusetts; Dr. Shigley is director of GIA Research in Carlsbad, California; and Dr. Butler is head of the Gas/Surface Dynamics Section in the Naval Research Laboratory, Washington, D.C.

ACKNOWLEDGMENTS: Constructive reviews were provided by Prof. Alan Collins of Kings College, London, and Dr. Emmanuel Fritsch of the University of Nantes, France. HPHT annealing of the CVD synthetic diamonds was performed by Sundance Diamond in Orem, Utah, and Phoenix Crystal Corp. in Ann Arbor, Michigan. The authors are grateful to Mates Witriol of New York for repolishing two of the HPHT-annealed diamonds. Afkari & Sons Inc. of New York kindly mounted some of the CVD synthetic diamonds in jewelry.

REFERENCES

Angus J.C. (1994) Development of low-pressure diamond growth in the United States. In K.E. Spear and J.P. Dismukes, Eds., *Synthetic Diamond: Emerging CVD Science and Technology*, John Wiley & Sons, New York, pp. 21–39.

Butler J.E., Woodin R.L. (1993) Thin film diamond growth mechanisms. *Philosophical Transactions of the Royal Society of London*, Vol. A342, pp. 209–224.

Burns R.C., Davies G.J. (1992) Growth of synthetic diamond. In J.E. Field, Ed., *The Properties of Natural and Synthetic Diamond*, Academic Press, London, pp. 395–422.

Crowningshield G.R. (1971) General Electric's cuttable synthetic diamonds. *Gems & Gemology*, Vol. 13, No. 10, pp. 302–314.

Davies G. (1994) *Properties and Growth of Diamond*. Electronic Materials Information Service (EMIS) Dataviews Series No. 9, Institute of Electrical Engineers, London.

Davis R.F. (1993) *Diamond Films and Coatings—Development, Properties, and Applications*. Noyes Publications, Park Ridge, NJ, 421 pp.

De Beers Industrial Diamonds, Spits R.A., Burns R., Fisher D. (2001) *High Temperature/Pressure Color Change of Diamond*. International (PCT) patent application WO 01/72404A1, filed April 2.

Deljanin B., Hainschwang T., Fritsch E. (2003) Update on study of CVD diamonds. *Jewellery News Asia*, No. 231, November 2003, pp. 134–139.
Field J.E. (1992) *The Properties of Natural and Synthetic Diamond*. Academic Press, London.
Fisher D., Spits R.A. (2000) Spectroscopic evidence of GE POL HPHT-treated natural type IIa diamonds. *Gems & Gemology*, Vol. 36, No. 1, pp. 42–49.
Fritsch E., Conner L., Koivula J.I. (1989) A preliminary gemological study of synthetic diamond thin films. *Gems & Gemology*, Vol. 25, No. 2, pp. 84–90.
Fritsch E. (1998) The color of diamond. In G. E. Harlow, Ed., *The Nature of Diamonds*, Cambridge University Press, pp. 23–47.
Fuchs F., Wild C., Schwarz K., Muller-Sebert W., Koidl P. (1995a) Hydrogen induced vibrational and electronic transitions in chemical vapor-deposited diamond, identified by isotopic substitution. *Applied Physics Letters*, Vol. 66, No. 2, pp. 177–179.
Fuchs F., Wild C., Schwarz K., Koidl P. (1995b) Hydrogen-related IR absorption in chemical vapor deposited diamond. *Diamond and Related Materials*, Vol. 4, Nos. 5/6, pp. 652–656.
Goodwin D.G., Butler J.E. (1997) Theory of diamond chemical vapor deposition. In M.A. Prelas, G. Popovici, and L.K. Bigelow, Eds., *Handbook of Industrial Diamonds and Diamond Films*, Marcel Dekker, New York, pp. 527–581.
Hunter G., Paparella A. (2003) New diamond age? Lab-made diamonds are dead ringers for natural ones. ABCNews.com, http://abcnews.go.com/sections/GMA/SciTech/GMA030909Diamond_synthetics_hunter.html, posted Sept. 9, 2003.
Lawson S.C., Fisher D., Hunt D.C., Newton M. (1998) On the existence of positively-charged single-substitutional nitrogen in diamond. *Journal of Physics C: Condensed Matter*, Vol. 10, No. 27, pp. 6171–6180.
Linares R.C., Doering P. (1999) Properties of large single crystal diamond. *Diamond and Related Materials*, Vol. 8, Nos. 2/5, pp. 909–915.
Linares R.C., Doering P.J. (2003) *System and Method for Producing Synthetic Diamond*. U.S. Patent 6,582,513, filed May 14, 1999.
Ravi K.V. (1994) Technological applications of CVD diamond. In K.E. Spear and J.P. Dismukes, Eds., *Synthetic Diamond: Emerging CVD Science and Technology*, John Wiley & Sons, New York, pp. 533–580.
Shigley J.E., Fritsch E., Reinitz I., Moses T.E. (1995) A chart for the separation of natural and synthetic diamonds. *Gems & Gemology*, Vol. 31, No. 4, pp. 256–264.
Spear K.E., Dismukes J.P. (1994) *Synthetic Diamond: Emerging CVD Science and Technology*. John Wiley & Sons, New York, 663 pp.
Wang W., Hall M., Moses T.M., Shigley J.E. (2003) Gem News International: Chemical vapor deposition (CVD)—A new source of gem-quality laboratory-created diamond. *Gems & Gemology*, Vol. 34, No. 3, pp. 237–239.
Welbourn C.M., Cooper M., Spear P.M. (1996) De Beers natural versus synthetic diamond verification instruments. *Gems & Gemology*, Vol. 32, No. 3, pp. 156–169.
Wilks E., Wilks J. (1994) *Properties and Applications of Diamond*. Butterworth-Heinemann, Oxford, 525 pp.
Zaitsev A.M. (2001) *Optical Properties of Diamond*. Springer-Verlag, Berlin, 502 pp.

PEZZOTTAITE FROM AMBATOVITA, MADAGASCAR: A NEW GEM MINERAL

Brendan M. Laurs, William B. (Skip) Simmons, George R. Rossman, Elizabeth P. Quinn, Shane F. McClure, Adi Peretti, Thomas Armbruster, Frank C. Hawthorne, Alexander U. Falster, Detlef Günther, Mark A. Cooper, and Bernard Grobéty

Pezzottaite, ideally $Cs(Be_2Li)Al_2Si_6O_{18}$, is a new gem mineral that is the Cs,Li–rich member of the beryl group. It was discovered in November 2002 in a granitic pegmatite near Ambatovita in central Madagascar. Only a few dozen kilograms of gem rough were mined, and the deposit appears nearly exhausted. The limited number of transparent faceted stones and cat's-eye cabochons that have been cut usually show a deep purplish pink color. Pezzottaite is distinguished from beryl by its higher refractive indices (typically n_o=1.615–1.619 and n_e=1.607–1.610) and specific gravity values (typically 3.09–3.11). In addition, the new mineral's infrared and Raman spectra, as well as its X-ray diffraction pattern, are distinctive, while the visible spectrum recorded with the spectrophotometer is similar to that of morganite. The color is probably caused by radiation-induced color centers involving Mn^{3+}.

Beginning with the 2003 Tucson gem shows, cesium-rich "beryl" from Ambatovita, Madagascar, created excitement among gem collectors and connoisseurs due to its deep purplish pink color (figure 1) and the attractive chatoyancy displayed by some of the material. Although it was sold during and after the Tucson gem shows as "raspberyl," "red beryl," "pink beryl," "hot pink-red beryl," and especially "raspberry beryl," subsequent examinations (see, e.g., Simmons et al., 2003) revealed properties that were anomalous for beryl and were associated with very high concentrations of cesium (Cs). In September 2003, the International Mineralogical Association approved the name *pezzottaite* (pe-zó-ta-ite) for this new species of the beryl group. It is named after Dr. Federico Pezzotta (Natural History Museum, Milan, Italy), who was among the first to investigate this new mineral, in recognition of his scientific contributions to the mineralogy of Madagascar (Hawthorne et al., 2003).

With the addition of pezzottaite—ideally $Cs(Be_2Li)Al_2Si_6O_{18}$—the beryl group consists of four members. The other three (all hexagonal) are: beryl ($Be_3Al_2Si_6O_{18}$; Aurisicchio et al., 1988), bazzite ($Be_3Sc_2Si_6O_{18}$; Armbruster et al., 1995), and stoppaniite ($Be_3Fe_2Si_6O_{18}$; Ferraris et al., 1998; Della Ventura et al., 2000). Pezzottaite, which is rhombohedral, is not a Cs-rich beryl but rather a new mineral species that is closely related to beryl. Another mineral, indialite ($[Al_2Si]Mg_2[Al_2Si_4]O_{18}$; Meagher and Gibbs, 1977), is also sometimes included in the beryl group. Of these, only beryl and pezzottaite have been found in gem quality. (Note: In this article, "beryl" refers to the mineral species, rather than the group, unless otherwise specified.)

Pezzottaite has been confirmed from just one deposit in Madagascar, the Sakavalana granitic pegmatite located near Ambatovita in a remote area of the central highlands. In addition to material from this locality, a sample of Cs-rich "morganite" from Afghanistan described by Hänni and Krzemnicki (2003) has now been recognized as pezzottaite (H. Hänni, pers. comm., 2003). Observations of the crystal morphology of pezzottaite from Madagascar

See end of article for About the Authors and Acknowledgments.
GEMS & GEMOLOGY, Vol. 39, No. 4, pp. 284–301.

Figure 1. Pezzottaite, a new gem mineral from Madagascar, is a Cs,Li–rich member of the beryl group. Small quantities have been cut into attractive faceted stones and cat's-eye cabochons (here, 1.01–6.26 and 3.05 ct, respectively). These are some of the samples used for this study. Photo by Robert Weldon, © GIA; courtesy of Tom Cushman.

were presented by Warin and Jacques (2003), and the chemical composition was investigated by Abduriyim and Kitawaki (2003). This article provides information on the history, geology, composition, and properties of pezzottaite, as a follow-up to the initial description of the material provided by Simmons et al. (2003). A separate article that will formally describe the new mineral (Hawthorne et al., in preparation) and will be submitted to the *Mineralogical Record*.

HISTORY

As recounted by Dr. Pezzotta (pers. comm., 2003), mining of the Sakavalana pegmatite (for tourmaline) by French colonists began in the 1940s. Subsequently, intermittent digging by local people with hand tools occasionally produced tourmaline and other minerals. In mid-November 2002, the local miners discovered a large crystal-bearing cavity that contained multicolored tourmaline prisms of carving or slabbing quality, as well as gem-quality spodumene crystals in green, blue, and purple hues. The production eventually reached the capital city of Antananarivo, where it was seen by gem dealer Laurent Thomas in early December 2002. He noticed some unusual deep pink crystals with a color that resembled tourmaline but with a morphology similar to tabular morganite. Mr. Thomas measured a refractive index of 1.619 on a shiny pinacoidal face on one of these crystals. Recognizing that this was too high for beryl, he sent samples to Dr. Pezzotta in Italy.

Preliminary chemical analyses of two samples with energy-dispersive X-ray spectrometry (by Dr. Alessandro Guastoni of the Natural History Museum, Milan) revealed very high concentrations of Cs, and calculation of the unit-cell parameters (by Dr. Franco Demartin of the University of Milan) yielded data consistent with a beryl-like mineral with extreme Cs enrichment. After the 2003 Tucson gem shows, the customs department of Madagascar temporarily froze the export of the material due to confusion over its identity and the rumor that it might be a new mineral. Subsequent studies proved that it was, indeed, a new mineral (see, e.g., Laurs, 2003; "Newly discovered beryl . . . ," 2003).

Some of the initial production was mistakenly sold in Madagascar as tourmaline (F. Pezzotta, pers. comm., 2003). Soon, rumors that it represented a new source of red beryl (such as that from Utah) spurred local traders to call it "bixbite," after the outdated trade term for such material. Due to the excitement of the discovery and strong demand, dealers frequently have encountered exorbitant prices for gem rough and crystal specimens, even in Madagascar.

LOCATION AND ACCESS

Dr. Pezzotta guided the senior author to the mine in July 2003. It is located about 140 air-km (87 miles) southwest of Antsirabe, in central Madagascar (figure 2). Paved roads lead from Antsirabe to Ambatofinandrahana, a distance of approximately 160 km that requires about six hours of driving time. From there, a rough dirt track proceeds approximately 140 km to the town of Mandrosonoro, and then another 25 km to the

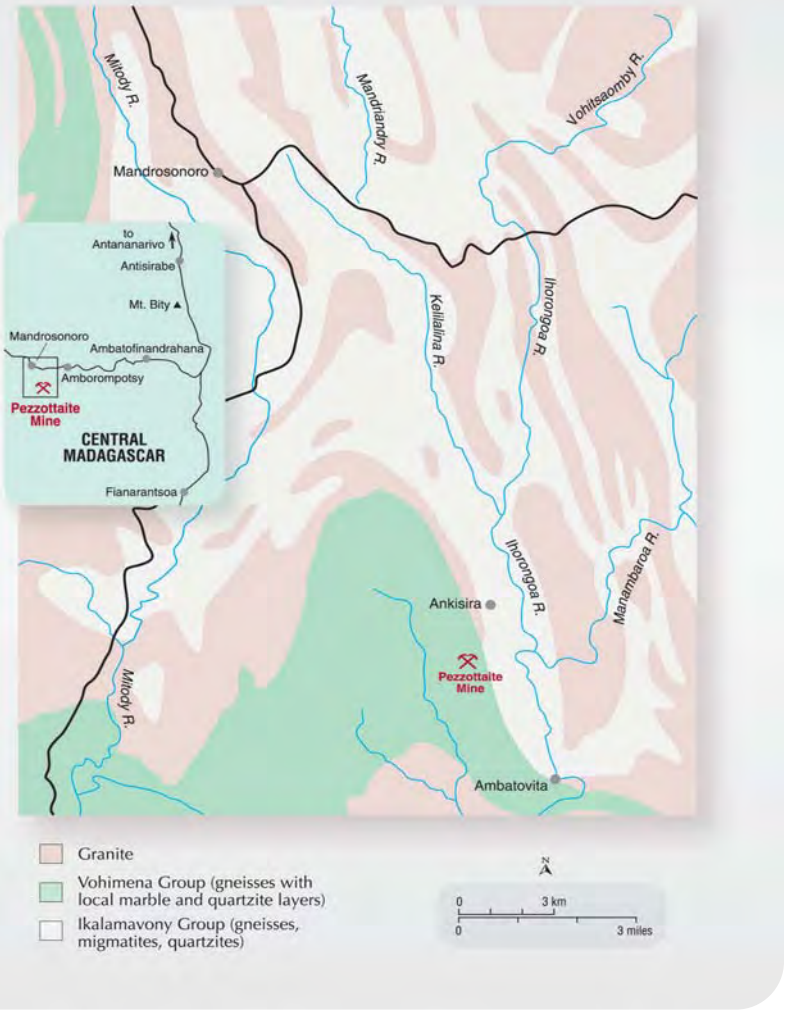

Figure 2. The pezzottaite deposit is located in central Madagascar, about 140 air-km southwest of Antsirabe and 130 km northwest of Fianarantsoa. From Antsirabe, a paved road leads south to Ambositra and west to Ambatofinandrahana, followed by a rough dirt track that passes through Amborompotsy and Mandrosonoro. The pegmatite is hosted by marbles, on the limb of a syncline that is composed mainly of quartzitic gneisses of the Vohimena Group. Geology from Chantraine (1966).

mine. The assistance of local guides was necessary for both navigational and safety reasons. This drive usually takes about 14 hours, although we encountered considerable delays due to multiple vehicular breakdowns caused by the rough terrain (figure 3). Our excursion was undertaken in "ideal" conditions during the dry season; the road is hazardous to impassible during the rainy season, from December to April.

The mine is situated on a low hill (figure 4), at coordinates 20° 44.78′ S and 46° 04.45′ E and an elevation of 920 m (3,020 feet). It is located a few kilometers northwest of the village of Ambatovita and southwest of the village of Ankosira, both of which lie along the Manambaroa River. Most of the miners live on-site, in several huts above the workings (figure 5).

GEOLOGY

The Sakavalana pegmatite, which hosts the pezzottaite, is located in the northern part of the famous Ampandramaika-Malakialina pegmatite district, one of many areas in central Madagascar that have produced gem minerals (see Pezzotta, 2001). A brief review of the regional geology of these pegmatites was provided by Dirlam et al. (2002). The geology of the Mandrosonoro-Ambatovita area was described and mapped by Chantraine (1966). The Sakavalana pegmatite is hosted by impure marbles that Chantraine (1966) assigned to the Vohimena Group, on the eastern limb of a synform that is composed mainly of quartzitic gneisses (again, see figure 2). This amphibolite-grade metasedimentary sequence is surrounded mostly by deformed granites. Pegmatites occur sparingly in the synform, but are much more abundant within mica schists that form the upper facies of the Vohimena Group, about 20 km to the west. This area (Malakialina)

Figure 3. Mechanical breakdowns were common because of the rough terrain, which required the use of a high-clearance four-wheel-drive vehicle. Photo by Brendan Laurs.

once was the most important producer of industrial beryl in Madagascar (Pezzotta, 2001).

Pezzottaite occurs at Sakavalana within a "mixed feature" granitic pegmatite—that is, one that has characteristics of both the LCT (lithium, cesium, and tantalum) and NYF (niobium, yttrium, and fluorine) families of the Rare-Element and Miarolitic classes (see Černý, 1991). The pegmatite (figure 6) is a subvertical dike that measures at least 4–6 m wide and more than 200 m long. The outer portion consists mostly of K-feldspar, quartz, plagioclase, and black mica, whereas the core zone consists of K-feldspar (green amazonite; figure 7), zoned crystals of black and purple mica, and smoky quartz, with traces of albite (bladed "cleavelandite" aggregates), danburite, zircon, and Nb-Ta oxides. In places, black tourmaline is intergrown with these minerals in the core zone, along with minor beryl, spessartine, and spodumene. Crystal-lined cavities are also locally present in the core zone, and they contain the core-zone minerals as well as pezzottaite in places. The paragenetic relations of the pocket minerals indicate that pezzottaite crystallized from the fluids in the cavities as late-stage crystals. Observations of numerous mineral samples by Dr. Pezzotta and some of the authors indicate that post-crystallization fluids caused etching or extensive corrosion on many of the pezzottaite crystals.

The main pezzottaite find occurred about 6 m below the surface, within a large cavity that may have measured up to 3.0 × 3.0 × 1.2 m. Below this pocket was a zone containing numerous vugs with smaller crystals of pezzottaite. All the pezzottaite produced to date came from this rather limited area within the pegmatite.

MINING AND PRODUCTION

The mine area consists of pits, shafts, and open cuts that explore at least one steeply south-dipping pegmatite dike. These workings were probably dug only with hand tools, although bulldozers available in the early days of mining may have been used. Illumination in the underground workings is by candlelight, and logs are used as crude scaffolding near the opening of the deepest shafts (approximately 30 m). Flooding is a problem in the lowermost shaft (which produced only tourmaline). The underground workings where the pezzottaite was mined (see, e.g., figure 8) consist of two small rooms, which are accessed from above and below by tunnels that are several meters long.

Figure 4. In this view (looking southwest) of the pezzottaite mining area, on the left are some of the miners' huts and on the right is a small open cut that has been worked for multicolored tourmaline since the 1940s. Photo by Brendan Laurs.

In the rush that followed the original find, approximately 120 people (including 60 miners and their families) lived at the deposit. Most of them left the area in April 2003 due to lack of production. As of July 2003, only about 20 people were actively working the pegmatite. Most of the pezzottaite-bearing zone appeared to have been mined

Figure 5. At the pezzottaite mine, most of the miners live on-site in several huts above the workings. One of the entrances to the pezzottaite-bearing part of the pegmatite is visible on the lower right (without a significant mine dump below it). Photo by Brendan Laurs.

Figure 6. The Sakavalana pegmatite is visible in this open cut as the light-colored dike on the left. The miners are standing in front of a 13-m-deep shaft that produced multicolored tourmaline crystals. The entrance to a separate tunnel that leads upward to the pezzottaite workings is visible behind the man on the far left. The green color of portions of the pegmatite and mine dump is due to the presence of amazonite feldspar. Photo by Brendan Laurs.

out, and the remaining areas were difficult to work with the hand tools available. Small amounts of pezzottaite were available at the mine, as well as elsewhere in Madagascar, but the material shown to us was of low quality. After another visit to the mine in November 2003, Dr. Pezzotta reported that the underground workings were in poor condition due to rockfalls and backfill generated by contin-

Figure 7. The core zone of the pegmatite is marked by concentrations of green amazonite. Note also the large crystals of black tourmaline above the miner. Photo by Brendan Laurs.

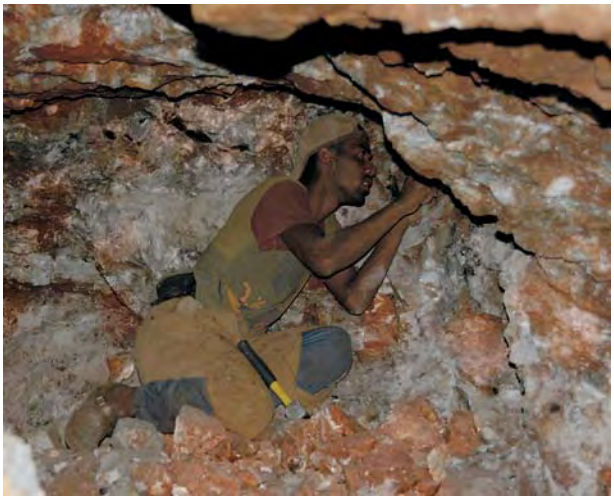

Figure 8. Numerous pezzottaite-bearing vugs were mined from this area, using simple hand tools and candlelight. Fractures in the pegmatite are coated by iron-stained clay, which obscures observation of the mineralogy and also causes stability problems in the ceiling, resulting in unsafe conditions. Photo by Brendan Laurs.

Figure 9. This pezzottaite specimen has been cleaned of dirt and clay, but otherwise shows the appearance as recovered from the mine. The pezzottaite crystal measures 3.6 cm in diameter, and is associated with "cleavelandite" feldspar (bladed albite, here partially covered with Mn-oxides) and quartz. Courtesy of Federico Pezzotta; photo by Brendan Laurs.

ued mining activities. Apparently this work produced little (if any) additional pezzottaite.

According to Dr. Pezzotta (pers. comm., 2003), the main pezzottaite pocket produced a total of about 700 kg of smoky quartz (in crystals up to 50 kg), 280 kg of tourmaline (multicolored, with a black "skin"), >40 kg of pezzottaite (see, e.g., figure 9), and 25 kg of transparent spodumene (see, e.g., figure 10). The three largest tourmaline crystals weighed 15, 25, and 50 kg, and reportedly were purchased by a Korean dealer for carving purposes. The pezzottaite was recovered as crystals, fragments, and masses typically weighing a few grams, and rarely up to 1,000 grams. In addition to the 40 kg mentioned above, there were many tens of kilograms of low-quality fragments and deeply corroded crystals. Pieces of gem-quality pezzottaite are rare and typically small (less than 1–2 grams). Much of the gem material is of carving quality only, although some contains abundant tubes oriented parallel to the c-axis that produce attractive chatoyancy in cabochons. One gem dealer estimated that perhaps 10% of the rough will produce the cat's-eye effect when cut ("Rare pink-red beryl. . . ," 2003).

The total amount of pezzottaite produced so far from the pegmatite is difficult to estimate. According to dealers Fabrice Danet, Denis Gravier, Dudley Blauwet, and Mark Kaufman (pers. comms., 2003), the total production may range up to 150 kg, with no more than 25% containing areas that could yield cabochons and faceted stones. Rarest of all are attractive specimen-quality crystals (see, e.g., figure 11). Most of the production was sold in Antananarivo in December 2002–February 2003, to European and American dealers. Additional smaller, lower-quality parcels were sold until September 2003. It is not clear how much of this material came from the original find, and how much resulted from later mining. African, Japanese, Thai, and Indian traders also bought the material directly in Madagascar or through local buyers. The largest transparent faceted pezzottaite of good quality known to the authors weighs approximately 11.31 ct, and the largest good-quality cat's-eye cabochon is 17.36 ct (see figure 12). Examples of other large pezzottaite gems seen at the GIA and GRS laboratories include faceted stones weighing 5.27, 6.26, and 10.07 ct, and cat's-eye cabochons weighing 7.98, 8.78, and 8.85 ct.

As of November 2003, Dr. Pezzotta reported there was practically no material available in the mine area, and only small, lower-quality material could be found in Antsirabe and Antananarivo.

Figure 10. Fine crystals of spodumene, some bicolored in violet and yellow as shown here (24.9 cm long), were recovered from the same pocket with pezzottaite (here, 4.9 × 3.1 cm). Courtesy of Brian Cook (pezzottaite) and the Brooke Collection (spodumene); photo by Maha Tannous.

MATERIALS AND METHODS

The samples and analytical techniques used in this study are summarized in table 1. Gemological properties were obtained on 19 samples (see, e.g., figure 1) using standard gemological instruments.

Figure 11. Attractive crystals of pezzottaite are relatively rare, particularly on matrix. This specimen measures 4.7 × 4.2 cm, and consists of bright pink pezzottaite, feldspar, smoky quartz, and black tourmaline. GIA Collection no. 30113; photo by R. Appiani.

Figure 12. At 17.36 ct, this is the largest good-quality cat's-eye pezzottaite known to the authors. Courtesy of K&K International; photo by Maha Tannous.

Internal features were examined with a gemological microscope, and absorption spectra were observed with a desk-model Beck prism spectroscope. The documentation of additional samples examined by one of the authors (AP) will be published in a separate article; these results are in general agreement with those obtained at GIA.

To test for color stability, one sample was sawn into four parts. Heating and irradiation experiments were conducted on three parts, while the other one was retained as a control.

Quantitative chemical analysis by electron microprobe was performed on 11 pezzottaite samples from which a total of 49 point analyses were obtained. Nearly all of these analyses were done on fragments that were donated for research; two of the gemstones mentioned above that could be borrowed long enough for chemical analysis also were analyzed. Analyses were obtained using an ARL-SEMQ electron microprobe with 15 kV (for sodium) and 25 kV accelerating voltages, 15 nA beam current, and 3 µm beam diameter. The measurements were calibrated with natural mineral and synthetic compound standards, and a ZAF correction procedure was applied to the data. Morphological observations of eight etched crystals also were performed.

Quantitative chemical analysis by laser ablation–inductively coupled plasma–mass spectrometry (LA-ICP-MS) using a GeoLas 193 nm excimer laser in combination with an Elan 6100 ICP-DRC (dynamic reaction cell) mass spectrometer was carried out on one sample. The water content of two additional fragments was determined by measuring the weight lost after heating them to 900°C. In addition, the lithium contents were measured in two other samples using an ARL 3520 AES inductively coupled plasma spectrometer.

Visible–near infrared spectra of pezzottaite and, for comparison, morganite and red beryl were obtained using a custom-built diode array spectrometer consisting of a tungsten-halogen source coupled to a microscope spectrometer. The detector, a 1025 element silicon diode array, was attached to a grating optical spectrograph that received its signal through fiber optics from the microscope.

Infrared spectra of pezzottaite, morganite, and red beryl were collected with a SensIR DuraScope diamond window attenuated total reflectance (ATR) apparatus. Spectra were obtained from a 0.1-mm-diameter area of finely powdered sample and were referenced to a blank window. These spectra closely resemble those obtained with the use of KBr pellets, but are considerably more convenient to obtain.

Raman spectra of pezzottaite, aquamarine, morganite, and red beryl were obtained with a Renishaw 1000 microRaman system. Spectra were generated with both a 514.5 nm argon-ion laser and a 782 nm laser diode. Similar spectra were obtained with both lasers, although less fluorescence was excited with the 782 nm laser. In no case, however, did the fluorescence hinder the measurement. All spectra were obtained with a depolarizer positioned before the samples, in orientations both parallel and perpendicular to the c-axis. The sloping baseline in the spectra was corrected using a built-in Grams software function and normalized to the intensity of the ~684 cm^{-1} band.

Powder X-ray diffraction analyses of pezzottaite and aquamarine were performed using a Scintag instrument with an accelerating voltage of 35 kV and a beam current of 15 mA.

RESULTS

Crystal Forms and Visual Appearance. *Rough.* The pezzottaite crystals showed hexagonal symmetry and consisted of three main forms in various degrees of prominence: the pinacoid *c* {0001}, pyramid *d* {10$\bar{1}$2}, and prism *m* {10$\bar{1}$0} (figures 13 and 14). Although not present on our samples, small second-order pyramid and prism faces have been documented (Warin and Jacques, 2003). The samples showed

TABLE 1. Samples of pezzottaite from Ambatovita, Madagascar, and other samples analyzed for this study.

Samples (pezzottaite unless otherwise noted)	Method of analysis	Analyzed at:[1]	Notes
19 total, all purplish pink: 10 faceted (0.89–6.26 ct) 7 cabochons (1.16–8.78 ct) 1 crystal (7.5 grams) 1 partially polished fragment (1.64 ct)	*Gemological characterization:* R.I., S.G.[2], optic character, Chelsea filter reaction, UV fluorescence, absorption spectroscopy, and microscopic examination	GIA	Two of the faceted stones (1.18 and 3.42 ct) were analyzed by electron microprobe at UNO.
4 purplish pink fragments (~2 mm), derived from one crystal	*Color stability:* One fragment held as a control, one fragment irradiated but not heated, and two fragments heated in air for 2 hours at different temperatures: 250, 350, and 450°C. The 450°C sample was irradiated by 6 Mrads of Cs-137 gamma rays, at 0.9 Mrads per day	Caltech	Another piece of this sample was also used for ATR IR spectroscopy.
11 total, all purplish pink: 3 faceted (0.31, 1.18, and 3.42 ct) 6 polished fragments 1 polished plate (5.08 mm thick) 1 sliced crystal	Chemical analysis by electron microprobe (total of 49 point analyses)	UNO	R.I. values were obtained at UNO on the fragment with the lowest Cs content. Polished plate also used for Vis-NIR spectroscopy.
8 purplish pink etched crystals (0.15–1 g)	Morphological observations	UNO	
2 fragments (~300 mg each)	Loss on ignition (for H_2O)	UNO	
2 samples (275.6 and 21.0 mg)	Inductively coupled plasma spectrometry (for Li)	UNO	
1 purplish pink fragment (~1 ct)	Laser ablation–inductively coupled plasma–mass spectrometry (LA-ICP-MS)	ETH	R.I. values and density (measured by a Berman balance) were obtained at GRS Swisslab on this fragment, which had the highest Cs content measured in this study.
1 purplish pink polished plate (5.08 mm thick)	Visible-NIR spectroscopy[3]	Caltech	Spectrum reported in Simmons et al. (2003).
1 polished plate of pale pink morganite, Brazil (1.97 g)			Same sample was used for Raman spectroscopy.
1 polished plate of red beryl, Wah Wah Mts., Utah (0.38 g)			Same sample was used for Raman spectroscopy.
1 polished plate of red beryl, Thomas Range, Utah			
1 purplish pink powdered sample	Attenuated total reflectance (ATR) IR spectroscopy	Caltech	
1 powdered sample of pale pink morganite, Brazil			From the same sample used for Vis-NIR and Raman.
1 powdered sample of red beryl, Wah Wah Mts., Utah			
2 purplish pink polished plates (6.9 and 0.4 mg)	Raman spectroscopy	Caltech	
1 polished plate of pale pink morganite, Brazil (1.97 g)			
1 polished plate of red beryl, Wah Wah Mts., Utah (0.38 g)			
1 polished plate of pale blue aquamarine, Minas Gerais, Brazil (0.38 g)			
1 purplish pink powdered sample (~80 mg) 1 powdered sample of pale blue aquamarine, Erongo Mts., Namibia (~80 mg)	X-ray powder diffraction	UNO	

[1] Abbreviations: Caltech = California Institute of Technology, ETH = Eidgenössische Technische Hochschule, UNO = University of New Orleans.
[2] Note that the S.G. value of the partially polished fragment was not included, owing to inconsistent results that were probably due to trapped air bubbles within surface irregularities.
[3] Spectra were obtained at approximately 1.5 nm resolution.

varying degrees of etching and corrosion, with residual light-colored spongy masses present along the prism areas of some crystals. The underlying vitreous surfaces (seen where the spongy masses broke off or were entirely removed by corrosion) commonly showed a series of microsteps in reflected light. Warin and Jacques (2003) interpreted these surfaces as resulting from the original crystal growth, rather than corrosion, but this interpretation is not supported by our observations.

Besides the spongy corroded areas mentioned above, all of the samples were purplish pink. Dichroism (described below) was not readily seen when observing our samples with the unaided eye (due to their relatively small size), but it is quite obvious in larger samples (see, e.g., figures 14 and 15).

Polished. The polished stones we examined were transparent to translucent, deep purplish pink, and evenly colored with no eye-visible color zoning (again, see figure 1). They displayed moderate to strong dichroism: pinkish orange to pink-orange when viewed down the c-axis (ω ray) and purplish pink to pink-purple perpendicular to the c-axis. In some larger stones, depending on how they were cut relative to the optic axis, the pink-orange pleochroism could be observed with the unaided eye.

GEMOLOGICAL CHARACTERISTICS

Physical and Optical Properties. The results of gemological testing are summarized in table 2. The refractive indices of the faceted stones generally were n_o = 1.615–1.619 and n_e = 1.607–1.610 (birefringence 0.008–0.009), with the cabochons giving a spot reading of 1.61. As expected, the R.I. values of the fragment with the lowest Cs content (as analyzed by electron microprobe) were somewhat lower than those obtained on the faceted stones, at n_o = 1.612 and n_e = 1.601. The samples yielded S.G. values of 3.09–3.14. Although the S.G. values of our cabochons were not significantly influenced by the presence of growth tubes, it would not be surprising to obtain a lower S.G. for samples containing large numbers of them.

Pezzottaite is uniaxial negative, although several samples were anomalously biaxial in their optic figures, where the "brushes" were seen to come together and move apart slightly as a stone was rotated around the optic axis. This effect was most likely due to strain, which was visible in some of the samples when viewed parallel to the optic axis between crossed polarizing filters. The samples appeared faint orangy pink to pink-orange when viewed through a Chelsea color filter with a diffused light source; too strong a light source overpowered the reaction and the stone appeared yellow-green. All samples were inert to long- and

Figure 13. This idealized diagram shows the prominent faces of pezzottaite crystals, which consist of c *{0001},* d *{10$\bar{1}$2}, and* m *{10$\bar{1}$0} forms. The drawing was generated using Kristall2000 software that was developed by Klaus Schilling.*

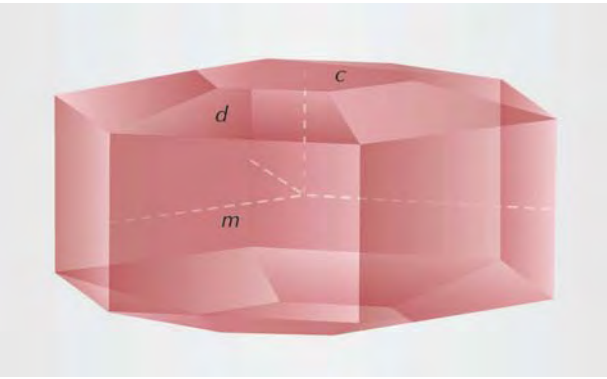

Figure 14. This well-formed crystal of pezzottaite (4.1 cm tall) exhibits a large pinacoid and subordinate pyramid faces. The small prism faces are not visible in this orientation, looking down the c-axis. Note the slightly pink-orange color that is typically seen down this axis. Corrosion resulted in the linear etch features on the crystal and the spongy matrix material that is stained brown by iron oxides. Courtesy of Dudley Blauwet Gems; photo © Jeff Scovil.

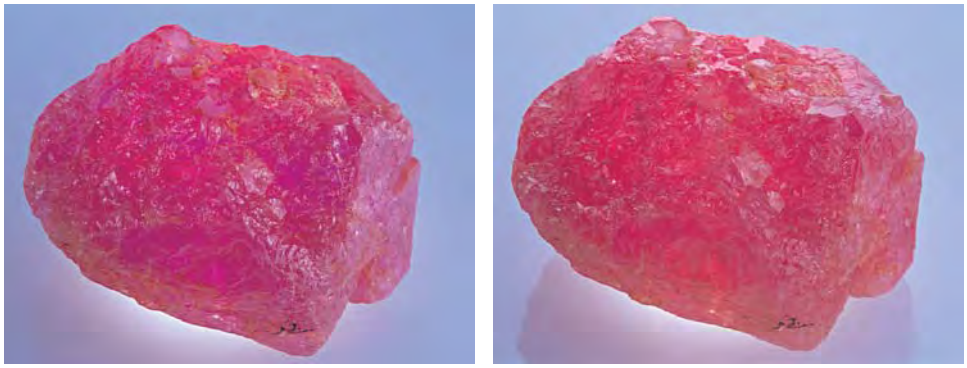

Figure 15. Pleochroism in purplish pink and pink-orange is clearly visible in this large piece of pezzottaite, which measures 4.9 × 3.1 cm. Photos by Maha Tannous.

short-wave UV radiation, although one sample did fluoresce a weak chalky yellow in the fractures, which indicated the presence of a filling material.

All samples displayed oriented absorption spectra with the desk-model spectroscope. When the spectrum was viewed with the stone parallel to the c-axis (down the optic axis), diffuse lines were visible at 465 and 477 nm, along with a band at approximately 485–500 nm. In some samples, these three features converged into a single broad absorption band. When viewed perpendicular to the c-axis, bands at approximately 485–500 and 550–580 nm were visible. In all other orientations, combinations of the above-listed absorption features were observed with varying intensities.

TABLE 2. Properties of pezzottaite from Madagascar.

Property	Description
Color	• Purplish pink • Moderate to strong dichroism: pinkish orange to pink-orange (ω ray) and purplish pink to pink-purple (ε ray)
Diaphaneity	Transparent to translucent
R.I.	• n_o = 1.615–1.619, n_e = 1.607–1.610 (faceted stones); spot reading = 1.61 (cabochons) • n_o = 1.612, n_e = 1.601 for polished fragment with the lowest Cs content • n_o = 1.620, n_e = 1.611 for polished fragment with the highest Cs content
Birefringence	0.008–0.009
Optic character	Uniaxial negative, with several samples showing anomalously biaxial optics
S.G.	Typically 3.09–3.11, with faceted stones—3.09–3.14, cat's-eye cabochons—3.09–3.11, and crystal—3.09
Chelsea filter reaction	Faint orangy pink to pink-orange
UV fluorescence	Inert to long- and short-wave UV radiation[a]
Spectroscope spectra	• Viewed parallel to optic axis: diffuse lines at 465 and 477 nm plus a band at 485–500 nm • Viewed perpendicular to optic axis: bands at approximately 485–500 nm and 550–580 nm
Internal features	Growth tubes, fractures, "fingerprints," and fluid inclusions (and, rarely, noticeable two-phase inclusions); transparent, near-colorless, low-relief birefringent crystals; transparent, grayish green tourmaline crystals; strain; rare color zoning

[a]*Weak chalky yellow fluorescence in fractures of one sample suggested the presence of a filling.*

Internal Features. All of the 19 samples we examined contained numerous fine growth tubes (figure 16) oriented parallel to the c-axis. When abundant, these tubes are responsible for the chatoyancy seen in cat's-eye pezzottaite. Some of these tubes had negative crystal "flare outs" along their length (figure 17). These features are indicative of an abrupt change in the growth environment (i.e., slower growth; J. I. Koivula, pers. comm., 2003). The intensity of strain seen between crossed polarizers seemed to increase with the number of growth tubes. Fractures, "fingerprints," and fluid inclusions also were present in all of the samples. Some of the samples contained transparent, near-colorless, low-

Figure 16. All of the pezzottaite samples examined contained numerous fine growth tubes oriented parallel to the c-axis. Some of the tubes shown here can be seen emanating from included crystals (identified as tourmaline). Photomicrograph by John I. Koivula; magnified 15×.

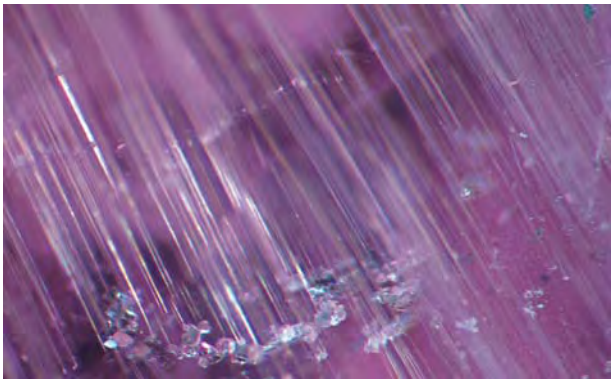

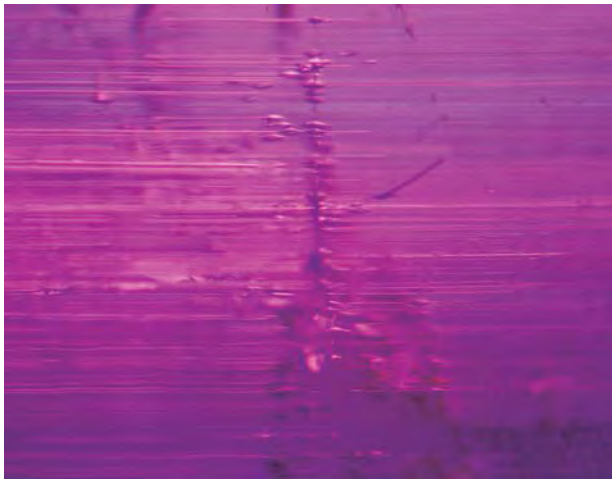

Figure 17. Negative crystal "flare outs" were sometimes seen along growth tubes in pezzottaite. Note the bipyrimidal form of these minute negative crystals. Photomicrograph by John I. Koivula; magnified 40×.

relief birefringent crystals, which could not be identified due to their small size and their position within the stones. A few samples contained transparent, grayish green, birefringent crystals that were identified (by Raman analysis) as tourmaline (figure 18). One sample contained obvious two-phase fluid and gas inclusions. This sample also showed color zoning, but we observed no notable growth or color zoning in the other samples.

Although the dealers who supplied the samples were not aware of any clarity enhancement, many of the samples showed fractures of low relief, some of which contained air bubbles that contracted when exposed to a thermal reaction tester, indicating the presence of a filling substance. Subsequently, we learned from Dudley Blauwet (pers. comm., 2003) that all of the pezzottaite rough he has purchased was oiled by the local Madagascar dealers. He reported that the oiling enables them to see into the rough easier (because of the slight etching on most of the crystal surfaces). While this may be true, pezzottaite, like many gem materials that tend to be fractured, can easily be clarity enhanced with oil or resin to improve its appearance.

Figure 18. Raman analysis identified the grayish green inclusions in this pezzottaite as tourmaline. Photomicrograph by John I. Koivula; magnified 15×.

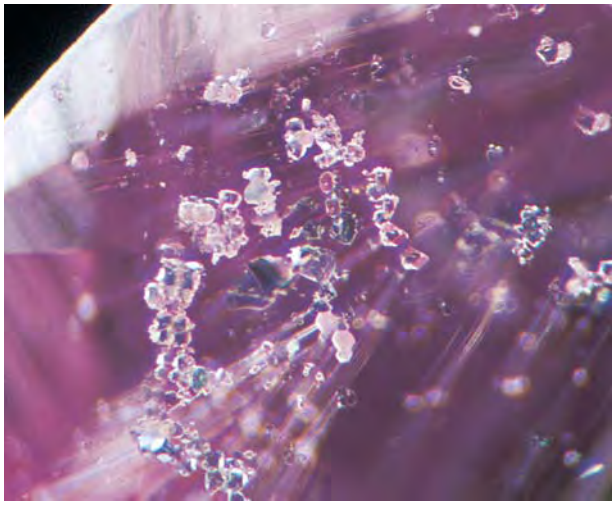

Heating and Irradiation Experiments. When heated at 450°C, a purplish pink fragment of pezzottaite suffered a near-total loss of color, although no effect was noted at lower temperatures. The sample regained nearly all of its purplish pink color on irradiation with gamma rays.

CHEMISTRY

The highest Cs content was obtained on the sample analyzed by LA-ICP-MS: 18.23 wt.% Cs_2O (table 3). The 11 samples analyzed by electron microprobe had cesium contents ranging from 11.23 to 15.13 wt.% Cs_2O (again, see table 3). A similar range also was obtained from four samples analyzed by electron microprobe at the University of Manitoba by one of the authors (FCH; unpublished data). Calculations of Cs ions per formula unit yielded 0.504 to 0.833.

Minor amounts of Rb and Na were also measured in all samples. Manganese, the chromophoric element in pink beryl, ranged up to 0.19 wt.% MnO, with the average being 0.11 wt.%. Mg, K, Sc, Ti, and Fe were either below the detection limit or present only in trace amounts in some samples. Many other elements were looked for, but not detected (see footnote to table 3). To view all 49 electron microprobe analyses, see table 1 in the *Gems & Gemology* Data Depository at www.gia.edu/gemsandgemology.

SPECTROSCOPY

Vis-NIR. With the beam oriented down the c-axis (or E⊥c), the Vis-NIR absorption spectrum of purplish pink pezzottaite is dominated by a band centered at 494 nm, with a distinct shoulder at 476 nm (figure 19). A second absorption band at 563 nm appears in the same polarization, along with a

TABLE 3. Chemical analyses of pezzottaite from Ambatovita, Madagascar, by LA-ICP-MS and electron microprobe.[a]

	LA-ICP-MS	Electron microprobe[b]		
		Lowest Cs[c]	Highest Cs[d]	Average[e]
Oxide (wt.%)				
SiO_2	54.58	57.01	56.27	56.77
TiO_2	0.01	bdl	bdl	bdl
Al_2O_3	16.88	16.69	16.11	15.99
Sc_2O_3	nd	0.05	0.01	0.03
BeO	8.14	8.25	8.09	8.14
FeO	0.02	bdl	bdl	bdl
MnO	0.02	0.18	0.11	0.11
CaO	0.22	bdl	bdl	bdl
Li_2O	2.12	2.16	2.16	2.16
Na_2O	0.46	0.43	0.26	0.41
K_2O	0.14	0.08	0.10	0.11
Rb_2O	0.44	0.78	0.77	0.85
Cs_2O	**18.23**	**11.23**	**15.13**	**13.55**
H_2O	nd	1.72	1.72	1.72
Total	101.26	98.58	100.74	99.84
Ions per 18 oxygens, anhydrous basis				
Si	5.860	6.001	6.004	6.030
Ti	0.001	0.000	0.000	0.000
Al	0.139	0.000	0.000	0.000
tet.	6.000	6.001	6.004	6.030
Be	2.098	2.086	2.073	2.077
Li	0.917	0.914	0.927	0.923
Be+Li	3.016	3.000	3.000	3.000
Al	1.996	2.070	2.026	2.000
Ca[f]	0.025	0.000	0.000	0.000
Sc	nd	0.005	0.001	0.002
Mn	0.002	0.016	0.010	0.010
Fe^{2+}	0.001	0.000	0.000	0.000
oct.	2.024	2.091	2.037	2.012
Na	0.095	0.087	0.054	0.085
K	0.019	0.011	0.014	0.015
Rb	0.030	0.053	0.052	0.058
Cs	**0.833**	**0.504**	**0.688**	**0.617**
channel	0.977	0.655	0.808	0.775

[a] *Abbreviations: nd = not determined, bdl = below detection limit.*

[b] *For the electron microprobe data, values for lithium (by ICP) and water (by LOI) were measured for two samples (Simmons et al., 2003). The measured Li_2O value was then used as the best approximation for calculating beryllium (Be+Li = 3) and the other ions per formula unit for all samples analyzed. The H_2O value is considered anomalously high due to the presence of microscopic tubules that are filled with an aqueous fluid (consistent with the granitic pegmatite environment). The low analytical totals (as calculated without water) are attributed to the abundance of these fluid-rich inclusions. Crystal structure refinement of a sample by FCH indicated only 0.28 wt.% H_2O in the channels. The following were analyzed by electron microprobe but were below the detection limits (shown in wt.%): MgO (0.01), TiO_2 (0.002), FeO (0.02), CaO (0.07). In addition, the following were checked for (scanned), but not detected: Cr_2O_3 (0.03), Bi_2O_3 (0.03), V_2O_3 (0.03), PbO (0.01), ZnO (0.08), BaO (0.03), Cl (0.04), F (0.05).*

[c] *Fragment of a purplish pink sample.*

[d] *Polished plate used for Vis-NIR spectroscopy reported in Simmons et al. (2003).*

[e] *Average of 49 analyses of 11 samples.*

[f] *Ca is assumed present in the octahedral site, but it may occur elsewhere in the beryl structure.*

broad band that is centered at 820 nm in the near-infrared region. The maximum transmission occurs near 630 nm (orange-red) and in the low-400 nm range (deep violet), which provides the pinkish orange pleochroic color in this direction. When the beam is oriented perpendicular to the c-axis (i.e., E⊥c), the spectrum is dominated by a band centered at 572 nm. A weak absorption band in the near-infrared region is also present at 820 nm. Transmission in the other regions of the spectrum combine to produce a purplish pink color for light polarized in this direction.

Other Methods. The infrared and Raman spectra, as well as X-ray diffraction patterns, of pezzottaite are briefly described here, and can be viewed in the *Gems & Gemology* Data Depository.

The ATR infrared spectrum generally resembled that of beryl (i.e., morganite and red beryl), with some shifts in wavenumbers and relative intensities. The most prominent differences were evident at higher wavenumbers; the absorption in the 1400–1100 cm^{-1} region occurs at a much higher wavenumber in pezzottaite than in the other minerals. The absorption in the region from about 1200 to 800 cm^{-1} correlates to various Si–O and Be–O bands (Hofmeister et al., 1987).

The characteristic feature of the pezzottaite Raman spectrum was the 1100 cm^{-1} band, which has not been observed in the spectra of other pink or red beryls or pale aquamarine. This band was present in Raman spectra obtained from both the (0001) and the ⊥c face.

In the X-ray diffraction pattern of pezzottaite, some important peaks typical of beryl were absent or very much weaker in intensity. Indexing of these patterns indicated that the affected peaks corresponded principally to *h*00 type reflections.

DISCUSSION

Cs in Beryl and Pezzottaite. Alkali beryls containing Cs have been informally referred to in the literature by some mineralogists as *vorobievite*—commonly for the pink Li-Cs variety—and *rosterite*—typically for the near-colorless Na-Li type (Beus, 1966; see also Zambonini and Caglioti, 1928; Rossovskiy, 1981). *Morganite* is the most common term used to refer to gem-quality pink beryl; this color variety commonly contains Cs. The amount of Cs (and other alkalis) that is incorporated into beryl has been correlated to the local abundance of

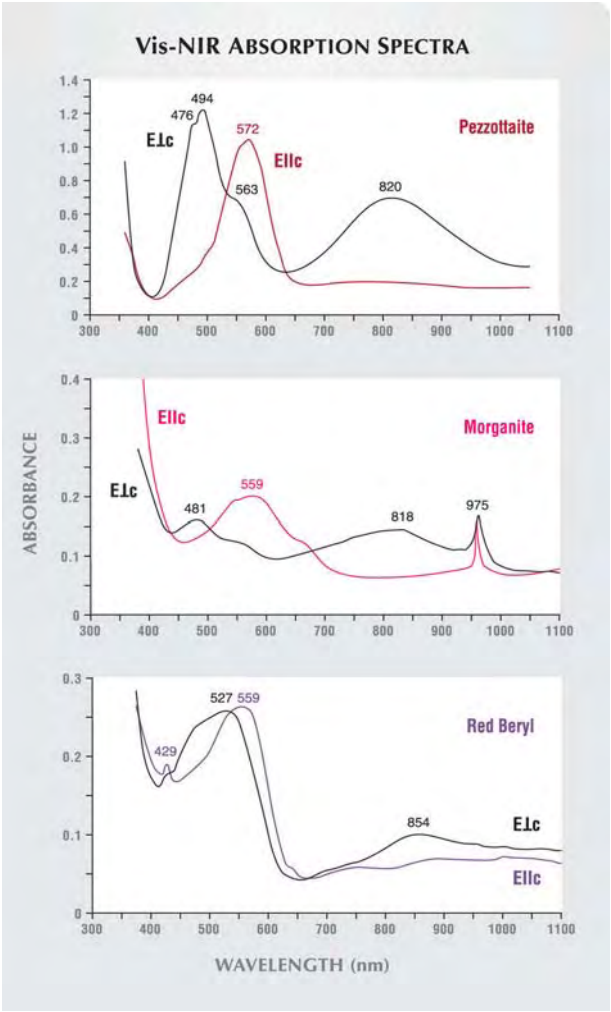

Figure 19. Representative polarized Vis-NIR spectra are shown here for a 5.08-mm-thick slice of pezzottaite (top), a 10.79-mm-thick slice of morganite from Brazil (middle), and a 0.72-mm-thick slice of red beryl from the Thomas Range, Utah (bottom). The pezzottaite is dominated by bands centered at 494 and 563 nm when the beam is oriented down the c-axis (or E⊥c), and a band centered at 572 nm when the beam is oriented perpendicular to the c-axis (i.e., E∥c). The difference in these absorptions accounts for pezzottaite's moderate dichroism in purplish pink and pink-orange. The morganite shows similar absorptions that are shifted somewhat and not as intense. This relatively thick sample also shows overtones of the water absorption near 975 nm. The red beryl shows intense absorptions centered at 527 and 559 nm; the minimal difference between the two red beryl spectra corresponds to the lack of noticeable pleochroism in this material.

such elements in the growth environment (Černý, 1975). The alkalis reside in the channel site, and are accommodated into the beryl structure through coupled substitutions (see box A).

The concentrations of the alkali elements Cs, Rb, and Li have been measured in beryl from a variety of geologic environments (Staatz et al., 1965). The greatest amounts of these elements have been found in beryl from the inner zones of granitic pegmatites, since this is where such elements—which are incompatible with common pegmatite minerals such as quartz and feldspar—are concentrated during crystallization (Beus, 1966; Černý, 1975; Zagorsky et al., 1999; Černý et al., 2003). Geochemically, pegmatitic beryl samples with the highest Cs contents generally also show low values of Na/Li. Typically, high-Cs beryls range up to 4 wt.% Cs_2O, although there are a few notable exceptions (table 4). At 11.3 wt.% Cs_2O, it is probable that the Madagascar sample studied by Evans and Mrose (1966) was pezzottaite. Furthermore, Černý (1972) reported that minute crystals of late hydrothermal beryl from the Tanco pegmatite had R.I. values exceeding those reported by Evans and Mrose (1966). Although they were not chemically analyzed, and specific R.I. values were not reported, these crystals also may have corresponded to pezzottaite.

According to Dr. H. A. Hänni (pers. comm., 2003), the Afghanistan sample with 9.70 wt.% Cs_2O reported by Hänni and Krzemnicki (2003) is actually pezzottaite (based on its unit-cell dimensions). Therefore, this sample has the lowest Cs content found in pezzottaite so far. The highest concentration of Cs measured in pezzottaite was obtained on samples from Madagascar by Abduriyim and Kitawaki (2003), who measured 19.76–21.33 wt.% Cs_2O by X-ray fluorescence spectroscopy and up to 23.37 wt.% Cs_2O by LA-ICP-MS.

Early studies showed a strong relationship between alkali content and refractive indices (as well as specific gravity) in beryl from Madagascar (see, e.g., Ford, 1910; Lacroix and Rengade, 1911; Lacroix, 1912). More recently, the relationship between composition and optical/physical properties was documented in beryl from several localities (reviewed by Deer et al., 1997).

Černý and Hawthorne (1976) pointed out that factors in addition to alkali content can influence R.I. values, so a simple mathematical relationship between them is impossible to generalize. This is shown by the high R.I. values reported for Cs-rich beryl in the literature (table 4). (Note that the high properties of the Arizona sample were attributed to enriched contents of both Fe [4.69 wt.% "oxides"] and Cs.) Since Cs is a relatively heavy element, significant concentrations of it would be expected to

BOX A: STRUCTURE OF BERYL AND PEZZOTTAITE, AND DEFINITION OF THE MINERAL

How is Cs (a relatively large ion) incorporated into the beryl structure? This mechanism was studied by Hawthorne and Černý (1977), and examined in more detail (particularly for lithium) by Sherriff et al. (1991). A useful review of beryl crystal chemistry was provided by Černý (2002), and the current consensus was summarized by Černý et al. (2003, p. 1006): "lithium substitutes for Be^{2+} in the tetrahedra linking the six-membered Si_6O_{18} rings, with the charge balance assured by Na^+ and Cs^+ in the channels passing through the centers of the vertically stacked rings. Sodium is accommodated in the centers of the individual rings of [silicate] tetrahedra, but the larger Cs^+ is located halfway between these centers" along the c-axis. The increase in charge caused by the incorporation of alkalis into the channel is compensated by replacement of Be by Li at a tetrahedral site.

Pezzottaite, ideally $Cs(Be_2Li)Al_2Si_6O_{18}$, is not isostructural with beryl, ideally $Be_3Al_2Si_6O_{18}$. However, the arrangement of the atoms in each structure is very similar, so the structures can be considered as very closely related. In beryl, the three Be atoms indicated in the formula occupy three symmetrically related positions. In pezzottaite, these three positions are occupied in an ordered fashion by Be_2Li rather than Be_3 (as in beryl). Thus, these positions in pezzottaite are no longer related by symmetry, so the symmetry of the mineral must change. As a result, pezzottaite differs from other members of the beryl group by having a different symmetry (rhombohedral rather than hexagonal) and a larger unit cell.

Further studies are needed to characterize the dividing line between pezzottaite and Cs-rich beryl, which is influenced by factors such as composition (Be-Li ordering), symmetry, and unit cell dimensions.

raise S.G. values as well. By comparison to the values reported in table 4, the theoretical specific gravity of beryl that has been calculated using X-ray diffraction measurements is 2.661 (Deer et al., 1997).

Origin of Color. An early study by Wood and Nassau (1968) attributed the color of morganite to Mn^{2+} and that of red beryl to Mn^{3+}, an assignment that Schmetzer et al. (1974) reiterated. Platonov et al. (1989) re-examined the spectra of manganese-containing beryls and concluded that Mn^{3+} is responsible for the color of both red beryl and morganite. Likewise, Solntsev and Bukin (1997) concluded that the pink morganite from Mozambique is colored by Mn^{3+} (specifically, *d-d* transitions in Mn^{3+} in the aluminum site).

In the visible range of the spectrum, the most significant difference between pezzottaite and morganite is the overall greater absorption intensity of pezzottaite, corresponding to its deeper color (figure 19). In fact, the spectra of the pezzottaites we studied have 5.3 times greater absorbance per centime-

TABLE 4. Properties of high-Cs beryls and pezzottaite.[a]

Description	Wt.% Cs_2O	n_o	n_e	S.G.	Reference
"Bluish" beryl from Arizona	6.68	1.608	1.599	2.92	Schaller et al. (1962)
Beryl from Tanco, Bernic Lake district, Canada	7.16	nr	nr	nr	Černý (1972)
Morganite from Madagascar	7.52	nr	nr	nr	Cabell and Smales (1957)
Pezzottaite from Afghanistan	9.70	1.604	1.598	2.91	Hänni and Krzemnicki (2003)
Pezzottaite from Madagascar	11.23	1.612	1.601	nd	This study (lowest Cs)
"Cesium beryl" from Antsirabe area, Madagascar	11.3	1.608	1.601	3.01	Evans and Mrose (1966)
Pezzottaite from Madagascar	18.23	1.620	1.611	3.09	This study (highest Cs)

[a] *nr = not reported, nd = not determined*

Figure 20. As seen in the photo on the left, cat's-eye pink tourmaline (left stone, 9.59 ct) is very similar in appearance to pezzottaite (right stone, 8.78 ct). However, they can be readily separated by their pleochroism, which is stronger in pezzottaite. This effect can be seen in the center and right photos, which were taken through a polarizing filter at different orientations. The pezzottaite is courtesy of William Pinch and the tourmaline is from the GIA Collection (no. 5738); photos by Maha Tannous.

ter than the one for morganite presented in Platonov et al. (1989). The spectrum of our morganite was similar to the Platonov et al. data, but was a factor of 10 less intense. While the spectrum of red beryl (again, see figure 19) shows absorption bands at generally the same wavelengths, their intensity distribution is distinct. The stability of the color of red beryl at high temperatures suggests that its color is not due to irradiation, and thus leads to the speculation that manganese in red beryl was originally present as Mn^{3+} during crystallization. In contrast, the instability of the manganese-derived color in morganite and pezzottaite at modest temperatures leads to the speculation that these gems originally formed containing Mn^{2+}, but became pink as a result of exposure to natural ionizing radiation after crystallization. The presence of such radiation in the Sakavalana pegmatite is demonstrated by the common association of smoky quartz with morganite and pezzottaite in the gem-bearing cavities; the radiation may be derived from radioactive trace minerals or the isotope ^{40}K in K-feldspars.

Previous studies (Nassau, 1984) have shown that some pink beryls, when decolorized by heat, regain their color upon irradiation with X-rays or gamma rays. This is consistent with our results for pezzottaite, and the sensitivity to heating and irradiation supports our proposal that the color of pezzottaite is caused by radiation-induced color centers involving Mn^{3+}.

It may be tempting to correlate the pink color of pezzottaite (as well as high-Cs morganite) with cesium, but this element has been ruled out as a chromophore in beryl (Ristic and Eichoff, 1955; Sinkankas, 1981). Although Cs-rich beryls do commonly have a pink color, this is probably due to the simple fact that Cs and Mn follow each other geochemically toward the end of crystallization in granitic pegmatites (see Černý et al., 1985). Thus, it is likely that both Cs and Mn will be present during the crystallization of beryl (or pezzottaite) in pegmatite pockets.

Identification. The identification of pezzottaite should be straightforward once the gemologist is familiar with its properties and a flat surface for an R.I. reading is available. The optical and physical properties of pezzottaite are distinct, particularly when compared to the varieties of beryl that it resembles—morganite and red beryl.

All of the samples of pezzottaite we examined were purplish pink. Although they varied somewhat in tone and saturation, their color was never the same as typical red beryl from Utah or its synthetic counterpart. This fact alone should prevent any confusion with these materials. In addition, the R.I. and S.G. values of pezzottaite are significantly higher than those of red beryl, for which the typical published values are n_o = 1.568–1.572, n_e = 1.564–1.569, and S.G. = 2.66–2.70 for natural material (Shigley and Foord, 1984), and n_o = 1.576–1.580, n_e = 1.569–1.573, and S.G. = 2.67–2.70 for the synthetic counterpart (Shigley et al., 2001). So far, pezzottaite has not been synthesized in the laboratory; the highest cesium content in synthetic beryl known to these authors is 2.39 wt.% Cs_2O (Shatskiy et al., 1981).

Some morganite may have a color similar to pezzottaite. However, the two can easily be separated gemologically by the distinctly lower R.I. and S.G. values of morganite (typically with R.I. values of n_o = 1.572–1.592 and n_e = 1.578–1.600, and S.G. = 2.71–2.90; Arem, 1987). Compared to pezzottaite, even high-Cs beryls have lower values (e.g., generalized by Schaller et al., 1962, as n_o = 1.599, n_e = 1.590, and S.G. ≈ 2.86).

The color of pezzottaite is almost the same as some tourmaline (figure 20, left). Pink tourmaline presents a more significant identification challenge

than do other beryls, particularly since many of the finest examples of pezzottaite are cat's-eyes. When encountering a pink cat's-eye, the gemologist is likely to think of tourmaline, since there are few other materials of this color that show chatoyancy. The refractive index of a pezzottaite cabochon measured by the spot method will read ~ 1.61, which is very close to the 1.62 that one would expect from tourmaline. Microscopically, the inclusions in pezzottaite also resemble those in tourmaline, being mostly parallel acicular tubes and planes of liquid inclusions. Even if the equipment is available for measuring the S.G. hydrostatically, the value will fall into the range of tourmaline (typically 3.01–3.06 for pink to red material [Arem, 1987]).

So, how does one separate these two materials? A faceted stone should not pose a problem, since an accurate refractive index measurement will clearly separate the two gem minerals. If a gemologist is good at taking spot R.I. readings, a value of 1.61 should be enough to warrant closer inspection. The pleochroism in pezzottaite is more pronounced than in pink tourmaline (figure 20, center and right). The purplish pink and pink-orange pleochroic directions also are different for these two materials, and their visibility in a sample will depend on the orientation of the polarizer. The best way to check the pleochroism would be to compare an unknown sample with a known piece of pink tourmaline. A desktop spectroscope can also be very useful, since the two minerals have distinctly different spectra; pink to red tourmaline typically shows narrow lines at 450 and 458 nm, and a broad region of absorption that is centered at ~ 525 nm (Webster, 1994). Of course, the best way to avoid misidentifying a pezzottaite cat's-eye as tourmaline is to be aware of the existence of this new mineral.

Additional Comparisons to Morganite and Utah Red Beryl. The chemical compositions of pezzottaite, morganite, and red beryl are distinct. Besides being virtually anhydrous, red beryl contains much higher amounts of Fe, Ti, Mn, and other trace elements (Shigley et al., 2003; see also table 2 in the *G&G* Data Depository). Morganite shows ranges of Fe, Ti, and Mn similar to those of pezzottaite, although the latter may contain significantly more Mn (typically <0.05 wt.% in morganite, vs. an average for this study of 0.11 wt.% MnO in pezzottaite).

Differences between pezzottaite and beryl in the infrared and Raman spectra, as well as in X-ray diffraction patterns (again, see Data Depository), appear distinctive and therefore provide additional criteria for separating the two minerals. What is not known at this time is how these properties vary with Cs content, and if beryls with intermediate levels of Cs can be distinguished from pezzottaite on the basis of these techniques.

Figure 21. Although considered a collector's stone due to its rarity, pezzottaite has been set into some attractive jewelry. This gold ring, containing a 5.25 ct pezzottaite, was created by Francis Bonnet of Polychrome France Co., Chambray-lès-Tours. Courtesy of Laurent Thomas.

Although these authors do not have first-hand experience with mounting pezzottaite in jewelry, the material is expected to behave similar to beryl in normal manufacturing, wear, and care conditions.

CONCLUSION

Due to its high Cs and Li contents and a structure that shows differences from beryl, pezzottaite has now been recognized as the fourth mineral of the beryl group. Unlike most new mineral species identified in recent years, pezzottaite was found as relatively large, well-formed crystals and fragments, and some of the rough proved suitable for cutting attractive gems (figure 21). The enriched Cs content gives

rise to some of its properties, which permit a straightforward separation from beryl and other pink gem minerals, except for cabochons of pink tourmaline, which can be identified by their dichroism and absorption spectra.

Significant amounts of gem-quality pezzottaite thus far have been found only at the Sakavalana pegmatite in a remote area of central Madagascar. Although the pegmatite has been mined since the 1940s for tourmaline, pezzottaite was not recovered there until mid-November 2002. The mineralized area has been mostly mined out by artisanal methods, so any future production of pezzottaite will depend on the use of mechanized mining and systematic exploration of the deposit. With the recognition of this material as a new gem mineral, it is also possible that it will be identified in other granitic pegmatites.

ABOUT THE AUTHORS

Mr. Laurs (blaurs@gia.edu) is editor of Gems & Gemology *at GIA in Carlsbad, California. Dr. Simmons is professor of mineralogy and university research professor, and Mr. Falster is senior research technologist, at the University of New Orleans, Louisiana. Dr. Rossman is professor of mineralogy at the California Institute of Technology, Pasadena. Ms. Quinn is staff gemologist, and Mr. McClure is director of Identification Services, at the GIA Gem Laboratory, Carlsbad. Dr. Peretti is director of the GRS Gemresearch Swisslab Ltd., Lucerne, Switzerland. Dr. Armbruster is professor of mineralogical crystallography at the University of Bern, Switzerland. Dr. Hawthorne is professor of mineralogy, and Mr. Cooper is laboratory technician, at the University of Manitoba, Winnipeg, Canada. Dr. Günther is professor for trace elements and microanalysis at the Laboratory for Inorganic Chemistry, ETH Zurich, Switzerland. Dr. Grobéty is professor of mineralogy at the University of Fribourg, Switzerland.*

ACKNOWLEDGMENTS: The authors are grateful to Dr. Federico Pezzotta (Natural History Museum, Milan, Italy) for supplying detailed information on the geology, mineralogy, and morphology of pezzottaite. The senior author is indebted to Dr. Pezzotta for guiding his visit to the mine in July 2003. We thank the following gem dealers for loaning and/or donating research samples: Mark Kaufman of Kaufman Enterprises, San Diego, California; Dudley Blauwet of Dudley Blauwet Gems, Louisville, Colorado; Laurent Thomas of Polychrome France Co., Chambray-lès-Tours, France; Denis Gravier and Fabrice Danet of Le Mineral Brut, Saint-Jean-le-Vieux, France; Tom Cushman of Allerton Cushman & Co., Sun Valley, Idaho; Marc Jobin and Steve Jaquith of MJ3 Inc., New York; Herb Obodda of H. Obodda, Short Hills, New Jersey; Stuart Wilensky of Stuart and Donna Wilensky Fine Minerals, Wurtsboro, New York; Irv Brown of Irv Brown Fine Minerals, Fallbrook, California; Edward Boehm of Joeb Enterprises, Solana Beach, California; K & K International, Falls Church, Virginia; William Pinch of Pittsford, New York; Rob Lavinsky of The Arkenstone, San Diego; Brian Cook of Nature's Geometry, Graton, California; G.E.O. International Co. Ltd of Bangkok; and Papas Gem Co. Ltd., Bangkok. We thank John I. Koivula of GIA, Carlsbad, for supplying samples and photomicrographs. Dr. Petr Černý of the University of Manitoba, Winnipeg, provided useful comments on the manuscript. Assistance with document scanning and computer-automated translations was provided by Denise Breceda of the GIA Gem Laboratory, Stuart Overlin of Gems & Gemology, *and Sheryl Elen of the Richard T. Liddicoat Library and Information Center in Carlsbad. Neil Barron and Ruth Patchick of the Liddicoat library obtained numerous publications via interlibrary loan. Portions of Zagorsky et al. (1999) were translated by Inna Saphonova, Novosibirsk, Russia.*

REFERENCES

Abduriyim A., Kitawaki H. (2003) Analysis on Cs pink "beryl" using a laser ablation system with inductively coupled plasma mass spectrometer (LA-ICP-MS). *Gemmology*, Vol. 34, No. 411, pp. 24–26 (in Japanese, with insert of English translation).

Arem J.E. (1987) *Color Encyclopedia of Gemstones*. Van Nostrand Reinhold Co., New York.

Armbruster T., Libowitzky E., Diamond L., Auernhammer M., Bauerhansl P., Hoffmann C., Irran E., Kurka A., Rosenstingl H. (1995) Crystal chemistry and optics of bazzite from Furkabasistunnel (Switzerland). *Mineralogy and Petrology*, Vol. 52, pp. 113–126.

Aurisicchio C., Fioravanti G., Grubessi O., Zanazzi P.F. (1988) Reappraisal of the crystal chemistry of beryl. *American Mineralogist*, Vol. 73, pp. 826–837.

Beus A.A. (1966) *Geochemistry of Beryllium and Genetic Types of Beryllium Deposits*. Ed. by L.R. Page, and transl. by F. Lachman and R. K. Harrison. W.H. Freeman and Co., San Francisco.

Cabell M.J., Smales A.A. (1957) The determination of rubidium and caesium in rocks, minerals and meteorites by neutron-activation analysis. *The Analyst*, Vol. 82, pp. 390–406.

Černý P. (1972) The Tanco pegmatite at Bernic Lake, Manitoba. VII. Secondary minerals from the spodumene-rich zones. *Canadian Mineralogist*, Vol. 11, pp. 714–726.

Černý P. (1975) Alkali variations in pegmatitic beryls and their petrogenetic implications. *Neues Jahrbuch fur Mineralogie, Abhandlungen*, Vol. 123, pp. 198–212.

Černý P. (1991) Rare-element granitic pegmatites. Part I: Anatomy and internal evolution of pegmatite deposits. *Geoscience Canada*, Vol. 18, pp. 49–67.

Černý P. (2002) Mineralogy of beryllium in granitic pegmatites. In E.S. Grew, Ed., *Beryllium: Mineralogy, Petrology, and Geochemistry*, Reviews in Mineralogy and Geochemistry, Mineralogical Society of America, Washington D.C., Vol. 50, pp. 405–444.

Černý P., Hawthorne F.C. (1976) Refractive indices versus alkali contents in beryl: General limitations and applications to some pegmatitic types. *Canadian Mineralogist*, Vol. 14, pp. 491–497.

Černý P., Meintzer R.E., Anderson A.J. (1985) Extreme fractionation in rare-element granitic pegmatites: Selected examples of data and mechanisms. *Canadian Mineralogist*, Vol. 23, pp. 381–421.

Černý P., Anderson A.J., Tomascak P.B., Chapman R. (2003) Geochemical and morphological features of beryl from the Bikita granitic pegmatite, Zimbabwe. *Canadian Mineralogist*, Vol. 41, pp. 1003–1011.

Chantraine J. (1966) Etude géologique et prospection au 1/100,000 des feuilles Janjina-Mandrosonoro (J-K, 51) [Geological investigation and prospection of the 1/100,000 sheets Janjina-Mandrosonoro (J-K, 51)]. *Travaux du Bureau Géologique*, No. 58, Service Géologique, Tananarive.

Deer W.A., Howie R.A., Zussman J. (1997) *Rock-forming Minerals—Disilicates and Ring Silicates*, Vol. 1B, 2nd ed. The Geological Society, London, pp. 372–409.

Della Ventura G., Rossi P., Parodi G.C., Mottana A., Raudsepp M., Prencipe M. (2000) Stoppaniite, $(Fe,Al,Mg)_4(Be_6Si_{12}O_{36}) \bullet (H_2O)_2(Na,\square)$ a new mineral of the beryl group from Latium (Italy). *European Journal of Mineralogy*, Vol. 12, pp. 121–127.

Dirlam D.M., Laurs B.M., Pezzotta F., Simmons W.B. (2002) Liddicoatite tourmaline from Anjanabonoina, Madagascar. *Gems & Gemology*, Vol. 38, No. 1, pp. 28–53.

Evans H.T., Mrose M.E. (1966) Crystal chemical studies of cesium beryl. *Program & Abstracts*, Geological Society of America Annual Meeting, San Francisco, p. 63.

Ferraris G., Prencipe M., Rossi P. (1998) Stoppaniite, a new member of the beryl group: Crystal structure and crystal-chemical implications. *European Journal of Mineralogy*, Vol. 10, pp. 491–496.

Ford W.E. (1910) The effect of the presence of alkalies in beryl upon its optical properties. *American Journal of Science*, Vol. 30, pp. 128–130.

Hänni H.A., Krzemnicki M.S. (2003) Caesium-rich morganite from Afghanistan and Madagascar. *Journal of Gemmology*, Vol. 28, No. 7, pp. 417–429.

Hawthorne F.C., Černý P. (1977) The alkali-metal positions in Cs-Li beryl. *Canadian Mineralogist*, Vol. 15, pp. 414–421.

Hawthorne F.C., Cooper M.A., Peretti A., Simmons W.B., Armbruster T., Rossman G.R., Günther D., Laurs B.M., Grobéty B. (2003a) Check-list for new mineral proposals: Pezzottaite. Proposal submitted to the International Mineralogical Association, 8 pp.

Hawthorne F.C., Cooper M.A., Simmons W.B., Falster A.U., Laurs B.M., Armbruster T., Rossman G.R., Peretti A., Günther D., Grobéty B. (in preparation) Pezzottaite, $Cs(Be_2Li)Al_2Si_6O_{18}$, a spectacular new mineral related to the beryl group, from Madagascar.

Hofmeister A.M., Hoering T.C., Virgo D. (1987) Vibrational spectroscopy of beryllium aluminosilicates: Heat capacity calculations from band assignments. *Physics and Chemistry of Minerals*, Vol. 14, No. 3, pp. 205–224.

Lacroix A. (1912) Sur la continuité de la variation des propriétés physiques des béryls de Madagascar, en relation avec leur composition chimique. *Bulletin de la Société Française de Minéralogie*, Vol. 33, pp. 200–208.

Lacroix A., Rengade (1911) Sur les propriétés optiques des béryls roses de Madagascar. *Bulletin de la Société Française de Minéralogie*, Vol. 34, pp. 123–125.

Laurs B.M. (2003) Gem News International: Update on sapphire, pezzottaite, and other gems from Madagascar. *Gems & Gemology*, Vol. 39, No. 3, pp. 229–231.

Meagher E.P., Gibbs, G.V. (1977) The polymorphism of cordierite; II, The crystal structure of indialite. *Canadian Mineralogist*, Vol. 15, pp. 43–49.

Nassau K. (1984) *Gemstone Enhancement*. Butterworths, London.

Newly discovered beryl now classified as mineral (2003) *Jewellery Net Asia*, http://www.jewellerynetasia.com/news/view.jsp?tid=5795 (accessible with password), posted October 16.

Pezzotta F., Ed. (2001) *Madagascar, a Mineral and Gemstone Paradise. extraLapis English*, No. 1, Lapis International LLC, East Hampton, CT, 100 pp.

Platonov A.N., Taran M.N., Klyakhin V.A. (1989) On two colour types of Mn^{3+}-bearing beryls. *Zeitschrift der Deutschen Gemmologischen Gesellschaft*, Vol. 38, pp. 147–154.

Rare pink-red beryl sparks market's interest (2003) *Jewellery Net Asia*, http://www.jewellerynetasia.com/news/view.jsp?tid=5693 (accessible with password), posted August 28.

Ristic S., Eichoff H.J. (1955) Les spectres d'absorption et réflexion de quelques variétés de béryls synthétiques et naturels. *Congrés Groupement pour l'Avancement des Méthods d'Analyse Spectrographiques des Produits Métallurgiques*, Vol. 18, pp. 385–411.

Rossovskiy L.N. (1981) Rare-metal pegmatites with precious stones and conditions of their formation (Hindu Kush). *International Geology Review*, Vol. 23, No. 11, pp. 1312–1320.

Schaller W.T., Stevens R.E., Jahns R.H. (1962) An unusual beryl from Arizona. *American Mineralogist*, Vol. 47, pp. 672–699.

Schmetzer K., Berdensinski W., Bank H. (1974) Über die Mineralart Beryll, ihre Farben und Absorptionsspektren. *Zeitschrift der Deutschen Gemmologischen Gesellschaft*, Vol. 23, pp. 5–39.

Shatskiy V.S., Lebedev A.S., Pavlyuchenko V.S., Kovaleva L.T., Koz'menko O.A., Yudin A.N., Belov N.V. (1981) Conditions for the entry of alkali cations into beryl. *Geochemistry International*, Vol. 18, No. 2, pp. 7–17.

Sherriff B.L., Grundy H.D., Hartman J.S., Hawthorne F.C., Černý P. (1991) The incorporation of alkalis in beryl: Multinuclear MAS NMR and crystal-structure refinement study. *Canadian Mineralogist*, Vol. 29, pp. 271–285.

Shigley J.E., Foord E.E. (1984) Gem-quality red beryl from the Wah Wah Mountains, Utah. *Gems & Gemology*, Vol. 20, No. 4, pp. 208–221.

Shigley J.E., McClure S.F., Cole J.E., Koivula J.I., Lu T., Elen S., Demianets L.N. (2001) Hydrothermal synthetic red beryl from the Institute of Crystallography, Moscow. *Gems & Gemology*, Vol. 37, No. 1, pp. 42–55.

Shigley J.E., Thompson T.J., Keith J.D. (2003) Red beryl from Utah: A review and update. *Gems & Gemology*, Vol. 39, No. 4, pp. 302–313.

Simmons W.B., Falster A.U., McClure S.F., Quinn E.P., Rossman G.R., Hawthorne F.C. (2003) Gem News International: A new saturated purplish pink Cs-"beryl" from Madagascar: Preliminary analyses. *Gems & Gemology*, Vol. 39, No. 1, pp. 50–54.

Sinkankas J. (1981) *Emerald and Other Beryls*. Chilton Book Co., Radnor, PA.

Solntsev V.P., Bukin G.V. (1997) The color of natural beryls from rare-metal Mozambique pegmatites. *Russian Geology and Geophysics*, Vol. 38, No. 10, pp. 1661–1668.

Staatz M.H., Griffitts W.R., Barnett P.R. (1965) Differences in the minor element compositions of beryl in various environments. *American Mineralogist*, Vol. 50, pp. 1783–1795.

Warin R., Jacques B. (2003) Le béryl-Cs d'Ambatovita, Madagascar—Morphologie et aspects macroscopiques [The Cs-beryl of Ambatovita, Madagascar—Morphology and macroscopic aspects]. *Le Règne Minéral*, No. 52, pp. 36–41.

Webster R. (1994) *Gems—Their Sources, Descriptions and Identification*, 5th ed. Revised by P.G. Read, Butterworth-Heinemann, Oxford, England.

Wood D.L., Nassau K. (1968) The characterization of beryl and emerald by visible and infrared absorption spectroscopy. *American Mineralogist*, Vol. 53, pp. 777–800.

Zagorsky V.Ye., Peretyazhko I.S., Shmakin B.M. (1999) *Miarolitic Pegmatites*. Volume 3 of B.M. Shmakin and V.M. Makagon, Eds. *Granitic Pegmatites*, Nauka, Siberian Publishing Firm RAS, Novosibirsk, Russia.

Zambonini F., Caglioti V. (1928) Ricerche chimiche sulla rosterite di San Piero in Campo (Isola d'Elba) e sui berilli in generale. *Gazetta Chimica Italiana*, Vol. 58, No. 131, pp. 131–152.

RED BERYL FROM UTAH: A REVIEW AND UPDATE

James E. Shigley, Timothy J. Thompson, and Jeffrey D. Keith

There is only one known commercial occurrence of gem-quality red beryl in the world: the Ruby Violet (or Red Beryl) mine in the Wah Wah Mountains of Beaver County, Utah. The beryl is found mostly along fractures (often clay-filled) in a topaz rhyolite. It crystallized as a vapor-phase mineral from the reaction between rhyolite-derived gases, vapors originating from heated groundwaters, and preexisting minerals and volcanic glass in the rhyolite. Production of red beryl over the past 25 years is estimated to be more than 60,000 carats, of which about 10% was facetable. Exploration and evaluation programs undertaken by two mining companies from 1994 to 2001, combined with field studies by some of the authors and others, have resulted in a greater understanding of the geology of the Ruby Violet deposit and the potential for productive areas beyond the current mine site.

Two decades ago, Shigley and Foord (1984) described the spectacular gem-quality red beryl (figure 1) found at the Ruby Violet mine in the Wah Wah Mountains of southwestern Utah (see also Ream, 1979; Sinkankas, 1976, 1997). Since that time, this material has remained one of the rarest color varieties of gem beryl, with its increased recognition and acceptance in the marketplace being offset by the continued limited scale of production.

Although gem beryls are common in granitic pegmatites (i.e., aquamarine, morganite, heliodor, and goshenite) and in certain metamorphic and metasedimentary rocks (emerald), their occurrence in rhyolites is unusual. Conversely, rhyolites occasionally contain crystals of quartz, topaz, and garnet in lithophysal (gas) cavities, or opal as veins or cavity fillings.

Besides the Ruby Violet mine, several other occurrences of red beryl (all in rhyolites) are known, but none has produced significant quantities of facet-grade material. These include: Utah—Wildhorse Spring, Topaz Valley, and Starvation Canyon, all in the Thomas Range, Juab County (Staatz and Carr, 1964; Ream, 1979; Sinkankas, 1981; Montgomery, 1982; Christiansen et al., 1986; Wilson, 1995; Foord, 1996; Baker et al., 1996); New Mexico—Beryllium Virgin prospect in Paramount Canyon, Black Range, Sierra County (Kimbler and Haynes, 1980; Sinkankas, 1981, 1997; Foord, 1996; Voynick, 1997), and East Grants Ridge, Cibola County (Voynick, 1997); and Mexico—San Luis Potosí (Ream, 1979).

Red beryl was initially called "bixbite" (Eppler, 1912), but this name never attained widespread usage—in part because of its confusion with bixbyite [$(Mn,Fe)_2O_3$], a mineral species that also happens to occur in topaz rhyolites in Utah in association with red beryl. More recently, some have attempted to market the gem as "red emerald" to enhance its status among consumers by calling attention to its relation to emerald (see, e.g., Spendlove, 1992; Weldon, 1999; Genis, 2000; Pesheck, 2000). Although this controversial terminology violates generally accepted gemological nomenclature, it has added to the public's recognition of red beryl (Roskin, 1998).

See end of article for About the Authors and Acknowledgments.
GEMS & GEMOLOGY, Vol. 39, No. 4, pp. 302–313.

Figure 1. Red beryl from the Wah Wah Mountains of Utah is among the rarest varieties of gem beryl, and crystals suitable for faceting have been found so far only at one locality. These crystals (3.5 and 2.2 grams) are from a collection that was donated to GIA by Rex Harris and Michael and Tina Nielson of Red Beryl Inc., Delta, Utah; the rings (the largest red beryl is 0.54 ct, set with a 0.54 ct emerald) are courtesy of Equatorian Imports, Dallas, Texas. Photo © Harold and Erica Van Pelt.

During the past decade, field studies of the Ruby Violet mine have provided new insights into the geologic conditions of red beryl formation (see, e.g., Keith et al., 1994; Christiansen et al., 1997). In addition, systematic exploration and sampling by two different mining companies (Kennecott Exploration Co. and Gemstone Mining Inc.) provided estimates of red beryl distribution and ore grade at the deposit. The present article reviews this new information on the geology of the Ruby Violet red beryl occurrence and the activities of these two mining companies. Also included is a brief gemological update on this unique American gemstone.

GEOGRAPHIC SETTING

Although red beryl was first reported nearly a century ago—from the Thomas Range, at a locality about 90 miles (145 km) north of the Ruby Violet mine (Hillebrand, 1905), it was discovered along the eastern flank of the Wah Wah Mountains in the late 1950s (Sinkankas, 1976). The Ruby Violet mine is situated approximately 40 km (25 miles) west-southwest of the town of Milford and is accessible for much of the year by paved and dirt roads (figures 2 and 3). The entrance to the property is secured by locked gates. Local elevations vary from 2,042 to 2,165 m (6,700 to 7,100 feet) above sea level. Average temperatures range from 38°C (100°F) in the summer to –12°C (10°F) in the winter. The area is uninhabited and has few landmarks. This portion of Utah lies within the "Basin and Range" physiographic province, which takes its name from the alternating parallel mountain ranges and valleys that dominate the topography.

GEOLOGY AND GENESIS

Geology. Topaz rhyolites of Cenozoic age are widely distributed across the western U.S. and Mexico. They are characteristically enriched in fluorine, and also contain elements such as Li, Rb, Cs, U, Th, and Be (Burt et al., 1982; Christiansen et al., 1983). The Thomas Range rhyolite, recognized as a source of topaz for over a century (Ream, 1979; Wilson, 1995), is located adjacent to Spor Mountain, the world's largest economic source of beryllium (Shawe, 1968; Christiansen et al., 1984; Barton and Young, 2002). At that deposit, the ore consists of disseminated bertrandite—$Be_4Si_2O_7(OH)_2$—and fluorite (CaF_2) in a water-deposited rhyolitic tuff (Lindsey, 1977). The geochemical association of beryllium and fluorine in some ore deposits has long been recognized, with fluorine bonding with—and acting to transport—beryllium as Be-F complexes in magmatic and hydrothermal systems (Ringwood, 1955; Levinson, 1962).

Rocks that predated the rhyolite and other volcanic rocks in the Wah Wah Mountains consist of Paleozoic and Mesozoic sediments that were deposited on Proterozoic crystalline basement rocks, and then were folded and thrust-faulted eastward during the Cretaceous-age Sevier Orogeny (Best et al., 1987; Keith et al., 1994). Volcanism in this part of Utah began during the middle Tertiary Period, about 34 million years (My) ago. Beginning about 23 My ago, extensional

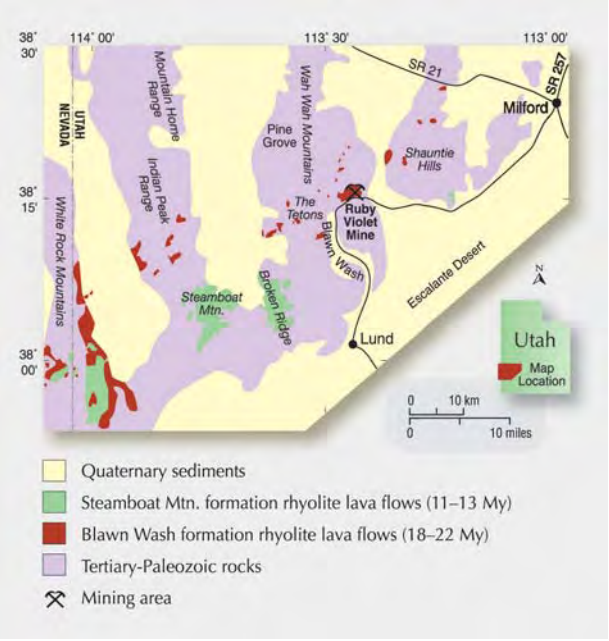

Figure 2. This simplified geologic map shows the location of the red beryl deposit on the eastern flank of the Wah Wah Mountains in southwestern Utah (approximately equal distances from both Salt Lake City, Utah, and Las Vegas, Nevada), as well as the general geology of the area. Both the Blawn Wash and Steamboat Mountain formations represent Cenozoic-age rhyolitic lava flows that occurred at several locations in this portion of Utah. Modified from Keith et al. (1994).

Figure 3. This view, looking westward, shows the Ruby Violet mine site in the mid-1990s, at the height of exploration activity. Since then, the site has been partially reclaimed, with most of the pits filled in to recreate the original shape of the hillside. Note that a dirt road leads directly to the site. Photo courtesy of William Rohtert.

(pulling apart) tectonism produced large, regional faults and associated volcanism in the area. The volcanism generated small-volume andesitic and rhyolitic domes, subvolcanic intrusions, and lava flows—including the red beryl–bearing rhyolite flow at the Ruby Violet deposit.

The red beryl forms hexagonal crystals that are hosted by a flow-banded, porphyritic, topaz rhyolite (figure 4). This light gray rock contains occasional crystals (phenocrysts) of alkali feldspar, quartz, and minor biotite mica in a fine-grained groundmass of these same minerals along with volcanic glass. At the mine site, this rock is exposed over an area of about 9 km^2, although portions may lie concealed beneath geologically younger rocks (Keith et al., 1994). The rhyolite forms part of the Blawn Wash formation (Abbott et al., 1983).

At the mine site, red beryl has been found within an area measuring 900 × 1,900 m, where the host rhyolite shows an unusual amount of argillic (clay) hydrothermal alteration (as compared to other topaz rhyolites; Keith et al., 1994). The more mineralized section of the deposit (figure 5) occupies a 50 × 850 m area that is currently exposed over an elevation range of about 90 m. This zone appears to lie within the central portion of the rhyolite flow (figure 6), which exhibits more prominent flow banding and phenocrysts (Keith et al., 1994).

The gem-grade red beryl mineralization occurs along or near discontinuous, near-vertical fractures that formed as a result of the cooling and contraction of the rhyolitic lava (figures 7 and 8). Not all fractures, or all portions of the same fracture, contain beryl. Within a productive fracture, the red beryl often occurs in locally dense concentrations of crystals that can extend over vertical distances of several meters and horizontal distances of 30 m or more. White (kaolinite) and brown (smectite-illite) clays, locally stained yellow-brown or black, fill many fractures, and often mark concentrations of red beryl crystals. The clay-filled fractures are also known to contain other vapor-phase minerals such as bixbyite, manganese-containing hematite, tridymite, cristobalite, and (rarely) topaz.

The walls of most of the beryl-bearing fractures have been altered to kaolinite over a width of several centimeters (Keith et al., 1994; Thompson et al., submitted). Some productive fractures lack clay alteration, possibly because they were sealed by the deposition of silica minerals (quartz, cristobalite, tridymite), oxide minerals (bixbyite and hematite),

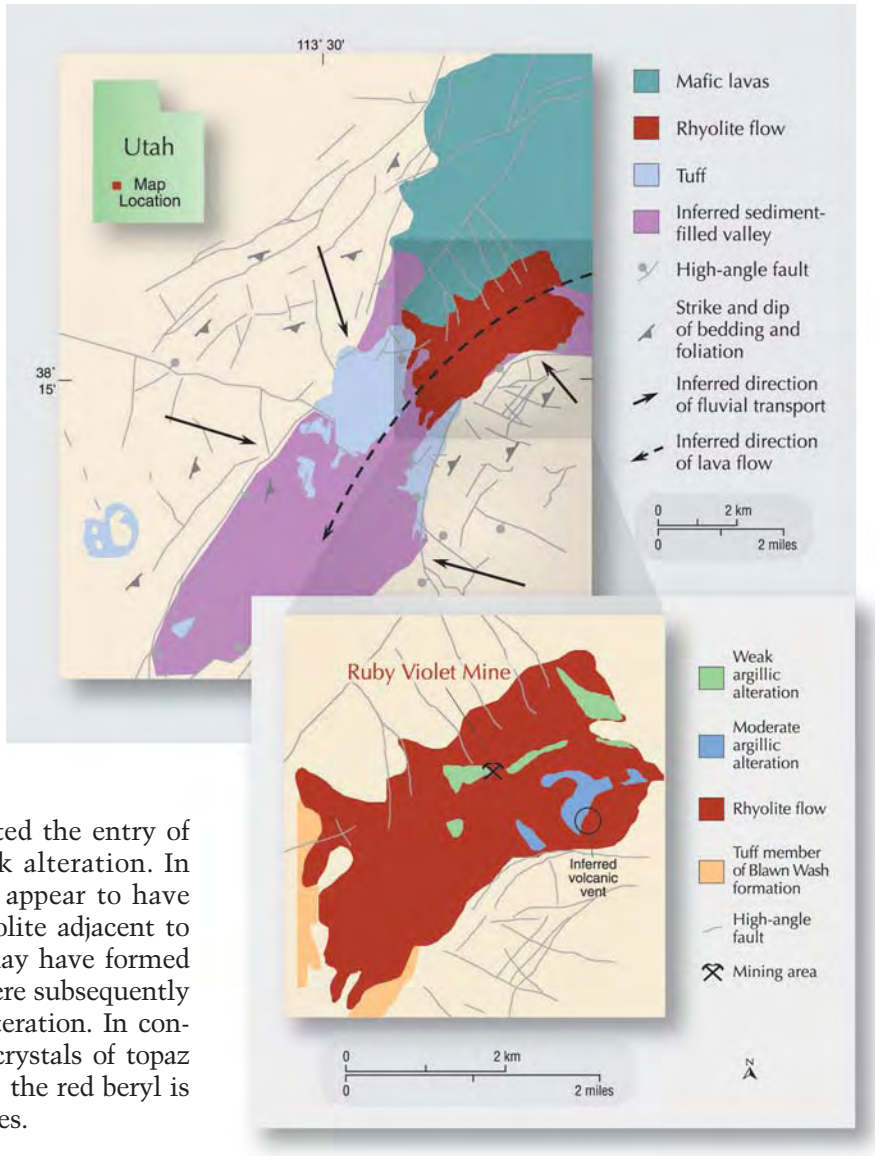

Figure 4. This simplified geologic map shows the location of the Ruby Violet mine within the rhyolite flow. Following its eruption, the lava is thought to have flowed southwestward through a valley, where it crystallized. Red beryl mineralization is locally concentrated along sets of near-vertical fractures that are oriented approximately parallel or perpendicular to the sides of this valley. These fractures resulted from the cooling and contraction of the solidifying rhyolite lava. Modified from Keith et al. (1994).

and alkali feldspar, which prevented the entry of fluids that produced the wallrock alteration. In addition, some red beryl crystals appear to have grown within the clay-altered rhyolite adjacent to the mineralized fractures; these may have formed along very narrow fractures that were subsequently obscured by mineral growth or alteration. In contrast to the typical occurrence of crystals of topaz and garnet in other topaz rhyolites, the red beryl is not found in lithophysal (gas) cavities.

Genesis of the Host Rhyolite and the Red Beryl. According to Keith et al. (1994) and Christiansen et al. (1997), after eruption the molten rhyolite flowed into a valley, where it solidified (again, see figure 4). The fractures that formed during cooling acted as conduits for the escape of gases released by the solidifying lava, as well as points of entry for surface waters into the flow (again, see figure 6).

Figure 5. In this mineralized section of the Ruby Violet mine, a number of discontinuous, near-vertical fractures are exposed in the rhyolite host rock. The rhyolite is excavated with earth-moving equipment and hand tools to expose productive areas for red beryl that occur along these fractures. Mine owner Rex Harris is shown for scale; photo courtesy of William Rohtert, taken in 1995.

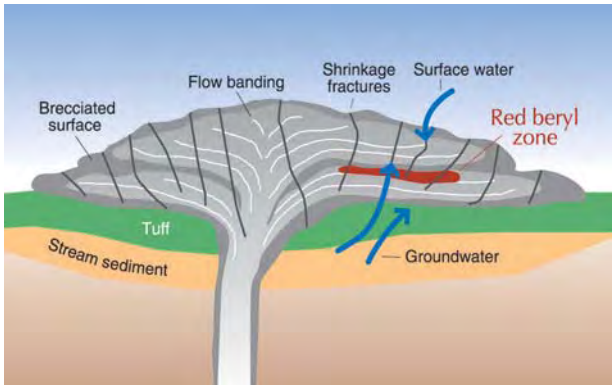

Figure 6. This cross section of the rhyolite lava flow is inferred from geologic field studies conducted at the Ruby Violet mine. The erupting lava flowed upward and outward from the vent of the volcano; as it cooled, conditions were achieved to allow for red beryl to form along fractures. Modified from Thompson (2002).

Figure 7. Typically, the red beryl crystals are locally concentrated along brown-stained, clay-filled fractures within the host rhyolite. Here, Rex Harris uses hand tools to carefully open up promising sections of the fractures. Photo courtesy of William Rohtert.

Keith et al. (1994) proposed that the beryllium necessary to form the red beryl was derived from the host rhyolite, from which it was mobilized as Be-F complexes within a favorable geochemical environment (see also Wood, 1992). Average whole-rock Be concentrations in the rhyolite range up to about 25 ppm—similar to Be values found in other topaz rhyolites (Christiansen et al., 1986). Even at only 25 ppm, there is sufficient Be in the rhyolite to crystallize the red beryl along fractures (for comparison, the organic black shales at Muzo Colombia, thought to be the source of beryllium for the emerald deposits, have an average Be concentration of only 3 ± 0.5 ppm; Ottaway et al., 1994). Be mobilization was enhanced by the very low Ca contents of the host rhyolite (<0.01–0.18 wt.% CaO, compared to about 0.5–0.9 wt.% for other topaz rhyolites; see Keith et al., 1994). This would allow the fluorine released from the cooling rhyolite to bond with and transport beryllium, rather than being removed by the crystallization of fluorite.

According to Keith et al. (1994) and Christiansen et al. (1997), red beryl crystallized when high-temperature fluorine-rich gases (released from the cooling rhyolite) mixed with vapors from heated waters (derived from sediments trapped beneath the flow) to produce a low-density, supercritical fluid that reacted with the rhyolite along fractures (figure 9). At certain depths within the flow, red beryl formed where Be-F complexes in the supercritical fluid

Figure 8. This red beryl crystal (just above the index finger) was found partly embedded in the rhyolite, along a clay-filled fracture. Crystals can range up to about 5 cm long, but 90% of those suitable for faceting are less than 1 cm. Photo courtesy of Rex Harris.

chemically reacted with rhyolitic glass, alkali feldspar, and Fe-Mn oxide minerals (bixbyite) along the fractures, primarily as a replacement of alkali feldspar (see also Aurisicchio et al., 1990; Barton and Young, 2002).* As temperatures continued to drop, subsequent reactions produced an acidic aqueous fluid that caused clay alteration along the fractures and within portions of the rhyolite. The absence of clay minerals as inclusions within the red beryl supports the theory that beryl formation occurred before the clay alteration. Therefore, the beryl formed at temperatures below the crystallization of rhyolite magma (i.e., <650°C), but above those of clay alteration (200–300°C).

HISTORY AND MINING

Lamar Hodges discovered red beryl in the Wah Wah Mountains in 1958, while prospecting (unsuccessfully) for uranium; his family worked the deposit, then known as the Violet Claims 1–8, as a hobby for the next 18 years (Barlow, 1979; Christensen and Austin, 1999; Garber, 2003). In 1976, the Harris family of Delta, Utah, purchased mining rights to the property. Over the next 18 years, the Rex and Ed Harris families and their partners worked the deposit on a more regular basis, usually for about 60 days per year, mainly in the spring and fall. Most of the mining then (as in recent years) took place in three open pits (lower, middle, and upper), with removal of ore

* According to Keith et al. (1994) and Christiansen et al. (1997), the nearly anhydrous red beryl crystallized from supercritical fluid that contained some water, but the activity of water in the fluid is thought to have been very low (i.e., only slightly higher than its activity in the rhyolite). Where water was absent in the flow, red beryl formation did not occur. The chemical reaction that formed red beryl consumed water and produced hydrofluoric acid, the principal agent of the clay alteration, as well as soluble fluorides.

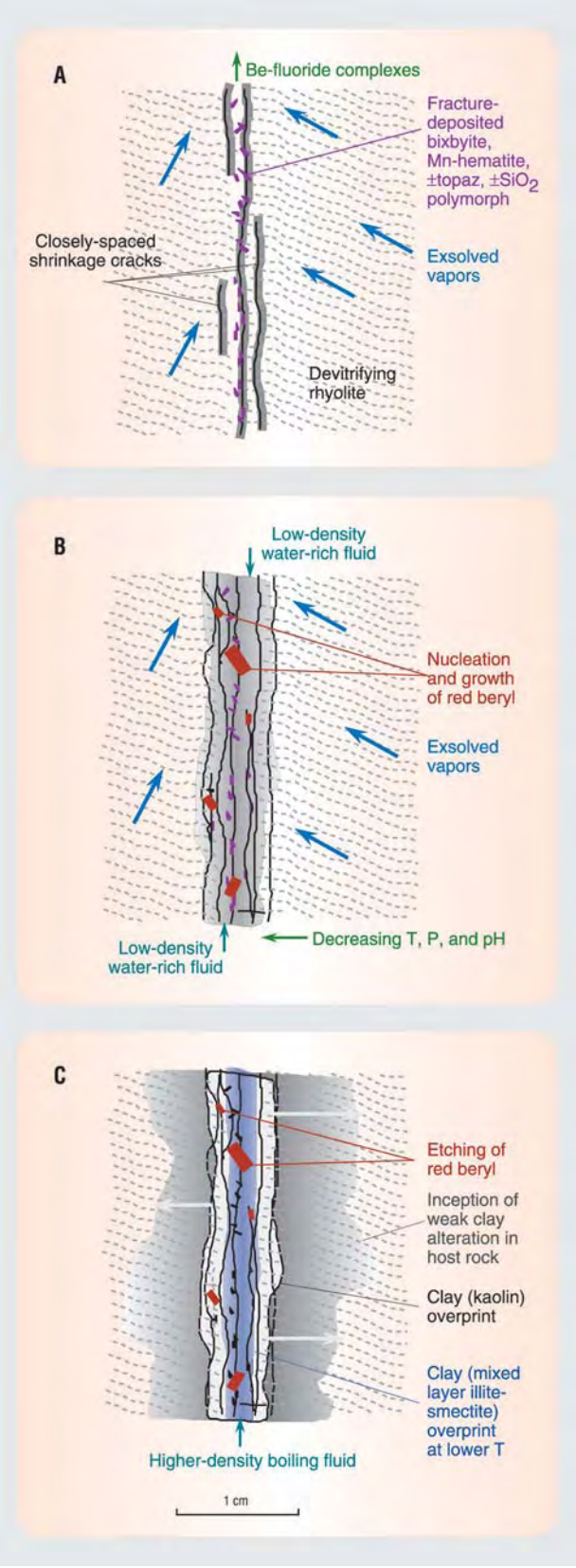

Figure 9. These diagrams depict the inferred sequence of events leading to the crystallization of red beryl and alteration of the host rhyolite. Shrinkage fractures in the cooling rhyolite provided channels for the upward release of supercritical fluids containing beryllium-fluoride complexes (A). These fluids interacted with preexisting minerals and rhyolitic glass, resulting in the formation of red beryl crystals along the fractures (B). Subsequently, acidic aqueous fluids caused clay alteration in the rhyolite and etched some of the beryl crystals (C). Modified from Keith et al. (1994).

ultimately reaching depths of about 20 m below the surface. Most of the gem-quality red beryl recovered to date has come from the lower pit, where red beryl–containing fractures occur every few meters (Keith et al., 1994). Mining has involved limited blasting to break up the host rock, the use of earth-moving equipment (backhoe and bulldozer) to clear access to productive areas, and digging with hand tools to locate and remove the beryl crystals from the fractures. According to Rex Harris (pers. comm., 2003), from 1976 to 1994 the deposit yielded about 0.5 carat of facetable red beryl per ton of ore, with at least 2,000 tons of ore extracted each year. Until 1994, the Harris family remained the single primary source of red beryl that could be marketed for faceting purposes or as mineral specimens.

On the basis of the recognized gem value of red beryl, and the geologic potential of the deposit identified through reconnaissance geologic mapping, in March 1994 Kennecott Exploration Co. (KEC) entered into a three-year lease with the Harris family, with the option to purchase the mine and surrounding claims as well as exploration rights (Verbin, 1994). Their intention was to determine whether sufficient red beryl reserves existed in the deposit and, if improved gem recovery was feasible, to allow the mine to be worked economically on a larger scale. KEC planned to quarry the mineralized rhyolite, crush the rock to a minimum size, and then chemically dissolve it to recover the red beryl crystals. Over the next three years, Kennecott conducted an extensive program of geologic mapping, core drilling, and bulk sampling.

According to an unpublished 1996 report by KEC project leader William Rohtert, nearly 3,962 m (13,000 feet) of core was recovered from 56 drill holes to investigate the subsurface geology of the deposit. In November 1995, KEC began an underground bulk-sampling program to confirm the extent of the deposit identified by core drilling, calculate the potential ore grade, and test the effectiveness of mechanized mining. In all, they removed nearly 11,000 tonnes of rock from almost 600 m of tunnels. This work resulted in a more complete understanding of the distribution and geologic controls of the red beryl mineralization. Proven and probable reserves were subsequently estimated to be over 1,000,000 tons of ore with a rough gem grade of 0.25 gram (1.25 ct) of beryl per ton (and locally up to 5 grams per ton). At a faceting yield of 10% (W. Rohtert, pers. comm., 2003), this would equate to 0.125 ct of faceted red beryl per ton of ore. Geologic and geophysical surveys suggested at least five additional exploration targets in the immediate area.

A proprietary method ("caustic fusion") to chemically dissolve the rhyolite and liberate the red beryl crystals was developed for KEC by the technical staff of Lakefield Research in Lakefield, Ontario, Canada, but it proved uneconomic compared to hand-picking crystals from the crushed ore. KEC also built a preliminary crushing plant capable of processing 10 tons of ore per hour near Cedar City (40 km from the site). Ore was crushed to two different feed sizes, and then passed by conveyor belt through a recovery room where it was hand-picked for red beryl crystals. The material was then hand-sorted into three categories: non-gem, near-gem (with less than 50% of a crystal being facet quality), and gem (with more than 50% facet quality). The beryl concentrate was cleaned and then re-sorted by professional gemologists to more accurately categorize facetable crystals by size, color, and quality. The rough was faceted in Thailand (and in Bogotá, Colombia, for some melee-size material), and then the polished goods were sorted by size, color, and clarity by gemologists at KEC's Salt Lake City offices. Unfortunately, production figures for this period remain proprietary.

Despite the technical successes of KEC's Ruby Violet exploration program, internal corporate politics and downsizing at RTZ (the parent company) led to the disbanding of Kennecott's colored gemstone initiative at the end of 1996, and the company decided to divest the property.

In March 1997, Utah-based Gemstone Mining Inc. (GMI)—the U.S. subsidiary of Gibraltar-based Amelia Investments Ltd.—purchased from the Harris family a one-year extension of the lease option, also to evaluate the feasibility of mining red beryl on a large scale (Lurie, 1997; Genis, 2000; Austin, 2002). In addition, GMI acquired all cut and uncut gem material that Kennecott had produced; their scientific, production, and marketing data; and the processing plant. Gem material from this stockpile and from further mining was then sold by GMI to a Gibraltar-based company, Red Emerald Ltd. (REL), for faceting, marketing, and sales. A third company, Canada-based Red Emerald Resources (formerly Neary Resources), provided investment funds for both companies in exchange for a portion of the profits. Later, additional funding was provided by another investor.

GMI performed further investigations of the geology and ore grade of the deposit, which included geologic mapping, core drilling, and bulk sampling. Favorable results prompted GMI to apply for a large-mine permit from state authorities. In December 1998, the option agreement was restructured, and GMI made a down payment to the Harris family to purchase the mine, agreeing to a payment schedule for the balance. At the same time, they began to work the deposit (which they referred to as the Red Emerald mine; Pesheck, 2000) using open-pit methods.

In June 2001, however, GMI did not make a scheduled payment to the Harris family, causing the mining contract to go into default. The U.S. Bureau of Land Management took control of the property on behalf of the Harrises, and GMI and REL ceased all mining and production activities. In August 2001, as required by state law as part of the large-mine permit, GMI began reclamation of the mine site. This action involved filling most of the open pits, hauling away waste rock, restoring much of the land surface to its original topography, covering the site with topsoil, seeding, and removing all structures. Efforts are underway to sell the remaining gem material obtained by GMI to pay investors and other costs (D. Merz, pers. comm., 2003).

The Harris family recently regained complete ownership of the mine, in accordance with the terms of the GMI purchase agreement, and they intend to resume small mining operations until a new purchaser is found for the property (R. Harris, pers. comm., 2003).

PRODUCTION AND DISTRIBUTION

A recent assessment of the gem material in possession of the Harris family listed over 1,600 carats of faceted stones and 56,000 carats of mixed-grade crystals, of which about 10% were suitable for cutting. The quantity of material held at the time by GMI has not been made public.

Red beryl is sold as both mineral specimens and faceted gemstones, as well as set in jewelry. The average weight of cut stones has been about 0.20 ct, with approximately 10% of the gemstone production exceeding 1 ct. To date, the largest faceted red beryl weighs 4.5 ct.

For the most part, the material has been marketed in the U.S. and Japan. Small cut goods have been used primarily in custom jewelry, while larger faceted stones have been sold loose to collectors or incorporated into exquisite jewelry pieces (similar to those on the cover of this issue of *Gems & Gemology*).

Figure 10. Red beryl crystals from the Ruby Violet mine display a simple prismatic morphology (dominated by basal pinacoid and prism faces) that is typical of most beryl. Shown here are two intergrown crystals (up to 2.1 cm long). Courtesy of Rex Harris; photo © Jeff Scovil.

PHYSICAL AND GEMOLOGICAL PROPERTIES

Crystals of red beryl (figure 10) usually occur as simple hexagonal prisms that are well formed and are terminated by flat or, less commonly, stepped basal pinacoid faces (Foord, 1996). They range up to more than 2 cm wide and 5 cm long. However, 90% of the gem-quality crystals are less than 1 cm in length. They are elongated parallel to the c-axis, with length:width ratios of approximately 4:1 or greater. Some crystals exhibit evidence of breakage and rehealing. Doubly terminated and multiple crystals have also been encountered (see again figures 1 and 10).

Shigley and Foord (1984) summarized the gemological properties of red beryl. A literature review revealed similar, but slightly expanded ranges for refractive indices (n_ε = 1.560–1.570 and n_ω = 1.567–1.572) and specific gravity (2.65–2.72), but no other differences in gemological properties (see Nassau and Wood, 1968; Schmetzer et al., 1974; Miley, 1980–1981; Bank and Bank, 1982; Flamini et al., 1983; Hosaka et al., 1993; Harding, 1995). These include the pleochroism (ε = purplish red, ω

Figure 11. Some crystals of red beryl from the Ruby Violet mine exhibit sector zoning, as shown here in these two samples. In the 0.23 ct polished crystal section on top, the zoning appears as a triangular orangy red interior portion that is surrounded by purplish red. The 0.97 ct crystal on the bottom grew in opposite directions from a central starting point, so it displays this same color zoning as two triangular portions that form an hourglass pattern. Photos by James Shigley.

= orange-red to red), lack of ultraviolet fluorescence, inclusions (described below), and an absorption spectrum displaying a weak 430 nm band plus strong broad bands centered at 500 and 570 nm.

As documented by Shigley and Foord (1984) and shown in figure 11, some red beryl crystals are color zoned with a central cone- or hourglass-shaped area of orange-red surrounded by purplish-red material. The color of faceted stones may vary according to where they were cut in relation to these zones, and is also influenced by the mineral's dichroism (figure 12). As a result of both factors, gemstones cut with the table facet oriented parallel to the c-axis typically appear red or purplish red. Conversely, those cut with the table facet oriented perpendicular to the c-axis tend to appear more orangy red. For maximum yield, the former often are usually given a rectangular shape, while the latter are round or oval.

Almost all red beryl crystals contain fractures and solid, fluid, or fluid-and-gas inclusions, often in such abundance that portions of many crystals are translucent or even opaque. Secondary fluid inclusions occur in isolation or along partially healed fractures ("fingerprints"; figure 13). Fractures sometimes mark the boundaries of the internal color zoning. Hexagonal growth zoning can be seen in some cut stones viewed in a direction parallel to the c-axis (figure 14). Mineral inclusions consist of colorless to white quartz and feldspar, and black grains of hematite or bixbyite (Shigley and Foord, 1984; Aurisicchio et al., 1990). One stone revealed an unusual spray of needle-like tubes that were filled with what is probably goethite (figure 15).

Chemically, red beryl is characterized by relatively high levels of Fe and Mn (generally 1–2 and 0.1–0.3 wt.% oxides, respectively), low contents of alkali elements (<0.4 wt.% Na_2O and <0.2 wt.% K_2O), and the near-total absence of water (Nassau and Wood, 1968; Shigley and Foord, 1984; Hosaka et al., 1993). Platonov et al. (1989) attributed the colors of both red beryl and pink morganite to Mn^{3+}, and suggested that this ion occupies different sites in the crystal structure of these two beryl varieties. Dr. G. Rossman (pers. comm., 2003) speculates that the Mn^{3+} was incorporated into red beryl during crystallization, whereas in morganite and pezzottaite (Hänni and Krzemnicki, 2003; Simmons et al., 2003; Laurs et al., 2003) it was produced from the oxidation of Mn^{2+} due to exposure to natural ionizing radiation after the minerals had crystallized in granitic pegmatites.

Figure 12. Faceted red beryl exhibits colors from orangy red to red to purplish red, as a result of color zoning present in many of the gem crystals and beryl's dichroism. The stones shown on the left (0.78–1.39 ct) are from a collection that was donated to GIA by Rex Harris and Michael and Tina Nielson of Red Beryl Inc., Delta, Utah. Those on the right weigh 0.22–1.09 ct, and are courtesy of Dominique Merz. Photos by Maha Tannous.

Red beryl is not treated by heating or irradiation. Furthermore, because it is nearly anhydrous, it can be heated to temperatures that could damage emerald or other beryls, as might accidentally happen during jewelry repair (R. Harris, pers. comm., 2002). Since much of the material is naturally fractured, crystals and faceted stones are commonly treated with colorless substances such as paraffin wax, Opticon, cedarwood oil, and Canada balsam to improve their apparent clarity. However, most clarity treatment done today uses Arthur Groom's Gematrat epoxy resin filler (R. Harris, pers. comm., 2003; see also Weldon, 1998).

The gemological properties of red beryl distinguish it from other natural red gems such as ruby, garnet, spinel, zircon, and tourmaline, all of which have higher refractive indices and other significant differences. Beginning in the mid-1990s, a hydrothermal synthetic red beryl from Russia became commercially available. However, it can be readily separated from its natural counterpart on the basis of its crystal shape, inclusions and other internal features, absorption spectra, and chemical composition (Henn and Milisenda, 1999; Shigley et al., 2001; Fumagalli et al., 2003).

Figure 13. "Fingerprint" inclusions such as the one shown here are typical of red beryl. Photomicrograph by James Shigley; magnified 20×.

Figure 14. This 1.02 ct orangy red round brilliant exhibited hexagonal growth zoning when viewed down the c-axis. Photomicrograph by James Shigley; magnified 10×.

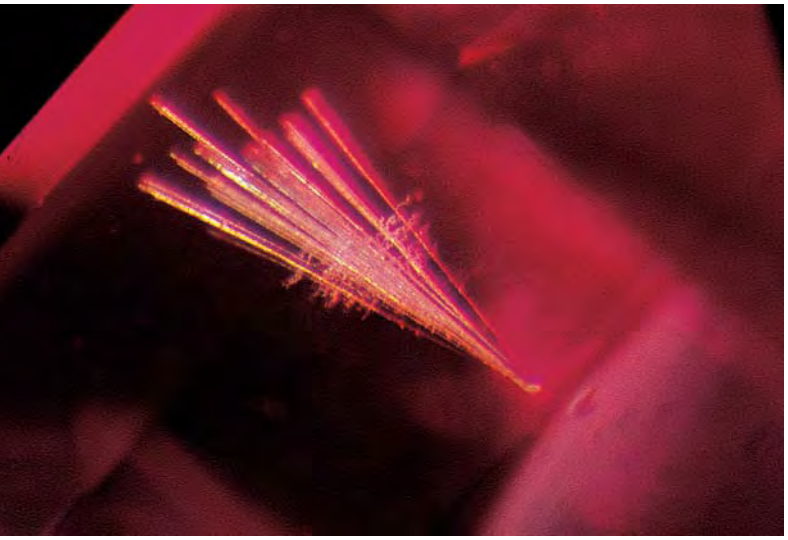

Figure 15. An unusual spray of needle-like tubes formed an interesting inclusion in this red beryl. These tubes are filled with an alteration mineral that is probably goethite, based on its Raman spectrum. Photomicrograph by John I. Koivula; magnified 40×.

CONCLUSION

The formation of gem-quality red beryl at the Ruby Violet mine resulted from a unique set of geologic conditions that occurred within a cooling rhyolite flow due to the reaction along fractures of magma-derived gases, groundwater, and preexisting minerals and volcanic glass in the host rhyolite. Over the past decade, significant projects were undertaken by two mining companies to investigate the potential for large-scale production of red beryl. While this large-scale mining has not continued, these efforts contributed to an increased knowledge of the deposit and recognition of red beryl in the gem trade. At the present time, gem material and mineral specimens are being sold from the inventory of the Harris family, as well as from the GMI stockpile. With the potential of the deposit not fully exploited, further work at the Ruby Violet mine is expected to begin again in the near future.

ABOUT THE AUTHORS

Dr. Shigley is director of GIA Research in Carlsbad, California. Mr. Thompson is a graduate gemologist and an engineering geologist with Intermountain GeoEnvironmental Services in Provo, Utah. Dr. Keith is professor of geology and chairman of the Brigham Young University Geology Department, in Provo, Utah.

ACKNOWLEDGMENTS: The authors thank the Rex Harris family for access to the Ruby Violet mine and for information on recent mining activities. William Rohtert of Hermosa Beach, California, provided photographs and information on the geology of the deposit. Kirsten Thompson of the Brigham Young University Geology Department drafted several of the illustrations. Helpful suggestions were provided by Edward Boehm of JOEB Enterprises LLC, Solana Beach, California; Dr. Kelly Hyslop of Knockeen, Ireland; Dr. Dominique Merz of Diligens Officium LLC, Newport Beach, California; and Dr. George Rossman of the California Institute of Technology, Pasadena.

REFERENCES

Abbott J.T., Best M.G., Morris H.T. (1983) Geologic map of the Pine Grove–Blawn Mountain area, Beaver County, UT. *U.S. Geological Survey Miscellaneous Investigations Series Map 1-1479*, Scale 1:24,000.

Aurisicchio C., Fioravanti G., Grubessi O. (1990) Genesis and growth of the red beryl from Utah (U.S.A.). *Atti Della Accademia Nazionale dei Lincei, Rendiconti Lincei, Scienze Fisiche e Naturali*, 9th Series, Vol. 1, No. 9, pp. 393–404.

Austin G. (2002) Red beryl company goes belly up. *Colored Stone*, Vol. 15, No. 2, pp. 14–15.

Baker J.M., Keith J.D., Christiansen E.H., Tingey D.G. (1996) Genesis of topaz rhyolite-hosted red beryl deposits, Starvation Canyon, Thomas Range, Utah. *Geological Society of America, Abstracts with Programs*, Vol. 28, p. A153.

Bank H., Bank F.H. (1982) Schleifwürdige rote Berylle aus Utah, USA, mit niedrigen Brechungsindizes. *Zeitschrift der Deutschen Gemmologischen Gesellschaft*, Vol. 31, No. 1/2, pp. 87–88.

Barlow F.J. (1979) Red beryl of the Wah Wah's. *Lapidary Journal*, Vol. 32, No. 12, pp. 2540–2546, 2568, 2570.

Barton M.D., Young S. (2002) Non-pegmatitic deposits of beryllium: Mineralogy, geology, phase equilibria and origin. In E.S. Grew, Ed., *Beryllium: Mineralogy, Petrology, and Geochemistry*, Reviews in Mineralogy and Geochemistry, Vol. 50, Mineralogical Society of America, Washington, DC, pp. 591–691.

Best M.G., Mehnert H.H., Keith J.D., Naeser C.W. (1987) Miocene magmatism and tectonism in and near the southern Wah Wah Mountains, southwestern Utah. *U.S. Geological Survey Professional Paper*, No. 1443-B.

Burt D.M., Sheridan M.F., Bikun J.V., Christiansen E.H. (1982) Topaz rhyolites—Distribution, origin, and significance for exploration. *Economic Geology*, Vol. 77, pp. 1818–1836.

Christenson C., Austin G. (1999) Red beryl. *Gems & Gemology*, Vol. 35, No. 3, p. 140.

Christiansen E.H., Burt D.M., Sheridan M.F., Wilson R.T. (1983) The petrogenesis of topaz rhyolites from the western United States. *Contributions to Mineralogy and Petrology*, Vol. 83, No. 1, pp. 16–30.

Christiansen E.H., Bikun J.V., Sheridan M.F., Burt D.M. (1984) Geochemical evolution of topaz rhyolites from the Thomas Range and Spor Mountain, Utah. *American Mineralogist*, Vol. 69, Nos. 3/4, pp. 223–236.

Christiansen E.H., Sheridan M.F., Burt D.M. (1986) *The Geology and Geochemistry of Cenozoic Topaz Rhyolites from the*

Western United States. Geological Society of America Special Paper 205, 82 pp.
Christiansen E.H., Keith J.D., Thompson T.J. (1997) Origin of gem red beryl in Utah's Wah Wah Mountains. *Mining Engineering*, Vol. 49, No. 2, pp. 37–41.
Eppler A. (1912) *Die Schmuck- und Edelsteine*. Verlag Felex Krais, Stuttgart, Germany.
Flamini A., Gastaldi L., Grubessi O., Viticoli S. (1983) Sulle caratteristiche particolari del berillo rosso dell'Utah. *La Gemmologia*, Vol. 9, No. 1/2, pp. 12–20.
Foord E.E. (1996) *Geology, Mineralogy and Paragenesis of the Ruby Violet Red Beryl Deposit, Southern Wah Wah Mountains, Beaver Co., Utah*. Consulting geologist report (unpublished) submitted to Kennecott Exploration Co., February 14, 76 pp. plus tables and illustrations.
Fumagalli M., Prosperi L., Pavese A., Bordiga S. (2003) Natural versus hydrothermal synthetic Russian red beryl: Chemical composition and spectroscopic measurements. *Journal of Gemmology*, Vol. 28, No. 5, pp. 291–301.
Garber W. (2003) Red beryl mining—Beaver County, Utah. *ICMJ's Prospecting and Mining Journal*, Vol. 72, No. 9, pp. 22–26.
Genis R. (2000) Here comes red emerald. *Rapaport Diamond Report*, Vol. 23, No. 27, pp. 109, 111.
Hänni H.A., Krzemnicki M.S. (2003) Caesium-rich morganite from Afghanistan and Madagascar. *Journal of Gemmology*, Vol. 28, No. 7, pp. 417–429.
Harding R.R. (1995) A note on red beryl. *Journal of Gemmology*, Vol. 24, No. 8, pp. 581–583.
Henn U., Milisenda C.C. (1999) Synthetic red beryl from Russia. *Journal of Gemmology*, Vol. 26, No. 8, pp. 481–486.
Hillebrand W.F. (1905) Red beryl from Utah. *American Journal of Science*, 4th series, Vol. 19, No. 112, pp. 330–331.
Hosaka M., Tubokawa K., Hatushika T., Yamashita H. (1993) Observations of red beryl crystals from the Wah Wah Mountains, Utah. *Journal of Gemmology*, Vol. 23, No. 7, pp. 409–411.
Keith J.D., Christiansen E.H., Tingey D.G. (1994) Geological and chemical conditions of formation of red beryl, Wah Wah Mountains, Utah. In R. Blackett and J. Moore, Eds., *Cenozoic Geology and Geothermal Systems of Southwestern Utah*, Utah Geological Association Publication, Vol. 23, pp. 155–170.
Kimbler F.S., Haynes P.E. (1980) An occurrence of red beryl in the Black Range, New Mexico. *New Mexico Geology*, Vol. 2, No. 1, pp. 15–16.
Laurs B.M., Simmons W.B., Rossman G.R., Quinn E.P., McClure S.F., Peretti A., Armbruster T., Hawthorne F.C., Falster A.U., Günther D., Cooper M.A., Grobéty B. (2003) Pezzottaite from Ambatovita, Madagascar: A new gem mineral. *Gems & Gemology*, Vol. 39, No. 4, pp. 284–301.
Levinson A.A. (1962) Beryllium-fluorine mineralization at Aguachile Mountain, Coahuila, Mexico. *American Mineralogist*, Vol. 47, No. 1/2, pp. 67–74.
Lindsey D.A. (1977) Epithermal beryllium deposits in water-laid tuff, western Utah. *Economic Geology*, Vol. 72, pp. 219–232.
Lurie M. (1997) Red beryl mine finds new investors. *Colored Stone*, Vol. 10, No. 6, pp. 26, 28.
Miley F. (1980–1981) An examination of red beryl. *Gems & Gemology*, Vol. 16, No. 12, pp. 405–408.
Montgomery A. (1982) Minerals of the Thomas Range, Utah. *Rocks and Minerals*, Vol. 57, No. 4, pp. 162–168.
Nassau K., Wood D.L. (1968) An examination of red beryl from Utah. *American Mineralogist*, Vol. 53, No. 5/6, pp. 801–806.
Ottaway T.L., Wicks F.J., Bryndzia L.T., Kyser T.K., Spooner E.T.C. (1994) Formation of the Muzo hydrothermal emerald deposit in Colombia. *Nature*, Vol. 369, No. 6481, pp. 552–554.
Pesheck L. (2000) The new red. *JQ Magazine*, Vol. 90, pp. 64–73.
Platonov A.N., Taran M.N., Klyakhin V.A. (1989) On two colour types of Mn^{3+}-bearing beryls. *Zeitschrift der Deutschen Gemmologischen Gesellschaft*, Vol. 38, No. 4, pp. 147–154.
Ream L.R. (1979) The Thomas Range, Wah Wah Mountains, and vicinity, western Utah. *Mineralogical Record*, Vol. 10, No. 5, pp. 261–278.
Ringwood A.E. (1955) The principles governing trace-element behavior during magmatic crystallization, Part II: The role of complex formation. *Geochimica et Cosmochimica Acta*, Vol. 7, pp. 242–254.
Roskin G. (1998) Selling beautiful gems with ugly names. *Jewelers' Circular Keystone*, Vol. 169, No. 7, pp. 120–123.
Schmetzer K., Bank H., Berdesinski W. (1974) Eine seltene rote Varietät der Mineralart Beryll (früher Bixbit genannt). *Zeitschrift der Deutschen Gemmologischen Gesellschaft*, Vol. 23, No. 2, pp. 139–141.
Shawe D.R. (1968) Geology of the Spor Mountain beryllium district, Utah. In J.D. Ridge, Ed., *Ore Deposits in the United States 1933–1967*, American Institute of Mining, Metallurgical, and Petroleum Engineers, Vol. 2, pp. 1148–1161.
Shigley J.E., Foord E.E. (1984) Gem-quality red beryl from the Wah Wah Mountains, Utah. *Gems & Gemology*, Vol. 20, No. 4, pp. 208–221.
Shigley J.E., McClure S.F., Cole J.E., Koivula J.I., Lu T., Elen S., Demianets L.N. (2001) Hydrothermal synthetic red beryl from the Institute of Crystallography, Moscow. *Gems & Gemology*, Vol. 37, No. 1, pp. 42–55.
Simmons W.B., McClure S.F., Quinn E.P., Rossman G.R., Hawthorne F.C. (2003) Gem News: A new saturated purplish pink Cs-"beryl" from Madagascar—Preliminary analyses. *Gems & Gemology*, Vol. 39, No. 1, pp. 50–54.
Sinkankas J. (1976) *Gemstones of North America*, Volume II. Van Nostrand Reinhold, New York.
Sinkankas J. (1981) *Emerald and Other Beryls*. Chilton Book Co., Radnor, PA.
Sinkankas J. (1997) *Gemstones of North America*, Volume III. Geoscience Press, Tucson, AZ.
Spendlove E. (1992) "Red emeralds" of Utah. *Rock & Gem*, Vol. 22, No. 5, pp. 32–36, 38.
Staatz M.H., Carr W.J. (1964) *Geology and Mineral Deposits of the Thomas and Dugway Ranges, Juab and Tooele Counties*, Utah. U.S. Geological Survey Professional Paper, Vol. 415, 188 pp.
Thompson T.J. (2002) A Model for the Origin of Red Beryl in Topaz Rhyolite, Wah Wah Mountains, Utah, USA. M.Sc. thesis, Department of Geology, Brigham Young University, Provo, Utah, 99 pp.
Thompson T.J., Keith J.D., Christiansen E.H., Griffen D.T., Tingey D.G. (submitted) A model for the origin of red beryl in topaz rhyolite, Wah Wah Mountains, Utah, USA. Submitted to *Journal of Volcanology and Geothermal Research*.
Verbin E. (1994) Argyle Diamond's RTZ options red beryl mine. *Colored Stone*, Vol. 7, No. 4, pp. 1, 25–26.
Voynick S.M. (1997) *New Mexico Rockhounding—A Guide to Minerals, Gemstones and Fossils*. Mountain Press Publishing Co., Missoula, MT.
Weldon R. (1998) Treatment tracer. *Professional Jeweler*, Vol. 1, No. 3, p. 50.
Weldon R. (1999) The case for red emerald. *Professional Jeweler*, Vol. 2, No. 6, pp. 66–67.
Wilson J.R. (1995) *A Collector's Guide to Rock, Mineral, and Fossil Localities of Utah*. Utah Geological Survey, Miscellaneous Publication 95-4.
Wood S.A. (1992) Theoretical prediction of speciation and solubility of beryllium in hydrothermal solution to 300°C at saturated vapor pressure: Application to bertrandite/phenakite deposits. *Ore Deposit Reviews*, Vol. 7, No. 4, pp. 249–278.

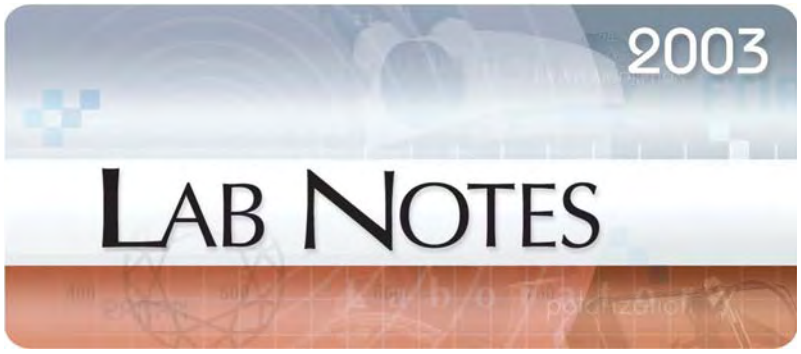

Chrysocolla "Owl" AGATE

Agates and other varieties of chalcedony are fascinating because their patterns vary so widely. While transparent single-crystal gems are much more uniform, chalcedony is one of nature's less-structured "painter's palettes," from which some quite imaginative jewelry and other decorative objects can be created. Among agates, some of the more interesting are the so-called eye agates, which develop as circular-to-semicircular concentrically layered agate through the cyclic deposition of chalcedony around a central acicular inclusion composed of some foreign substance, usually a mineral.

Recently, the West Coast laboratory had the opportunity to examine a well-polished bevel-edged oval plate of attractively patterned eye agate, which measured approximately 21.3 × 14.8 × 4.3 mm and weighed 12.71 ct. As shown in figure 1, the gem displayed a double "eye" structure of blue chrysocolla (identified by Raman analysis), with each eye individually surrounded by concentric bands of clear, near-colorless, and white agate. These in turn were surrounded by densely packed and interlocked macroscopic white-to-colorless quartz crystals that somewhat resembled white feathers.

Figure 1. This striking 21.3-mm-long Arizona "eye" agate shows an interesting double-eye pattern that could be set in a unique owl-themed brooch. Note the concentric formational banding of the agate around the chrysocolla-centered "eyes." Magnified 5×.

This distinctive piece was cut by Leon M. Agee of Agee Lapidary, Deer Park, Washington, from an inexpensive scrap of material that reportedly was from the Ray copper mine in Pinal County, Arizona. This locality is well-known among gem and mineral collectors for its magnificent specimens of chrysocolla in chalcedony.

In the past we have encountered and documented other agates showing pleasing and interesting patterns (see, e.g., Gem News: Summer 1998, pp. 136–137, and Winter 1999, p. 210; Lab Notes, Winter 2002, p. 340). With a little imagination, it is not hard to see how this piece could be featured as the "all knowing" eyes in a one-of-a-kind snowy owl brooch.

JIK and Maha Tannous

Editor's note: The initials at the end of each item identify the editor(s) or contributing editor(s) who provided that item. Full names are given for other GIA Gem Laboratory contributors.

Gems & Gemology, *Vol. 39, No. 4, pp. 314–321*

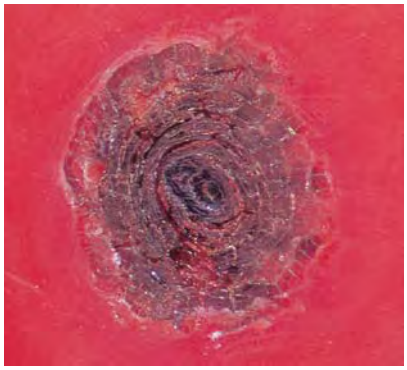

Figure 2. This dark brown area on a polished coral bead appears to be where a form of conchiolin coral was intersected and overgrown by red calcareous coral. Magnified 5×.

Figure 3. Surrounded by red coral, this white-to-light pink zone marks where a smaller branch of protruding coral was removed from the main mass during fashioning. Magnified 5×.

Interesting Red CORAL

While gems such as diamonds, rubies, sapphires, and emeralds are frequently submitted for identification, only occasionally do we see specimens fashioned from conchiolin or calcareous coral. Recently, an interesting necklace composed of what were believed to be red calcareous coral beads was submitted to the West Coast laboratory to determine if the beads were natural coral and whether they had been dyed.

Since calcareous coral has a well-known characteristic structure that is visible even with low magnification, it is relatively simple to identify this form of red coral and separate it from its various substitutes, such as dyed massive calcite, Gilson simulated coral, plastic, or glass. As is generally the practice, one bead in the necklace was randomly selected for gemological testing. Although examination with magnification easily proved it to be calcareous coral, there was still the question of whether it had been dyed or was natural color.

To determine if the bead had been dyed, we used the gemological microscope to examine the surface and the drill hole for signs of dye concentration or other color irregularities. During this search, we observed two interesting and unusual structural features on the surface of the polished bead. One of these features was a dark brown, off-round area of more or less concentric rings that looked quite literally like a cross section cut through a tree branch (figure 2). Testing with a hot point yielded an odor consistent with that of burning hair or a similar organic. From the shape of the feature and its reaction to heat, we suspect that it resulted when a branch of conchiolin coral was intersected and overgrown by the red calcareous coral.

The other surface characteristic was a web- or flower-shaped white-to-light pink zone (figure 3) that showed where a smaller branch of protruding coral had been polished off the main mass during fashioning of the bead. Since no dye was detected in either of these surface features or anywhere else on the bead, we concluded that the color was natural as well.

JIK and Maha Tannous

Coated DIAMONDS

A number of new diamond treatments have appeared in the last decade. Between fracture filling and high pressure/high temperature (HPHT) treatment, one sometimes forgets about the older, once-popular treatment of diamond coating. This practice was discussed by early GIA gemologist Eunice Miles in her groundbreaking article, "Diamond-coating techniques and methods of detection," in the Winter 1962–63 issue of *Gems & Gemology* (pp. 355–364).

Diamonds may be coated to deepen their color (in the case of fancy colors) or to diminish the amount of apparent color (in the D–Z range). Since the majority of gem diamonds are type Ia, with varying degrees of yellow due to nitrogen impurities, historically the most common coating technique has been to paint a thin blue film on diamonds of a near-colorless or lower color grade. This type of coating is typically confined to the crown and pavilion facets close to and on the girdle edge, though it can completely cover the diamond's surface. Since blue and yellow are complimentary colors, they appear to cancel each other out to produce a more colorless appearance. (Ever wonder why the flutes in most parcel papers are light blue?) It has been almost 20 years since a Lab Note on a coated diamond was last published (see Summer 1984 Lab Notes, p. 107). While, as then, it is true that only a few coated diamonds are submitted to the lab each year, the practice has not completely disappeared.

Recently, two round brilliant diamonds (1.09 and 3.03 ct) were submitted, by separate clients, to the East Coast laboratory. In the course of grading, the presence of a coating in the form of pale blue spots was observed while the diamonds were being examined with magnification. Figure 4 shows the coating on the 3.03 ct stone, which displays what Eunice Miles reported in 1962 as a faint blue "flux" that is characteristic of this treatment. Although GIA does not grade coated diamonds, for the purposes of this report we determined that the color of the smaller stone was equivalent to the "Q–R" range, while the larger appeared to be "M." In many instances, the lab has observed this treatment with diamonds in the near-colorless range, but over the years staff members have seen it applied to dia-

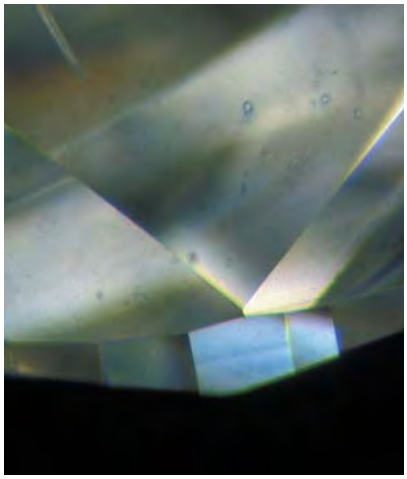

Figure 4. Seen here on the bezel and upper girdle facets of this 3.03 ct round brilliant diamond, multiple blue spots are indicative of a coating. Magnified 33×.

monds with color grades through light yellow. Another clue to this type of treatment is often a "grayish" overall body color evident when these stones are observed table-down in a standard color grading environment.

Upon detection of the treatment, these two diamonds were returned to the clients to remove the coating before grading could continue. Since they were not resubmitted as of this writing, we do not know their true colors.

Joshua Sheby

EMERALD

Natural, with Abundant Nail-head Spicules

Separation of natural and synthetic gems frequently requires a variety of techniques, although observation of internal features is often sufficient to make a conclusive identification. For example, curved striae or curved color banding and large gas bubbles quickly reveal flame-fusion synthetic corundum. In some instances, however, synthetics may have inclusions that resemble those found in natural stones.

The West Coast laboratory recently received for identification a 9.69 × 9.47 × 6.30 mm green ring-set gem. The refractive index, specific gravity, fluorescence, and spectra matched those of natural or synthetic emerald. When examined with magnification, however, the sample revealed a large number of what appeared to be nail-head spicules in several parallel planes (figure 5). Nail-head spicules are commonly associated with hydrothermally grown synthetic emeralds, but they can also occur in natural stones (see Spring 1992 Lab Notes, pp. 54–55). They are formed when a small piece of material is deposited on the surface of the growing crystal, and a tapered void is created as the crystal continues to grow past the inclusion. In synthetic emeralds, the solid material is usually phenakite, beryl, chrysoberyl, or gold (the last is derived from the vessel in which the emerald is grown). In this emerald, the crystals at the base of the tapered void were flat platelets that were not easily resolved, and the voids were liquid two-phase inclusions with a gas bubble.

Because the appearance of the nail-head spicules in this particular specimen was inconclusive, we asked senior research associate Sam Muhlmeister to perform energy-dispersive X-ray fluorescence (EDXRF) analysis to test for the presence of nickel. In Russian hydrothermally grown synthetic emeralds, NiO is found in greater concentrations than is known in natural emeralds. Our test results showed the presence of a trace amount of nickel that was more consistent with that found in natural emeralds (H. W. Schrader, "Contributions to the study of the distinction of natural and synthetic emeralds," *Journal of Gemmology*, Vol. 18, pp. 530–543). Infrared spectroscopy also did not show any of the peaks that are considered diagnostic of synthetic emerald. Nevertheless, these tests, too, were inconclusive. Ultimately, the determination of natural vs. synthetic was made based on the refractive indices and the presence of skeletal platelets of ilmenite (figure 6).

Hydrothermally grown synthetic emeralds usually have R.I. values very similar to those of natural emeralds, particularly those from Colombia, although they generally do not exceed an upper limit of 1.585. The R.I.'s of this stone were 1.584–1.590, which is consistent with an emerald of natural origin.

Ilmenite is found more commonly in aquamarine as opaque black to dark brown dendritic or skeletal platelets, but it has not been observed in synthetic emeralds. The ilmenite in this emerald was visually identi-

Figure 5. Nail-head spicules, a common feature in hydrothermal synthetic emeralds, are also seen in natural emeralds, as shown here. Magnified 22×.

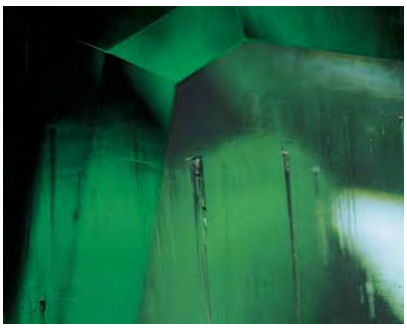

Figure 6. The presence of these skeletal platelets of ilmenite helped prove the emerald's natural origin. The white appearance of some of the inclusions is due to light reflecting off them. Magnified 40×.

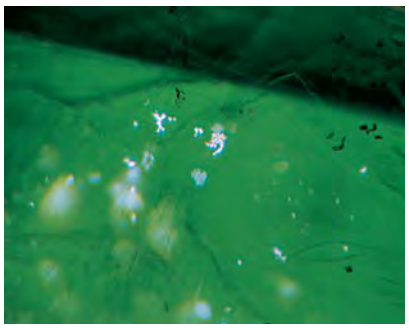

fied by chief research gemologist John Koivula through its distinctive skeletal or snowflake-like structure. These two pieces of evidence were enough to conclude that this emerald was indeed a natural stone.

Kimberly Rockwell

With Strong Dichroism

An unusually colored transparent bluish green pear-shaped gem (figure 7) recently arrived at the West Coast laboratory for identification from the private collection of Dale Dubin. The stone was reportedly a beryl that had been mined from Paraíso do Norte, Goiás State, Brazil. The client inquired as to whether the stone was indeed a beryl and, if so, whether the strong blue color component would prevent it from being classified as an emerald.

The 1.12 ct stone (8.52 × 6.44 × 4.04 mm) was moderately to heavily included, with numerous internal characteristics typical of emerald. Fourier-transform infrared (FTIR) and Raman spectroscopy both revealed spectra that were consistent with those of emeralds we have on file. There was no luminescence to long- or short-wave UV radiation, and the stone displayed a uniaxial optic figure in the polariscope.

Additional examination and testing revealed several unusual characteristics. The R.I.'s (~ 1.595–1.601) and S.G. (~ 2.76, by the hydrostatic method) were both high compared to other Brazilian emeralds we have seen. These high properties are more typical of emeralds from African countries such as Zambia (R. Webster, *Gems*, 5th ed., Butterworth-Heinemann, London, 1994, pp. 117–118).

Figure 7. This 1.12 ct bluish green emerald, reportedly from Brazil, displayed several unusual gem properties.

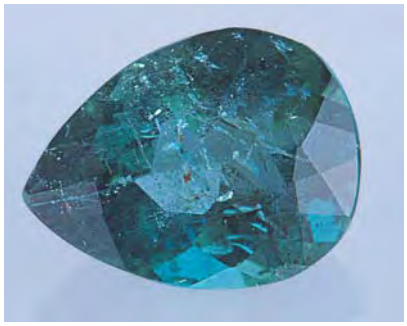

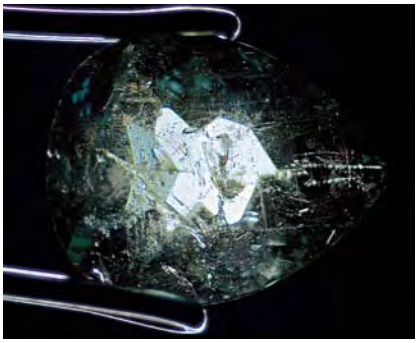

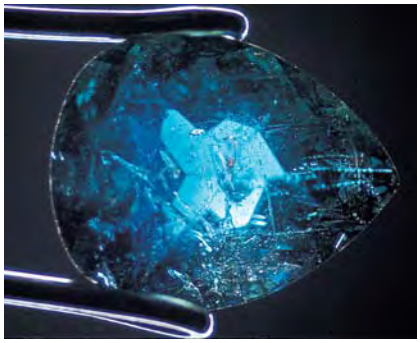

Figure 8. The dichroism of the emerald in figure 7 was unusually strong and distinct, with a very saturated blue component.

However, the most unusual quality of this stone was its strong and distinct dichroism, of medium yellowish green and vivid blue (figure 8). The absorption spectrum as seen with a desk-model spectroscope revealed chrome lines typical of emerald and a 427 nm line typical of aquamarine, indicating the presence of iron as a coloring agent in addition to chromium. This seemed to explain the presence of both the green and blue components of the color.

In an attempt to confirm the elemental coloring agents, Sam Muhlmeister performed EDXRF analysis as well as UV-Vis spectroscopy. Trace elements revealed by EDXRF were V, Cr, Fe, and Rb. UV-Vis analysis corroborated the presence of Cr and significant amounts of Fe. This, along with the 427 nm line visible in the desk-model spectroscope, led us to conclude that iron was responsible, at least in part, for the strong blue component of the color.

Several properties confirmed that the material was indeed beryl, and the predominantly green color of the stone was sufficient to classify it as an emerald. The owner stated that he had seen a few other similar stones from his supplier, but none as blue as this one. Indeed, this emerald displayed perhaps the most intensely saturated blue dichroic color component we at the laboratory had ever seen in a Brazilian emerald.

CYW

High-R.I. GLASS Imitation of Tanzanite

Glass has long been used to imitate a wide variety of gem materials. In recent years, we have seen an increased amount of blue to violet glass being used to simulate the very popular gem tanzanite (see, e.g., L. Kiefert and S. T. Schmidt, "Some tanzanite imitations," Winter 1996 *Gems & Gemology*, pp. 270–276). As shown in figure 9, the West Coast

Figure 9. The high R.I. of this 5.42 ct violetish blue specimen of manufactured glass, very close to that of tanzanite, could lead to a misidentification.

laboratory recently received a 5.42 ct transparent violetish blue oval modified brilliant for identification. The specimen, submitted to us by Martinek's Jewelers of Traverse City, Michigan, was brought to them by one of their customers, who had purchased it in Mexico as tanzanite. Upon recording the gemological properties, we could see how a quick examination could lead to a misidentification.

The most interesting characteristic of this material was its high refractive index, which was very close to that of tanzanite. We recorded a single R.I. of 1.700, which is the high value for tanzanite (1.690–1.700). The glass imitations of tanzanite we have examined in the past have seldom had refractive index readings that exceeded 1.66. The fact that the specimen was singly refractive (with weak anomalous double refraction) was the main distinguishing property separating it from tanzanite, and this also meant that it lacked tanzanite's characteristic pleochroism. Additional features of the stone included a specific gravity of 4.11; weak blue fluorescence to long-wave UV radiation, and weak-to-moderate chalky yellow and blue fluorescence to short-wave UV; and weak bands seen at approximately 500 and 600 nm with a desk-model spectroscope. The stone was fairly free of inclusions, and magnification revealed only a few pinpoints.

Both FTIR and Raman spectroscopy provided spectra similar to those previously recorded for manufactured glass, which confirmed the identification. EDXRF analysis by Sam Muhlmeister showed silicon as a major constituent with numerous trace elements, including calcium, zinc, strontium, barium, zirconium, antimony, and lanthanum.

The important point with an imitation such as this is one that we continue to mention on a regular basis: Always use all the available information in making an identification. A quick R.I. reading coupled with the violetish blue color could easily lead to the wrong conclusion. However, if tanzanite is suspected, the characteristically strong pleochroism should be readily detectable if the material is genuine.

Elizabeth Quinn

Figure 10. This antique brooch showcases a very rare clam "pearl" that measured approximately 20 mm in diameter.

Large Clam "PEARL"

An antique brooch received in the East Coast laboratory generated great interest among our staff members. It showcased a single large clam "pearl" that was bezel set in a yellow and white metal mounting and surrounded by a single row of brilliant old mine and old European cut diamonds (figure 10). The almost round button-shaped mottled purple-and-white clam "pearl" measured approximately 20 mm in diamester and showed a prominent alveolar (honeycomb) growth pattern readily visible with the naked eye. This distinct growth structure is predominantly found in such concretions as clam pearls. On closer scrutiny, we noticed another feature commonly found in other non-nacreous pearls: Each individual honeycomb cell also displayed a microstructure similar in appearance to the flame-like structure that characterizes so many concretions from various mollusks. Even though this microstructure was only moderately developed, it still produced a sheen-like effect in those areas where the surface was still smooth and had not been slightly worn off over time. Such a remarkable non-nacreous "pearl"—with an alveolar structure and a flame-like microstructure—is indeed rare. G. F. Kunz and C. H. Stevenson report in *The Book of the Pearl* (Dover Publications, New York, 1908) that the common hard clam *Venus mercenaria* from the Atlantic Coast of the U.S. can, on rare occasions, produce such large "pearls."

KNH

Figure 11. These five sapphires, 3.07–9.22 ct, all have the unusual color zoning associated with what may represent a "new" treatment.

Blue SAPPHIRES with Unusual Color Zoning

A possible new treatment for blue sapphires has begun raising questions throughout the industry. The appearance of this treatment has already been reported on the Internet and in a few trade publications (see, e.g., K. Scarratt, "A review of preliminary data on heated blue sapphires with an unusual color distribution—A work in progress," http://www.agta.org/consumer/news/20031112gemstone-update.htm, Nov. 12, 2003; D. Federman, "Blue devils," *Modern Jeweler*, November 2003, p. 9).

The concern with these stones, which typically are an attractive blue (figure 11), focuses on the presence of unnatural color zoning, which consists of a dark blue central zone with curved irregular edges that is surrounded by a light blue to near-colorless zone (figure 12). The pale outer zone varies dramatically in depth and does not conform to the outside surface of the faceted stone. Rather, it appears to conform to the surface of the original rough. This feature has been seen primarily in sapphires of Sri Lankan and Madagascar origin that show evidence of exposure to high temperatures.

The GIA laboratory has examined dozens of these treated sapphires since they were first noticed on the market in the beginning of this year. When this zoning was first observed, it had so many characteristics similar to those seen in some Be-diffused blue sapphires that we expected it to be, in fact, the result of Be diffusion. We have seen several known Be-diffused stones with surface-conformal colorless rims surrounding blue cores, at times with blue color bands ending abruptly in a scalloped pattern (figure 13). Although the pale (near-colorless to light blue) rims around the new sapphires tended to be significantly deeper and usually did not conform to the faceted shape of the stone, the similarities were nonetheless striking.

To date, however, no significant amounts of beryllium have been found in these suspicious stones. Closer inspection of the zoning revealed other interesting distinctions from known Be-diffused corundums.

When viewed in certain directions, many of these sapphires showed a scalloped appearance at the interface between the darker center and the lighter rim (figure 14). This

Figure 12. Sapphires subjected to this treatment typically have a dark blue central zone that is separated from a paler outer zone by curved edges, as can be seen in this 6.55 ct stone at 10× magnification with immersion.

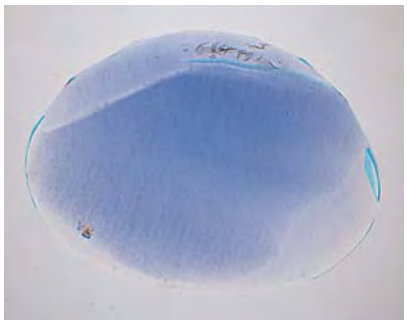

Figure 13. Be-diffused blue sapphires also typically have blue cores, but the pale rims are surface conformal, and the blue color bands in the core end abruptly at the outer rim. Immersion, magnified 40×.

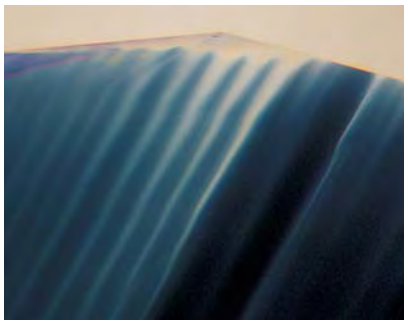

Figure 14. Note the scalloped edge characteristically seen at the interface of the darker core and paler rim in these "new" treated sapphires. Immersion, magnified 10×.

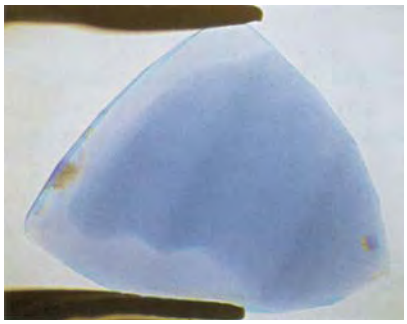

Figure 15. In many of these treated sapphires, when observed from certain orientations, the interface between the light and dark areas was marked by a colorless line all along the dark core. Immersion, magnified 12×.

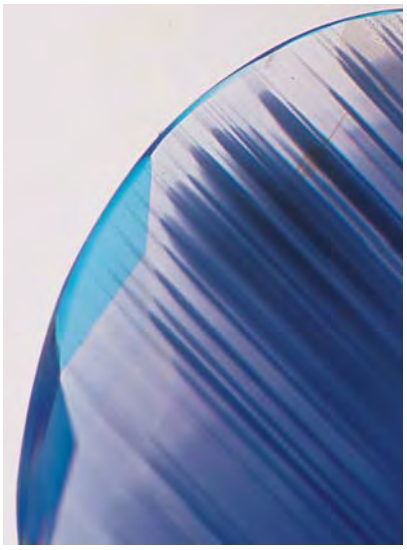

Figure 16. Often the color bands in the possibly new treated sapphires do not end at the light blue or near-colorless rim, but rather get abruptly lighter and appear curved. Immersion, magnified 10×.

scalloped edge seemed to be directly related to the tone of the color banding: The pale rim extended deeper into the lighter blue bands of the core than into the darker bands. This seemed to suggest that, as with Be diffusion, the depth of penetration of this treatment is dependent on the inherent chemistry of the stone.

The color banding of these stones often did not simply disappear at the light/dark interface. Rather, this interface usually manifested itself as a very narrow, colorless line extending all the way around the darker blue core (figure 15). In many examples, the color banding abruptly became much lighter on the other side of this line, and appeared distinctly curved (figure 16), but continued on, making the outer area light blue rather than colorless.

As stated earlier, the depth of this outer portion varied considerably from stone to stone. It sometimes encompassed the majority of the sapphire, leaving an area of darker color that represented only 25–30% of the whole (figure 17).

The exact nature of this treatment, as well as its specific effect on the stones treated, is still not understood. One theory that has received considerable attention involves the partial dissolution of the original sapphire during this "new" heating process and subsequent regrowth (i.e., of synthetic sapphire) over the remaining, original stone. To investigate this new treatment further, in mid-December GIA researchers Christopher P. Smith and Matthew Hall traveled to Sri Lanka, where they attended experiments by Tennakoon Punsiri of Punsiri Gems, the man who developed this process. The heat treatment procedure (which is proprietary to Mr. Punsiri) had a dramatic effect on the color of most of the samples they had treated during their visit (figure 18), and initial observation suggested that the unusual color concentrations indicated above were produced in more than two-thirds of them.

On the basis of detailed microscopic examination of the samples after treatment, Smith and Hall concluded unequivocally that no synthetic sapphire growth had taken place. Furthermore, they did not witness the use of any fluxing agents during the heating experiments, and no evidence of flux was present on or around the samples brought back to the U.S. for additional analyses. To further our understanding of this

Figure 17. In some samples, such as this 4.80 ct sapphire, the light area encompassed most of the stone. This sapphire, the center one in the back row of figure 11, was also lighter than those we examined that had a smaller light area. Immersion, magnified 10×.

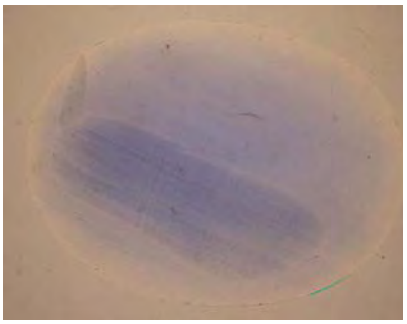

Figure 18. This 9.74 ct sample (approximately 16.1 × 10.3 × 6.3 mm) was sawn in two prior to the heat treatment experiment, and the half on the left was retained as a control. Note the dramatic change in color in the half on the right following treatment.

Figure 19. This sequence of photomicrographs shows two resin-filled cavities on the pavilion of a Sri Lankan spinel under different lighting conditions. In the left and center images—taken with darkfield and surface-reflected fiber-optic illumination, respectively—excess filler on the surface and its relationship to the filled cavities is evident. The image on the far right clearly shows the largest apatite-shaped cavity as well as the gas bubbles in the fillers in both pits. Magnified 10×.

treatment, a cooperative effort between GIA researchers, colleagues from other laboratories, and outside experts has brought full resources to bear on this problem. We will continue to report significant developments as they occur.

SFM

SPINEL with Filled Cavities

While the filling of cavities and surface-reaching fissures in emerald, ruby, and sapphire with resin or glass is relatively common and always suspected by gemologists, this type of treatment is virtually unknown in spinel. During a buying trip to Sri Lanka, gemologist Mark Smith of Thai Lanka Trading Ltd., Bangkok, encountered an oval mixed-cut spinel that appeared to have been treated in this manner. A cursory field examination with a 10× hand loupe revealed the presence of several rounded crystal inclusions, as well as two pits on the pavilion that obviously had been filled.

Routine gemological testing of this transparent 4.79 ct stone at the West Coast laboratory confirmed the identification as spinel. Examination with a gemological microscope and a fiber-optic illuminator also confirmed the presence of several slightly rounded (corroded) near-colorless transparent-to-translucent mineral inclusions, which had the general morphology of those that have previously been identified as apatite in Sri Lankan spinel. In addition, the two cavities clearly visible on the pavilion apparently had been filled after polishing, since no attempt had been made to clean the excess filler from the surface (see figure 19, left and center). Both pits contained gas bubbles in the filler, and the largest of the two (as shown in figure 19, right) had the general shape of an apatite crystal, so we suspect that the pits were created when some of the mineral inclusions were plucked out during faceting.

Since spinel is a very durable gem material with a high melting temperature, some form of glass filling was suspected, as this type of treatment is frequently encountered for pits and surface-reaching cracks in rubies and sapphires. Micro-hardness and indentation testing, however, revealed that the filler was much softer than glass. When a small spot of the filler was tested with a thermal reaction tester (hot point), the immediate reaction and odor produced were similar to what would be expected for some type of clear-drying organic resin.

In this instance, the identification of these resin-filled cavities was made relatively easy by the presence of the gas bubbles and the complete lack of repolishing to remove the excess filler. Such obvious surface evidence is rarely encountered even in stones that are routinely filled, such as rubies and sapphires, since they are commonly repolished after treatment. This is the first spinel we have seen treated in such a manner.

JIK and Maha Tannous

PHOTO CREDITS
Maha Tannous—1, 7, 9, and 11; John I. Koivula—2, 3, 8, and 19; Vincent Cracco—4; Shane F. McClure—5, 6, and 12–17; Elizabeth Schrader—10; Matthew Hall—18.

DIAMONDS

A comparison of three historic blue diamonds. This summer's "Splendor of Diamonds" exhibition at the Smithsonian Institution in Washington, D.C., presented a unique opportunity for the public to view seven of the world's rarest diamonds (see, e.g., J. M. King and J. E. Shigley, "An important exhibition of seven rare gem diamonds," Summer 2003 *Gems & Gemology*, pp. 136–143). The closing of the exhibition brought another opportunity—for the contributors of this entry to compare the properties of three of the largest documented strongly colored blue diamonds. Two of these diamonds, the 45.52 ct Hope and the 30.62 ct Blue Heart, are part of the Smithsonian's permanent collection; the third, the 27.64 ct Heart of Eternity, was part of the special exhibit (figure 1). Arrangements were made to remove the Hope and the Blue Heart from their mountings and to allow the contributors one evening to examine and test them in conjunction with the Heart of Eternity prior to its being returned to its owner.

GIA has graded all three diamonds since the 1995 introduction of enhancements to its colored diamond color grading system (see J. M. King et al., "Color grading of colored diamonds in the GIA Gem Trade Laboratory," Winter 1994 *Gems & Gemology*, pp. 220–242). The Hope diamond was described as Fancy Deep grayish blue in an updated grading performed in 1996; the Blue Heart was graded Fancy Deep blue in 1997, and the Heart of Eternity was graded Fancy Vivid blue in 1999. Given the different color descriptions for each of these diamonds, this was a special chance to see how the color appearances related to the terms defined by the grading system.

In GIA's system, fancy-grade terminology is used to describe a range of the combined effect of tone (the lightness to darkness of a color) and saturation (the strength or purity of a color). For blue diamonds, for example, *Fancy Deep* describes those of medium to dark tone and moderate to strong saturation. *Fancy Vivid* describes those that are medium to dark in tone and strong to very strong in saturation. These fancy-grade ranges are further divided by color terms such as blue, blue-gray, or bluish gray to refine the location of the color appearance. "Cooler" colors, such as blue, appear more grayish or gray as they become darker in tone and/or weaker in saturation, and modifiers of *grayish* or *gray* are used in the color description to reflect this aspect. When the color space for blue diamonds was discussed by J. M. King et al. ("Characterizing natural-color type IIb blue diamonds," Winter 1998 *Gems & Gemology*, pp. 246–268), the authors noted that the range of saturation in which blue diamonds occur is relatively compressed. This means the appearance differences between color terms can be more subtle than similar terms for other colors.

From the report descriptions, one would expect these three diamonds to have similar tone (with small variations) and subtle differences in saturation. The Hope, which has been described as "steely" in appearance, is less saturated than the other two. The Heart of Eternity has the strongest color, with the Blue Heart falling between them. The Heart of Eternity's color is strong

Editor's note: Interested contributors should send information and illustrations to Brendan Laurs at blaurs@gia.edu (e-mail), 760-603-4595 (fax), or GIA, 5345 Armada Drive, Carlsbad, CA 92008. Original photos will be returned after consideration or publication.

GEMS & GEMOLOGY, Vol. 39, No. 4, pp. 322–346

Figure 1. Shown here from left to right, the 30.62 ct Blue Heart, the 45.52 ct Hope, and the 27.64 ct Heart of Eternity are three of the largest strongly colored blue diamonds that have been documented gemologically. To encounter one such diamond is extremely rare, and to have an opportunity to observe all three together was a unique experience. Photo by Shane McClure.

enough for it to merit a different grade range (i.e., Fancy Vivid). Figure 2 shows the relationship of these three diamonds on a section of a tone/saturation grid.

This occasion also presented a chance to view the unique phosphorescence associated with some natural-color type IIb blue diamonds. Type IIb blue diamonds that phosphoresce do so almost solely in response to short-wave UV radiation and do not react to long-wave. King et al. (1998) noted that three-quarters of the blue diamonds that phosphoresced showed a very weak to weak reaction. The most common color was a chalky blue to green, with rare red or orangy red reactions. The Hope diamond's strong red phosphorescence to short-wave UV radiation has been described a number of times (and is illustrated in R. Crowningshield, "Grading the Hope diamond," *Gems & Gemology*, Summer 1989, p. 93), so it was interesting to note a similar reaction in the Heart of Eternity. When the UV source was turned off, both diamonds showed a similar intensity of phosphorescence; however, while the Hope's could be observed for more than a minute, the Heart of Eternity's faded rather quickly. In addition, the Hope's reaction was a slightly warmer red than that of the Heart of Eternity. The Blue Heart exhibited a more typical, very subtle white to

Figure 2. The three blue diamonds described here are placed on a portion of a tone/saturation grid to illustrate their relationship in color space. All are relatively similar in tone (lightness to darkness) but differ in saturation (the strength or purity of the color). The Hope is the least saturated, the Heart of Eternity is the most saturated, and the Blue Heart is between them in saturation and slightly lighter in tone.

Figure 3. While the cutting of each diamond is approached individually, a general difference in cutting philosophy is seen here in the profile view of the two heart-shaped diamonds. The Blue Heart (left) was cut in the early part of the 20th century and the Heart of Eternity (right) was cut in the 1990s. The two faceting approaches result in different face-up appearances. Photo by Shane McClure.

chalky blue reaction that also faded quickly. There is no known explanation for why two of these diamonds show such a dramatic reaction and the third does not.

The differences in cutting philosophy between the two heart-shaped diamonds also were intriguing (figure 3). Smithsonian records indicate that the Blue Heart was cut in the early part of the 20th century; we know that the Heart of Eternity was cut in the 1990s. Bearing in mind that each piece of rough is approached individually to achieve the best weight retention, color, clarity, and cut, there are still distinct differences in style between the two. The culet on the Blue Heart is near the center of the diamond, and is surrounded by radiating facets similar to how sapphires are cut. The edges between facets are sharp and well-defined, which often results in more brilliance in the face-up position (see again figure 1). The Heart of Eternity has a French culet (four pavilion mains) and a number of relatively large flat facets on the pavilion near the girdle. The angle between adjacent facets is rather shallow in a number of areas on the pavilion, making these facets appear less distinct. These cutting aspects help deepen and intensify the face-up color appearance of the Heart of Eternity.

These contributors also performed infrared spectroscopy on all three diamonds. The Hope has a large culet facet, and the infrared beam entered through the table and passed out the culet, for a path length of 12 mm through the diamond (assuming no internal reflections). The Blue Heart has a small culet that is subparallel to the table (11.9 mm in this dimension); thus, the infrared beam was aimed directly through these two facets. The Heart of Eternity does not have a culet facet, so the spectrum was taken across the width of the heart, with a beam path length of approximately 20 mm (again, assuming no internal reflections).

Mid-infrared spectra (8000–400 cm^{-1}) were obtained with a Bio-Rad Excalibur Fourier-transform infrared spectrometer using a KBr beam splitter and DTGS detector at 4 cm^{-1} resolution. The infrared spectrum of the Hope diamond is shown in figure 4. The absorption characteristics of the Blue Heart and the Heart of Eternity were essentially identical to that of the Hope diamond, but due to lower transmission of light through these samples the spectra were of lower quality.

There are two principal causes for the absorption features in this energy range: lattice vibrations of the diamond and electronic transitions due to substitution

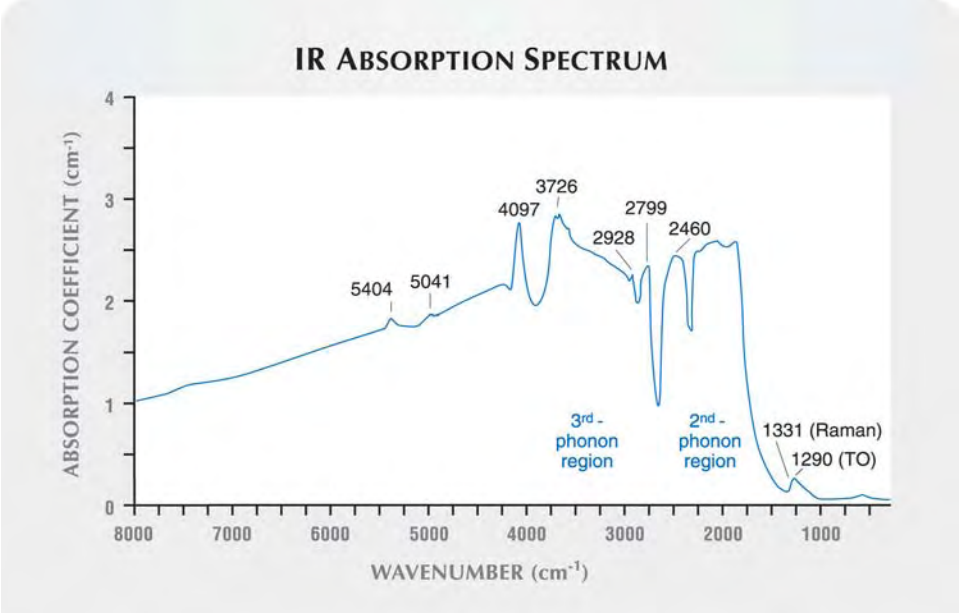

Figure 4. The infrared spectrum of the Hope diamond shows features that are consistent with boron-induced blue color and type IIb diamonds in general (see text). Note that portions of some bands in the 3800–1600 cm^{-1} region were actually off the scale of the spectrometer.

of boron into the diamond structure. The lattice vibrations appear from 4000 to 1200 cm^{-1}, and consist of the transverse optic (TO) mode, the Raman-active mode, and bands in the second- and third-phonon regions (King et al., 1998). The broad absorbance that results from substitution of small amounts of boron for carbon in the diamond structure starts roughly at 3000 cm^{-1} and extends into the near-infrared and red region in the visible spectrum; it is the cause of the blue color (see S.D. Smith and W. Taylor, "Optical phonon effects in the infra-red spectrum of acceptor centres in semiconducting diamond," *Proceedings of the Physical Society, London*, Vol. 79, 1962, pp. 1142–1153; I. G. Austin and R. Wolfe, "Electrical and optical properties of a semiconducting diamond," *Proceedings of the Physical Society*, Vol. 69B, No. 3, 2003, pp. 329–338). As reported by Smith and Taylor (1962), the other absorption features seen in figure 4 are due to boron-related electronic transitions (2928, 2799, and 2460 cm^{-1}) and the combination modes of the boron transitions and lattice vibrations (5404, 5041, 4097, and 3726 cm^{-1}). The spectra of all three blue diamonds lacked any detectable nitrogen bands in the 1400–1000 cm^{-1} region, consistent with the definition of type II diamonds.

To our knowledge, this is the first mid-infrared spectrum obtained on the Hope diamond; it shows features consistent with the presence of boron as the cause of the blue coloration and its categorization as a type IIb diamond.

John M. King (jking@gia.edu)
GIA Gem Laboratory, New York

Elizabeth A. Johnson and Jeffrey E. Post
Smithsonian Institution, Washington, D.C.

A natural yellow diamond with nickel-related optical centers. A Fancy Light yellow 2.95 ct round brilliant diamond was recently submitted to the SSEF Swiss Gemmological Institute for color authenticity determination (figure 5). In the course of standard testing, we noticed the presence in its UV-visible spectrum of clear nickel-related optical centers, which are usually encountered in flux-grown synthetic diamond. Further spectroscopic analysis, as described below, in combination with the growth patterns, proved that this Ni-containing diamond was natural and not a synthetic. Although the presence of nickel in natural diamonds has been previously documented (C. J. Noble et al., "Electron paramagnetic resonance investigations of nickel defects in natural diamonds," *Journal of Physics: Condensed Matter*, Vol. 10, 1998, pp. 11781–11793), we are not aware of any previous mention of this in the gemological literature.

Microscopic observation of this diamond revealed several small black-to-brown inclusions of unknown origin. Numerous swirl-like patterns were visible with darkfield illumination, and were more distinct when crossed polarizers were used. With long-wave UV radiation, the stone showed a strong "lemon" yellow reaction, which was mostly even except for a few weaker zones close to the culet. The short-wave UV reaction was similar in color though weaker in intensity. No magnetic test was performed.

The infrared spectrum showed a strong platelet-related peak (higher than the two-phonon zone) and a large and saturated absorption band between 1300 and 1050 cm^{-1}. These features are typical for type Ia diamonds that contain significant concentrations of nitrogen. Several characteristic peaks in both the one- and three-phonon zones indicated that the diamond also contained a moderate concentration of hydrogen. This is consistent with its yellow UV fluorescence. If we consider both the presence of a well-defined 1010 cm^{-1} peak and the absence of the 484 cm^{-1} peak, it is reasonable to assume that the majority of nitrogen was present as B aggregates.

The UV-Vis absorption spectrum, recorded at approximately –120°C, showed a strong N3 center, with an absorption coefficient of 2.0 cm^{-1} at 415.2 nm. A series of weak peaks (343.6, 347.3, 360.3, 363.5, and 366.9 nm) were recorded that so far have been described only in synthetic diamonds (J. E. Field, *The Properties of Natural and Synthetic Diamond*, Academic Press, London, 1992). Also present was another series of weak peaks (467.9, 473.0, 477.5, and 546.7 nm) that have been previously attributed to nickel- and nitrogen-related absorptions in annealed type Ib synthetic diamonds (J. E. Shigley et al., "The gemological properties of Russian gem-quality synthetic yellow diamonds," Winter 1993 *Gems & Gemology*, pp. 228–248). In addition, a weak peak was recorded at 793.3

Figure 5. This 2.95 ct Fancy Light yellow natural diamond was found to contain Ni-related absorption features in the UV-visible region that have previously been associated only with synthetic diamonds. Photo by M. Krzemnicki, © SSEF.

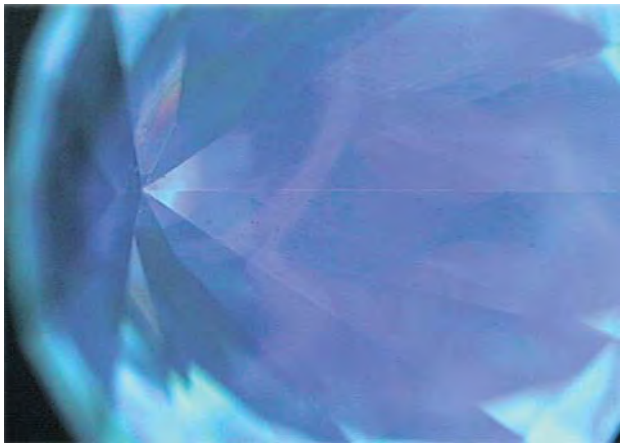

Figure 6. This De Beers DiamondView image of the Fancy Light yellow diamond with Ni-N–related optical centers shows irregular patterns of blue fluorescence, indicative of natural origin. Photo by J.-P. Chalain, © SSEF.

nm (with an absorption coefficient of 0.1 cm^{-1}), which is commonly observed in both natural and synthetic nickel-containing diamonds and is almost certainly due to a nickel-nitrogen complex (D. Fisher, pers. comm., 2003).

The Raman photoluminescence spectrum of this diamond, recorded at approximately –120°C with a 514.5 nm (green) laser, showed two peaks of moderate intensity at 640.5 and 693.9 nm, and a very strong peak at 700.5 nm. This last peak is usually seen in natural type Ia diamonds. None of the Raman photoluminescence peaks could be ascribed to Ni-related optical centers.

Notwithstanding the features seen in the UV-Vis spectrum, the natural origin of this diamond was supported by many properties, the first of which was the presence of irregular growth patterns. A DiamondView image (figure 6) revealed blue fluorescence with irregular patterns close to the culet and no phosphorescence (a synthetic diamond would have displayed regular cubo-octahedral growth patterns, as shown in C. M. Welbourn et al., "De Beers natural versus synthetic diamond verification instruments," Fall 1996 *Gems & Gemology*, pp. 156–169). The high concentration of nitrogen, especially in the form of B aggregates, the presence of a high platelet peak, and a strong N3 center are also valuable indications for natural diamond.

In conclusion, examination of this interesting diamond allowed us to observe, for the first time, Ni-related defects in a natural diamond by means of UV-visible absorption spectroscopy. The natural origin of the diamond's color was proven by the absence of any coating, as well as the lack of any spectroscopic features indicative of HPHT treatment or irradiation and annealing.

This contributor is grateful to Dr. D. Fisher for providing constructive comments.

J.-P. Chalain (gemlab@ssef.ch)
SSEF Swiss Gemmological Institute, Basel

COLORED STONES AND ORGANIC MATERIALS

Gem-quality afghanite. While on a gem-buying expedition in Peshawar, Pakistan, Dudley Blauwet, a gem dealer from Louisville, Colorado, obtained five cabochons and an excellent crystal specimen of afghanite. The stones were said to have come from Kiran, Kokcha Valley, Badakhshan Province, Afghanistan. Although in the past these contributors have seen a few afghanite crystals at various gem and mineral shows, we had never seen gems fashioned from this rare mineral, so for us this was a first opportunity to examine polished samples of afghanite. A member of the cancrinite group, the chemical formula of afghanite is $(Na,Ca,K)_8(Si,Al)_{12}O_{24}(SO_4,Cl,CO_3)\cdot H_2O$. It has a hardness of 5 11¼ 2–6 on the Mohs scale.

The crystal measured 23.0 ↔ 14.5 mm and was partially embedded in white calcite matrix (figure 7). Although we could not find it reported in the literature, an interesting feature of afghanite that should prove useful in its identification is its strong, bright orange fluorescence to long-wave UV radiation (see, e.g., figure 8), which we also observed in all five cabochons. All of the samples were inert to short-wave UV radiation, and no phosphorescence was observed in either case.

The five cabochons (ranging from 2.87 to 7.25 ct) yielded refractive index readings of 1.52, which, given that these are spot readings, is consistent with published R.I. values for afghanite (n_o = 1.522–1.528, n_e = 1.528–1.533; R. V. Gaines et al., *Dana's New Mineralogy*, John Wiley & Sons, New York, 1997, p. 1634). The hydrostatic specific gravity ranged from 2.52 to 2.56, with one cabochon giving a 2.60 value. The S.G. value reported in the literature is 2.55–2.65 (Gaines et al., 1997), and the slightly low reading of some of the samples is probably due to variable amounts of lazurite inclusions, which were present in all of our samples. In addition, inclusions of calcite and pyrite were identified with Raman analysis in some of the samples. In the previously published descriptions of afghanite, no mention was made of any inclusions.

To the unaided eye, the samples appeared translucent light blue; the mineral is described in the literature as "bluish" to colorless (Gaines et al., 1997). All the polished cabochons we examined contained numerous intense blue inclusions of lazurite that certainly added color to their host. As shown in figure 9, the lazurite inclusions also gave the polished cabochons a speckled appearance. With magnification, the irregularly shaped lazurite inclusions stood out in high relief due to their color (figure 10), while the (essentially colorless) calcite inclusions were much harder to see. It is not clear how much of the blue color in these afghanites is derived from the deep blue inclusions, and how much is actually intrinsic to the mineral.

John I. Koivula (jkoivula@gia.edu) and Maha Tannous
GIA Gem Laboratory, Carlsbad

Figure 7. This 23-mm-long crystal of afghanite on calcite is from Badakhshan Province, Afghanistan. GIA Collection no. 30110; photo by Maha Tannous.

Figure 8. On exposure to long-wave UV radiation, the afghanite crystal in figure 7 fluoresced a strong, bright orange. Photo by Maha Tannous.

Blue beryl discovery in Canada. In August 2003, an unusually dark blue beryl was discovered in Canada's Yukon Territory by Bill Wengzynowski (Archer Cathro & Associates, Vancouver, British Columbia; figure 11) and one of these contributors (LAG). Mr. Wengzynowski also is credited with the 1998 discovery of the Regal Ridge emerald deposit in the Yukon Territory, which is ~100 km east-southeast of the blue beryl occurrence. These efforts were financed by True North Gems Inc. of Vancouver. The new gem is noteworthy for its dark blue color and strong dichroism, and is being referred to as "True Blue" beryl.

One of the contributors (WRR) visited the True Blue property shortly after it was discovered. The beryl occurs in a swarm of closely spaced quartz-carbonate-tourmaline veins (figure 12) that cut a Mississippian-age (320 million years) fluorite-bearing syenite stock. The veins range from 0.5 to 20 cm thick, and locally comprise up to 30% of the rock overall. The vein zone measures 700 × 200 m in outcrop at the surface, and is exposed over an elevation range of 100 m. Within this area, more than 100 individual occurrences of the beryl have been found on the surface.

In September 2003, True North Gems Inc. hand collected 65 kg of samples from outcrop in the vein zone,

Figure 9. These three cabochons of afghanite (2.87, 3.00, and 3.26 ct) are speckled with inclusions of lazurite. Courtesy of Dudley Blauwet; photo by Maha Tannous.

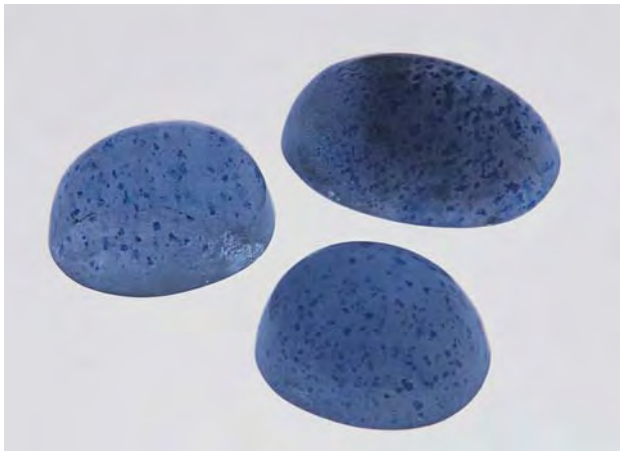

Figure 10. With magnification, the irregular shape of the lazurite inclusions is apparent. These inclusions are at least partially responsible for the light blue color of their afghanite host. Photomicrograph by John I. Koivula; magnified 15×.

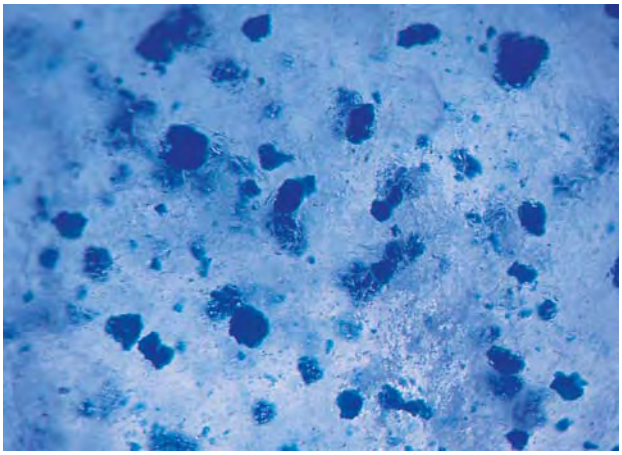

Figure 11. In August 2003, dark blue beryl was discovered in a remote area in the Yukon Territory of Canada. Here, that same month, Bill Wengzynowski uses a diamond saw to remove a beryl-bearing sample from a boulder at the deposit. Photo by Lee Groat.

which contained 57.9 grams of blue beryl. Individual crystals ranged up to 38 mm long and 11 mm in diameter. Five stones have been faceted thus far (figure 13): two elongated emerald cuts (0.82 and 0.79 ct) and three round brilliants (0.06–0.11 ct). Prior to cutting, the pieces of rough were stabilized with Epo-Tek 301 epoxy. The stones were resin-impregnated again after preforming, and then once more, if needed, after faceting. The hue is maintained at exceptionally small sizes for aquamarine (e.g., in the 1 mm round brilliants). The main constraints on the size of the stones faceted to date are the abundant fractures present in the material gathered from the surface, and the typically small diameter of the crystals.

Figure 13. Gemological properties were obtained on these samples of the dark blue beryl (0.06–0.82 ct). Courtesy of True North Gems Inc.; photo by Maha Tannous.

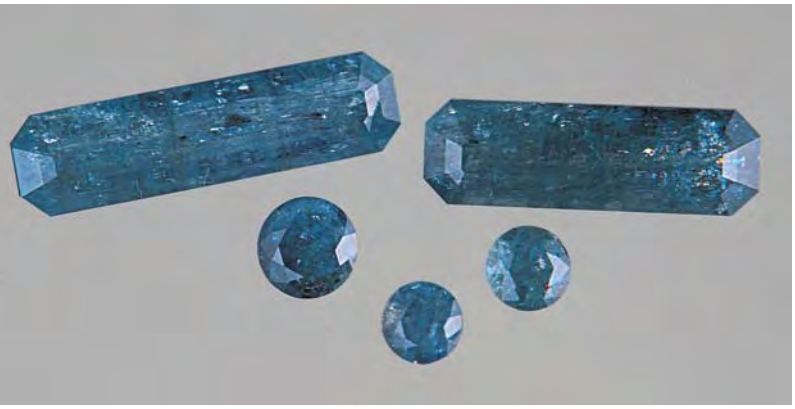

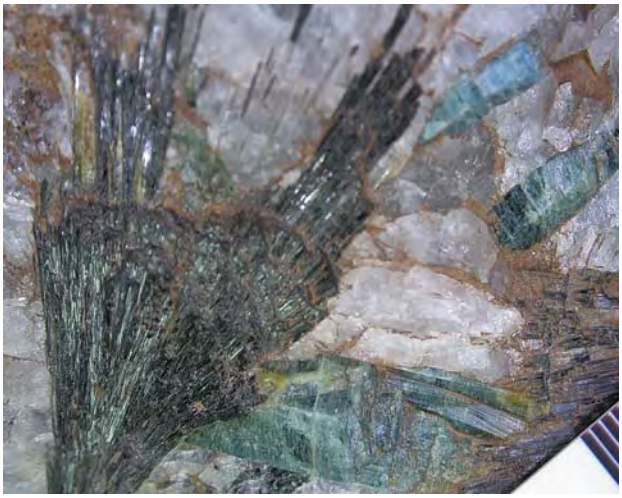

Figure 12. The dark blue beryl is hosted by veins containing quartz-carbonate-tourmaline assemblages. The bars on the ruler are millimeters; photo by David Turner.

The five faceted samples were examined by one of us (EPQ) at GIA, and the following properties were obtained: color—dark grayish greenish blue, with strong dichroic colors of deep blue to violetish blue and pale greenish blue to near colorless; diaphaneity—semitransparent to translucent; R.I.—n_o=1.597–1.601, n_e=1.589–1.594; birefringence—0.008–0.009; S.G. of the two larger stones (measured hydrostatically)—2.78 and 2.79; Chelsea color filter reaction—none; fluorescence—inert to long- and short-wave UV radiation; and only general absorption to approximately 430 nm was observed with the desk-model spectroscope.

Microscopic examination revealed that all five samples were fairly heavily included, which significantly affected their transparency. Internal features included fractures, "fingerprints," growth tubes, two-phase fluid-and-gas inclusions, transparent near-colorless quartz crystals (identified with Raman spectroscopy), and evidence of clarity enhancement; one stone had parallel planar clouds. One of the small stones had a surface-reaching inclusion that was surrounded by a thin layer of a dark brown submetallic material. With Raman analysis, the interior portion was identified as a carbonate (probably siderite) and the surrounding material was identified as pyrrhotite.

Seven fragments of the beryl, ranging from deep blue to medium blue, were chemically analyzed by electron microprobe by one of us (LAG) at the University of British Columbia. These samples showed relatively high iron contents, ranging from 1.54 to 5.81 wt.% FeO. The highest Fe content was found in the darkest blue sample, and surpasses the highest value for Fe in beryl that these con-

tributors are aware of: 4.69 wt.% Fe oxides for a "bluish" beryl from Arizona (W. T. Schaller et al., "An unusual beryl from Arizona," *American Mineralogist*, Vol. 47, 1962, pp. 672–699). The analyses also showed relatively high concentrations of Na and Mg, and traces of K, Ca, Sc, Ti, V, Cr, Mn, and Cs.

Polarized Vis-NIR absorption spectra (figure 14) of a deep blue, 0.68-mm-thick sample were recorded at the California Institute of Technology by GRR. The spectrum taken with light polarized parallel to the c-axis was dominated by a strong, wide band centered at about 850 nm. With light polarized perpendicular to the c-axis, this band was weak. The difference in absorption between these two orientations accounts for the strong dichroism shown by this beryl. The spectroscopic features indicate that iron is the chromophore responsible for the blue color.

There are two distinct varieties of blue beryl: aquamarine and Maxixe. In the material studied here, we observed that the lighter pleochroic color (pale greenish blue to near colorless) was carried on the ordinary ray (viewed with polarized light down the optic axis.) This is typical of aquamarine and not of the deep blue Maxixe beryl, where the colors are reversed and carried on opposite rays. Aquamarine sometimes has a spectrum that is visible (but not pronounced) with a desk-model spectroscope, comprising a line at 427 nm and occasionally a weak band at 456 nm, whereas Maxixe beryl typically has a series of six bands between 550 and 695 nm. None of the lines commonly seen in Maxixe beryl were found in the five faceted samples, but the general absorption to 430 nm may be due to the aquamarine 427 nm band (related to iron). The R.I.'s recorded for this material were a bit higher than those previously recorded for aquamarine (n_o = 1.572–1.590 and n_e = 1.567–1.583), whereas the S.G. values of the two samples tested fell within the reported range for aquamarine, 2.66–2.80 (R. Webster, *Gems*, Butterworth-Heinemann, Oxford, England, 1994, p. 124).

Figure 14. The Vis-NIR absorption spectra of the dark blue beryl are strongly polarized. When the beam was polarized parallel to the c-axis, the spectrum was dominated by a strong, wide band at about 850 nm. Relatively little absorption was recorded when the beam was polarized perpendicular to the c-axis.

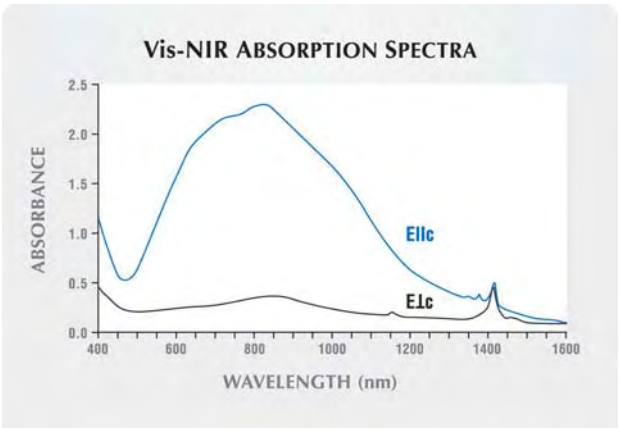

William R. Rohtert (william.rohtert@gte.net)
Hermosa Beach, California
Elizabeth P. Quinn
GIA Gem Laboratory, Carlsbad
Lee A. Groat
University of British Columbia
Vancouver, British Columbia, Canada
George R. Rossman
California Institute of Technology
Pasadena, California

Gem-quality corundum from Colombia: Localities and inclusions. Although Colombia is well-known for producing fine emeralds, for years the country has also been a modest producer of ruby and sapphire (see, e.g., P. C. Keller et al., "Sapphire from the Mercaderes–Río Mayo area, Cauca, Colombia," Spring 1985 *Gems & Gemology*, pp. 20–25, and the Fall 2000 Gem News section, p. 268). The gem corundum has been mined from alluvial deposits on both sides of the Río Mayo, which forms part of the border between the departments of Cauca and Nariño. This contributor recently completed a detailed study of rubies and sapphires from four mining areas in Colombia, which included 41 polished stones and nearly 2,800 pieces of rough obtained from several sources (see J. M. Duroc-Danner, "A study of Colombian corundum," Diplôme d'Université de Gemmologie, University of Nantes, France, 2002, 217 pp.). Among these samples, some of which are shown in figure 15, were rubies (eight polished and one minute piece of rough) and sapphires of various colors (including multicolored and change-of-color stones). Following is a brief summary of these

Figure 15. This 6.24 ct ruby cabochon, 2.58 ct oval multicolored sapphire (pale blue, gray, and pink), and 2.19 ct marquise sapphire from Colombia formed part of the study samples. Photo by J.-M. Duroc-Danner.

Figure 16. In southwestern Colombia, ruby and sapphire are mined from four principal regions within the Cauca, Nariño, and Caquetá Departments. Caquetá is located just east of the map area shown. After Keller et al. (1985).

Colombian localities and inclusions identified in the gem-quality corundum studied.

All of the corundum deposits reported to date are located in southwestern Colombia, in four principal regions of three departments—Cauca, Nariño, and Caquetá (figure 16):

1. Cauca—Near the village of Mercaderes (at Quebrada Senegetas, La Maria ranch, Río Sangandinga), close to the village of Sombrerillo and hamlet of Sombrerillos (at Quebrada del Rubí and Quebrada Limoncito), and in the region of Arboledas village (at Quebrada Las Cañadas, Quebrada Paloverde, Quebrada Honda, Quebrada Monserrate, Quebrada Monteoscuro, and Alto La Cañada).
2. Along the border of the Cauca and Nariño Departments—Together with garnet and amethyst in the Río Mayo.
3. Nariño—At San Pablo (about 20 km northwest of the Doña Juana volcano) and near Pasto (8 km east of the Galeras volcano).
4. Caquetá—From sands of the Río Platoyaco, a tributary of the Río Caquetá.

Although production figures are not available, most of the corundum appears to have come from Quebrada del Rubí, Quebrada Paloverde, Quebrada Honda, Quebrada Monserrate, and Quebrada Monteoscuro. Due to the political instability and guerrilla activities in the region, there are no organized mining activities. Rather, the material is collected by local people using artisanal methods.

In both the rough and faceted corundum samples, various inclusions were observed with the microscope and identified using Raman spectroscopy. Zircon was common; it typically occurred as doubly terminated colorless crystals (figure 17), with or without tension fractures. Occasionally seen were dark, opaque zircon inclusions with associated tension cracks. Rutile formed black or dark brown to red doubly terminated crystals that sometimes showed twinning. Some stones contained small, densely woven nests composed of very short needles that were probably also rutile; these appeared similar to those found in corundum from Myanmar. Boehmite also was common, typically occurring as white needles lying at the junction of intersecting twin planes; polysynthetic twinning was present in nearly all of the rough corundum examined. Boehmite also

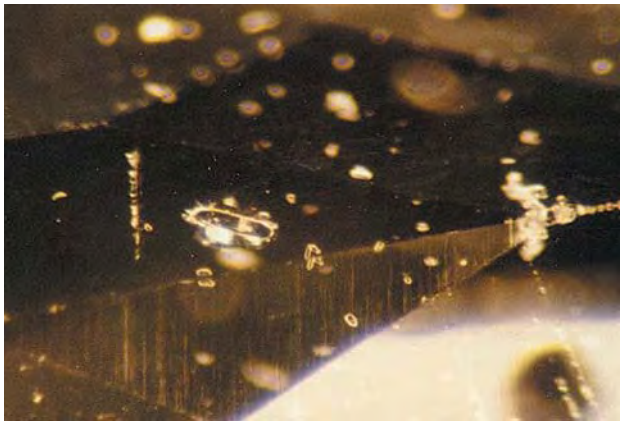

Figure 17. Zircon inclusions were common in the Colombian corundum, and often formed doubly terminated, colorless crystals. Photomicrograph by J.-M. Duroc-Danner; magnified 40×.

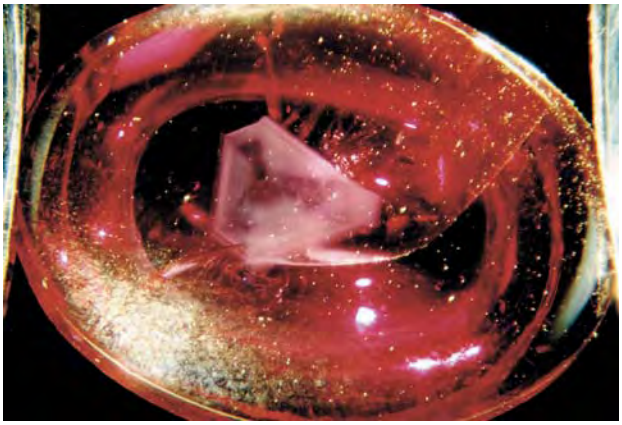

Figure 18. Pseudohexagonal growth zoning is clearly visible in this 6.24 ct Colombian ruby. Photomicrograph by J.-M. Duroc-Danner; magnified 12×.

was seen as coarse needles intersecting in three directions, similar to those found in Thai rubies, and as fine white needles in a scaffold-like arrangement, as observed in some East African corundum. Pinpoint inclusions (zircon, rutile, and apatite, among others) were present in many of the stones. Larger apatite inclusions were seen in some samples, and plagioclase feldspar occurred in abundance in one specimen.

In addition to mineral inclusions, partially healed fractures and internal stress fractures were occasionally observed, as were a few "fingerprints," some of which were similar to those encountered in Sri Lankan sapphires. Pseudohexagonal growth zoning was visible as distinct cloud-like zones in a few samples (figure 18). Many of the stones were color zoned, particularly with pronounced areas of yellow color.

Consistent with the gemological properties, the chemical composition and spectroscopy (UV-Vis and FTIR) of the samples demonstrated that most of the corundum was of basaltic origin. However, a small number had characteristics that were consistent with a non-basaltic source. Since many of the characteristics shown by the Colombian corundum overlap those from other world localities, they could not be separated according to geographic origin.

Jean-Marie Duroc-Danner (durocdanner@bluewin.ch)
Gemgrading, Geneva, Switzerland

Emeralds from Madagascar with strong blue/green dichroism. M. Guillet, a mineral dealer from St. Nazaire, France, brought to this contributor's attention a new production of emeralds from Madagascar (the exact locality was not disclosed to him). Most of the over 200 carat parcel was composed of small, commercial quality, fairly included polished stones up to about 2 ct.

Gemological properties were obtained on five of the emeralds. The R.I. values were 1.585–1.592, specific gravity (determined hydrostatically) was 2.75, and the stones displayed a uniaxial negative optic figure. All were inert to ultraviolet radiation, and showed no reaction to the Chelsea filter. Most remarkable was their very strong dichroism: from yellowish green to dark "aquamarine" blue (figure 19). The relatively high R.I. and S.G. values are reminiscent of emeralds from Zimbabwe and Zambia, whereas the strong blue/green dichroism was previously found only in Nigerian emeralds (see H. A. Hänni, "Considérations terminologiques au subjet des émeraudes du Nigéria de couleur bleu-vert," *Revue de Gemmologie*, No. 113, 1992, pp. 2–4).

Editor's note: An emerald represented as originating in Goiás State, Brazil, that shows a noticeably blue color component is reported in the Lab Notes section of this issue (p. 317).

EF

Figure 19. Strong dichroism is evident in this emerald, which reportedly is from a new locality in Madagascar. Photomicrographs by John I. Koivula; magnified 12×.

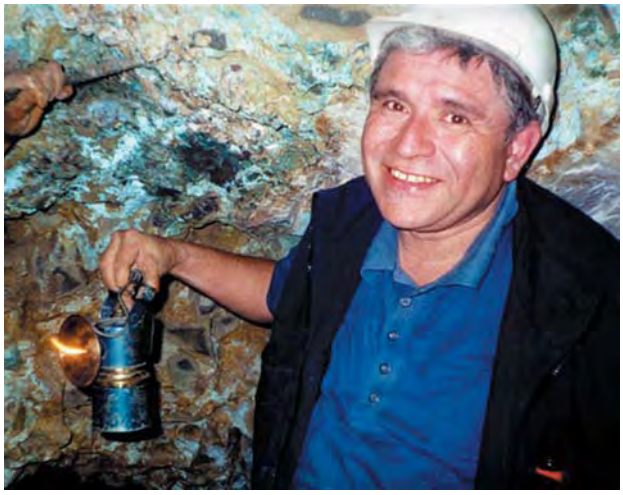

Figure 20. At the Lily mine in Peru, blue opal is mined from underground workings, where it forms in association with calcite, chalcedony, quartz, and chalcotrichite. Carbide lamps are used for lighting the tunnels, as shown by mine owner Felix Rocha. Courtesy of Roxanne Kremer.

Peruvian blue opal. Small quantities of attractive blue opal from the Andes Mountains of Peru have been seen in the gem trade for years (see Summer 1991 Gem News, pp. 120–121, and Spring 1994 Lab Notes, pp. 43–44). Recently we were provided with a notable sample and updated information on mining and production of this opal from Roxanne Kremer of Collectors Co., Rosemead, California, who visited Peru in November 2003. Ms. Kremer reported that there are two principal sources of blue opal in Peru: the Acari and Lily mines. The Acari mine, located in the department of Arequipa, has been worked for two decades.

Figure 21. This 17.58 ct blue opal reportedly is an example of the finest material produced from the Lily mine in Peru. Courtesy of Roxanne Kremer; photo by Maha Tannous.

The Lily mine, in the department of Ica, has produced blue opal for approximately 10 years.

According to Ms. Kremer's sources at the Lily mine, about 10 tonnes of opal are produced there every 2–3 months, but only 1–2 kg are gem quality. The blue opal forms in association with calcite, chalcedony, quartz, and chalcotrichite (a variety of cuprite), and is mined from underground workings (figure 20) with small charges of dynamite. Although pieces of blue rough up to 100 kg have been recovered, only small areas have the purity and color that are appropriate for jewelry use. The low-grade material is carved in China and Hong Kong, while the gem-quality opal is polished locally in Peru.

Ms. Kremer loaned an attractive 17.58 ct polished freeform opal (figure 21) from the Lily mine to GIA for examination. The following gemological properties were obtained by one of us (EPQ): color—slightly mottled, greenish blue; diaphaneity—semitransparent to translucent; R.I.—1.45 by the spot method; S.G.—2.11; Chelsea filter reaction—none; luminescence—very weak bluish green fluorescence to long- and short-wave UV (with a slightly stronger reaction to the former) and no phosphorescence. With the desk-model spectroscope, only a cutoff was observed at around 650 nm. Microscopic examination revealed yellowish brown and wispy white clouds, small yellowish orange crystals, small dark metallic-appearing crystals (possibly hematite), and transparent near-colorless crystals (probably quartz). The properties of this sample were consistent with those reported in the *Gems & Gemology* entries listed above for similar blue opal from Peru.

Elizabeth P. Quinn (equinn@gia.edu)
GIA Gem Laboratory, Carlsbad
oBML

Some interesting pearls from the North American West Coast. Although they are not common on the retail market, occasionally in the GIA Gem Laboratory we see natural and cultured pearls from North America, such as those from the *Pteria sterna* and *Pinctada mazatlanica* oysters in Mexico's Gulf of California, as well as the natural and cultured freshwater pearls from the *Unionidae* mussels of Tennessee, Mississippi, Texas, Ohio, and other states. We also are fortunate to see natural abalone pearls from the coast of North America. These currently originate predominantly from the green abalone (*Haliotis fulgens*) and the pink abalone (*H. corrugata*). Occasionally, pearls from the red abalone (*H. rufescens*) and the black abalone (*H. cracherodii*) are seen, but they are usually from older collections as these abalones have become more scarce and are no longer fished commercially.

Jeremy Norris of Oasis Pearl in Albion, California, recently loaned GIA some of his rare-pearl inventory for examination. These included two pen shell pearls (one brown and one black) from the Pacific coast of Baja

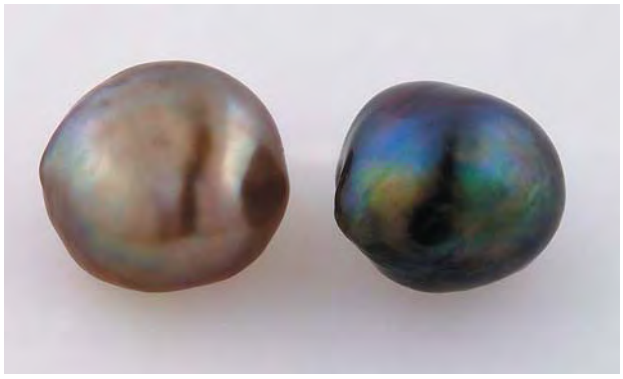

Figure 22. These pen shell pearls (7.6 × 7.1 × 4.8 mm and 7.3 × 6.7 × 6.0 mm) originate from the Pacific coast of Baja California, Mexico. Photo by C. D. Mengason.

Figure 23. These abalone pearls (40.13 and 29.37 ct) were unusual in shape, appearance, and growth structure. Photo by Maha Tannous.

California, Mexico, as well as two unusual abalone pearls and a nacreous pearl from a turban snail.

The pen shell pearls (figure 22), which probably came from *Atrina maura* or *Pinna rugosa,* had an interesting nacre structure when viewed with magnification. Instead of the usual overlapping platelets with a stepped appearance, the nacre appeared as a network of tiny shallow elongated rectangular "webs." The different appearance of the nacre in pen shell pearls from the *Pinna* species has been explained by the fact it is not constructed of concentric layers of nacre, but rather of numerous small prisms arranged around the center (see J. Taburiaux, *Pearls: Their Origin, Treatment & Identification*, 1985, Chilton Book Co., Radnor, Pennsylvania). Unfortunately, the structure was too subtle to show clearly on a photograph.

Each of the abalone pearls was unusual in shape and appearance (figure 23). The nearly round shape of the 29.37 ct freely formed pearl (18.4 × 17.7 × 17.4 mm) was notable, since abalones' strong muscular bodies typically deform pearls into baroque shapes as they grow. To obtain a nearly round abalone pearl is quite rare.

The 40.13 ct abalone pearl (23.5 × 19.9 × 18.0 mm) was very unusual in that part of it had extruded through to the outside of the abalone shell during growth. External shell material was deposited on this end, creating a series of red ridges. The ridges were non-nacreous, and a band of irregularly arranged structural patches formed at the junction between the ridges and the nacre. The red ridges imparted an intriguing appearance, calling to mind a sea anemone or other natural creature. X-radiographs of both abalone pearls revealed that the nearly round pearl was partially hollow, and the ridged pearl was nearly solid.

One of the most interesting items provided by Mr. Norris was a 19.80 ct nacreous turban snail pearl (22.9 × 16.1 × 10.9 mm; figure 24), which was presumed to be from the wavy turban, *Astraea undosa*. It was the first such pearl this contributor had examined closely. The pearl was off-white, with high luster and orient, and exhibited striking iridescent colors similar to those seen in some North American freshwater pearls. The structure displayed an undulating wave-like pattern. The nacre was very smooth, resembling that of abalone. In numerous

Figure 24. This 19.80 ct nacreous pearl (shown here in two views) originated from a turban snail. Photos by Maha Tannous.

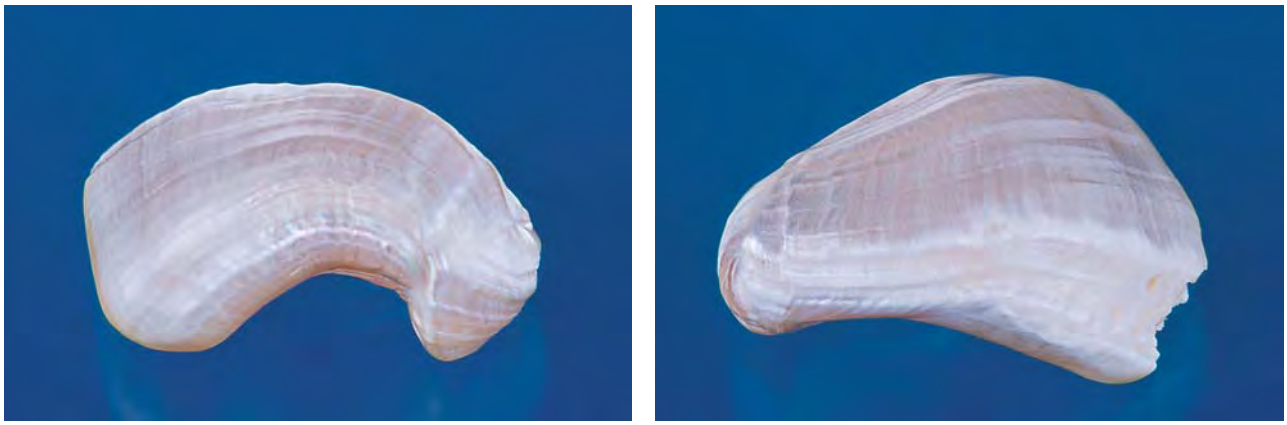

Figure 25. These two polished crystals of "platinum quartz" from Curvelo, Minas Gerais, Brazil, weigh 222.26 and 94.73 ct. The inclusions are composed of rutile and brookite. Photo by Maha Tannous.

areas on the pearl, the nacre was so smooth and glassy that it appeared to have a polished "wet" appearance; Mr. Norris said that this appearance and high luster was natural for this turban snail pearl.

Cheryl Wentzell (cwentzell@gia.edu)
GIA Gem Laboratory, Carlsbad

"Platinum quartz." Over the past several years, we have seen examples of rough and polished rock crystal and pale smoky quartz crystals, as well as polished free-form pieces of quartz, that contain inclusions of silvery reflective rutile needles. The rutile inclusions in these pieces, all from Brazil, grow from and are oriented on light brown elongated blades of brookite, another titanium-oxide mineral.

Figure 26. As identified by Raman analysis, slender needles of rutile are clearly visible extending from the underlying central crystal of brookite in this "platinum quartz" from Brazil. Photomicrograph by John I. Koivula; magnified 5×.

Shortly after this material entered the marketplace, one of the present contributors (JIK) obtained a few specimens (see, e.g., figure 25) for photomicrography and inclusion analysis from Luciana Barbosa, of the Gemological Center in Belo Horizonte, Minas Gerais, Brazil, and two lapidaries/jewelry designers—Falk Burger of Los Alamos, New Mexico, and Kevin Lane Smith of Tucson, Arizona. Although the inclusion study was completed, the results were never published.

Then, at a recent jewelry trade show in New York, James Shigley, GIA director of Research (and *Gems & Gemology* and GNI contributing editor), spoke with a supplier of the material, Ricardo Viana of Belo Horizonte, Brazil. Mr. Viana was marketing the material as "platinum quartz." He subsequently sent several specimens to Dr. Shigley, which were then provided to these contributors for gemological examination. Mr. Viana also informed us that the quartz reportedly is from Curvelo, in Minas Gerais. At about the same time, an additional sample of the material was provided by David Epstein of Precious Resources Ltda. in Teófilo Otoni, Brazil.

The inclusions in both the older and newer samples looked virtually identical in morphology, having a feathery to insectile appearance, and Raman analysis proved that they were indeed the same materials (rutile and brookite).

With magnification, the inclusions generally appeared as blades of light brown or tan brookite from which numerous slender silvery rutile crystals extended in more-or-less parallel arrangements. As shown in figure 26, in some samples the central blade of brookite was still apparent, while in others the rutile was so dense that the brookite nucleus could no longer be seen. More rarely, the brookite blades were clearly visible with only a sparse number of rutile fibers extending from them (figure 27). In these few samples, the precise orientation of the rutile on the brookite suggested that the rutile had grown epitaxially on the substrate. Since brookite is a lower-temperature form of titanium oxide (rutile is the higher-temperature variant), the presence of the associated oriented rutile suggests that as the inclusions (which are protogenetic to the host quartz) developed, the temperature increased so that rutile was preferred.

John I. Koivula and Maha Tannous

Some rare faceted gem materials. This contributor recently had the opportunity to examine specimens of three gem materials that are very rarely seen in faceted form: chlorargyrite, stolzite, and sulfoborite.

Chlorargyrite. Faceted silver minerals are perhaps the rarest of all collector gems (see figure 28). By far the most

beautiful of them is deep red proustite, trigonal Ag_3AsS_3, which has been found as facetable crystals in Germany and the Czech Republic, among other locations. However, the best specimens are from Chanarcillo, Chile, and faceted stones from this locality have been seen in sizes up to 55.48 ct (Patricia Gray, pers. comm., 2003). Much less interesting is pyrargyrite, trigonal Ag_3SbS_3, which is usually red only in transmitted light; the best facetable crystals come from Colquechaca, Bolivia. Both proustite and pyrargyrite are light sensitive and should be kept in darkness.

Chlorargyrite (cubic AgCl) is quite common in many silver deposits as small cubes or grains. This contributor recently examined seven faceted stones (see example in figure 28) up to 10 ct that were cut from a single 1-cm-thick vein of massive translucent chlorargyrite. The 7 × 5 cm specimen came from Chanarcillo, and was probably found in the mid-19th century (R. B. Cook, "Famous mineral localities: Chanarcillo, Chile," *Mineralogical Record*, Vol. 10, No. 4, 1979, pp. 197–204). Cutting and polishing were very difficult because of chlorargyrite's very low hardness of 2 on the Mohs scale. The material also proved to be highly corrosive: The wheel used to facet the stones became so badly corroded it was useless a few days after cutting.

The faceted chlorargyrites were "creamy" yellow in color and had a waxy luster. According to the literature, the R.I. of chlorargyrite is 2.07 (R.V. Gaines et al., *Dana's New Mineralogy*, John Wiley & Sons, New York, 1997, pp. 377–378). Specific gravity, measured hydrostatically, was 5.55. The stones examined showed anomalous interference colors under crossed polarizers, had no reaction to UV radiation, and displayed no visible spectrum in a handheld spectroscope. Because chlorargyrite is light sensitive (becoming darker with exposure to light), the stones should be kept in darkness.

Other silver-bearing minerals have been polished into gems, as well. Boleite, an Ag-Cu-Pb-chloride from Boleo, Mexico, may be faceted into small dark blue stones, and native silver embedded in calcite (e.g., from Canada and the Czech Republic) can be cut into cabochons.

Stolzite. Another extremely rare gem is stolzite, $PbWO_4$ (figure 29). It is known only from a few localities; J. E. Arem mentions a few tiny bright orange faceted stones from Broken Hill, New South Wales, Australia (*Color Encyclopedia of Gemstones*, 1987, Van Nostrand Reinhold, New York, p. 181). It has also been grown synthetically for industrial applications at Turnov, Czech Republic (again, see figure 29). By far the best-known stolzite crystals were found between 1987 and 1991 in the Sainte Lucie mine in southern France (see S. Weiss, "Stolzit aus Sainte Lucie, Frankreich: Die grössten und besten Kristalle der Welt," *Lapis*, Vol. 27, No. 1, 2002, pp. 17–20; see also figure 30). These yellow-to-orange tabular crystals measured up to 8 cm across. Many of them had a

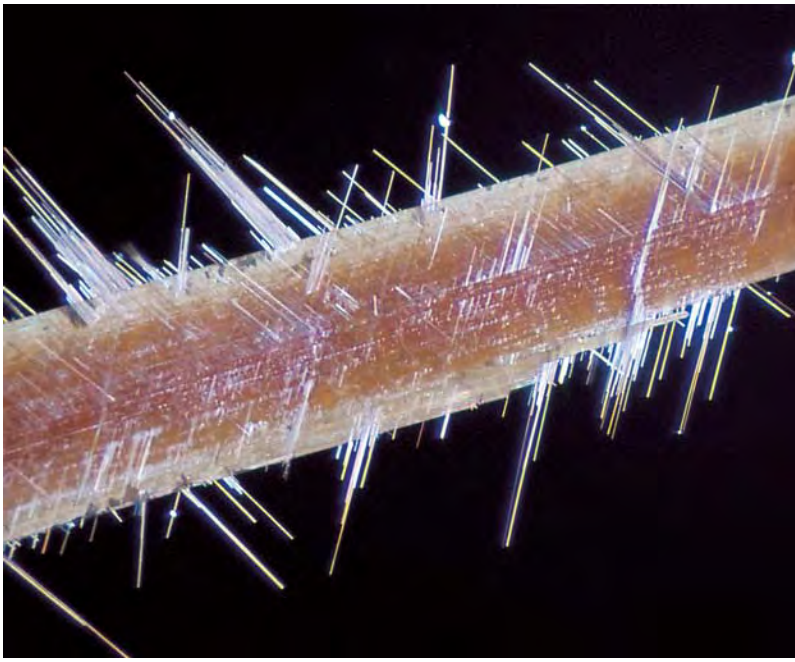

Figure 27. The precise orientation of rutile needles from the brown blade of brookite is apparent in this unusual example of "platinum quartz" from Brazil. Photomicrograph by John I. Koivula; magnified 10×.

semitransparent core that corresponded chemically to pure stolzite. The core was covered, sandwich-like, by almost opaque yellow layers of Mo-rich stolzite (i.e., containing a wulfenite component).

According to Gaines et al. (1997, pp. 1000–1001), the Mohs hardness of stolzite is 2.5–3, and the refractive index is very high: 2.18–2.27. The three faceted stolzites from

Figure 28. These faceted silver minerals are among the rarest of collector stones. Shown here, from left to right, are a 5.22 ct proustite from Germany, a 9.45 ct chlorargyrite from Chile, and a 2.17 ct pyrargyrite from Bolivia. Photo by J. Hyrsl.

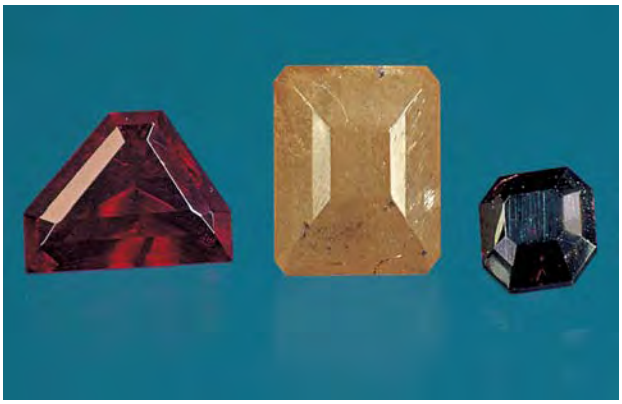

Figure 29. The 3.84 ct faceted yellow stolzite shown here is from the Sainte Lucie mine in France; the 56.49 ct near-colorless round brilliant is a synthetic stolzite grown in the Czech Republic. Photo by J. Hyrsl.

Figure 30. This well-formed 2.5 cm stolzite crystal was found at the Sainte Lucie Mine, France. Photo by J. Hyrsl.

France examined by this contributor (0.76–3.84 ct) had a specific gravity of 8.23–8.32 (measured hydrostatically). The stones exhibited yellow fluorescence to short-wave UV radiation, and were inert to long-wave UV. They also showed two thin lines in the yellow region of the spectrum when viewed with a handheld spectroscope, and had a negative optic character.

Sulfoborite. Many rare minerals, especially sulfates and borates, are found at the Inder borate deposit on the north shore of the Caspian Sea in western Kazakhstan (I. V. Pekov and D. V. Abramov, "Boron deposit of the Inder and its minerals," *World of Stones*, Vol. 1, 1993, pp. 23–30). Small faceted examples of preobrazhenskite and kaliborite from Inder were described in the Summer 1995 Gem News section (pp. 129–130); the görgeyite in that entry was most likely from Inder as well.

Sulfoborite, $Mg_3B_2(SO_4)(OH)_8(OH,F)_2$, has been found at Inder in several forms. The most beautiful are very rare prismatic water-clear crystals that are similar in shape to topaz and have been known to reach 5 cm long. This contributor obtained five faceted stones (0.10–1.27 ct) and several crystals of sulfoborite (see, e.g., figure 31). Their measured refractive indices were 1.532–1.550, as compared to published values of 1.527–1.552 (Gaines et al., 1997, p. 566). Specific gravity, measured hydrostatically, was 2.44–2.46. The stones were inert to UV radiation, and no absorption lines were observed with a handheld spectroscope. The Mohs hardness was 4–4.5.

In addition to görgeyite, preobrazhenskite, kaliborite, and sulfoborite, many other rare minerals have been found at Inder, some of them in transparent crystals suitable for faceting, especially hydroboracite, pinnoite, inyoite, and inderborite.

Jaroslav Hyrsl (hyrsl@kuryr.cz)
Kolin, Czech Republic

Large scapolite from Tanzania. Gem-quality yellow scapolite has been known for years from the Mpwapwa area near Dodoma, Tanzania (see G. Graziani et al., "Observations on some scapolites of central Tanzania," *Journal of Gemmology*, Vol. 18, No. 5, 1983, pp. 379–381). Recently, a scapolite from this locality produced a stone that was notable for both its size and color. At 147.62 ct, the exceptionally clean cushion cut was a deep "golden" orange (figure 32). According to David Atkinson (of Terra, in Sedona, Arizona), who brought the stone to this contributor's attention, the rough was probably mined in the early 1990s, at the same time abundant smaller sizes also were available. He indicated that most scapolite crystals from Mpwapwa form elongated prisms (usually less than 2.5 cm in diameter). For maximum yield, stones usually are cut with their tables parallel to the c-axis, resulting in a "straw" yellow color. However, the scapolite shown in figure 32 was faceted from a 580 ct crystal cross section with a diameter of more than 6 cm. As a result, the cutter

Figure 31. The Inder borate deposit in Kazakhstan is a source of many rare minerals, such as these sulfoborites. The faceted stone in the center is 1.27 ct. Photo by J. Hyrsl.

Figure 32. This 147.62 ct scapolite from Tanzania, faceted by Maria Atkinson, shows an unusually attractive deep "golden" orange color that results from cutting the stone with the table perpendicular to the c-axis. Photo by Jeff Scovil, © Terra, 2003.

could orient the stone to take advantage of the deeply colored c-axis direction. *BML*

Update on tanzanite mining by AFGEM. Since the discovery of tanzanite in the Merelani Hills of Tanzania in 1967, recovery of this attractive violet-blue gem (figure 33) has been subject to erratic production and resulting price fluctuations, due largely to informal mining using primitive methods. Several mining accidents over the past few years have claimed the lives of numerous workers (see, e.g., Summer 1998 Gem News, p. 145). Fortunately, the recent introduction of modern mining methods in one portion of the deposit has helped stabilize production. Since 1999, African Gem Resources Ltd. (AFGEM) of Johannesburg, South Africa, has been solely developing Block C of the tanzanite claims. Block C is the largest of the three main blocks covering an area of 8 km^2; Blocks B and D are divided into 50 ↔ 50 m plots and mined informally. Block A is roughly 2 km^2 and is mined by a Tanzanian individual.

As at the other claim blocks, extraction of tanzanite at Block C has historically been similar to artisanal mining of colored gem minerals at other primary deposits, with local miners braving dangerous conditions to extract the gem material as quickly and cheaply as possible. With these techniques, mine shafts are typically narrow, steep, and poorly ventilated—and the use of explosives releases noxious fumes that have proved deadly to the miners.

The new, mechanized operation at Block C is operated by AFGEM Tanzania, and is designed to maintain a high level of efficiency and safety. The miners work in large (2 ↔ 3 m) shafts with extensive roof bolting and timber support, as well as meshed concrete where necessary. All of the working faces are properly ventilated, and the miners are required to wear appropriate safety equipment. Although water is used during drilling to reduce dust, the use of underground channels, water collection pits, and large pumps minimizes the risk of flooding. Emergency equipment is provided in each shaft, and a well-equipped emergency clinic is available on site (although there have been no serious injuries to date). The miners are provided room and board in modern accommodations, with electricity supplied by a connection to the national grid, and back-up generators are available in the event of a power failure. The mine was in a developmental phase until the first quarter of 2003 and therefore has only recently begun regular production of tanzanite.

There are five active shafts on the property, known as JW, Main, Delta, CT, and Bravo. The most consistent production has come from the JW shaft, while the biggest finds have come from the Bravo shaft, where in July 2002 exquisite collector-quality crystals were extracted (some as large as 600 to 800 grams). In the six months leading up to September 30, 2003, 12,311 tonnes of ore were extracted, which yielded 812,526 carats of gem-quality tanzanite. Thus, the ore grade during this period averaged 66 carats/tonne of mixed-quality gem material (classified into A, B, and C grades, based on transparency, color before heating, and size).

Underground blasting is strictly controlled. In tanzanite-rich zones, the larger visible crystals (known as "face pickings") are removed by hand, and the remaining material is processed via dense media separation (DMS). Ore is removed from the shaft by both fixed-rail and monorope

Figure 33. Tanzanite (here, 62.97 ct) has enjoyed strong demand in the gem trade, but has been subject to erratic production and resulting price fluctuations. Recent developments in the mining, recovery, and marketing of tanzanite from the Block C portion of the deposit are helping to stabilize the production of this material. Courtesy of H. Krupp; photo by Maha Tannous.

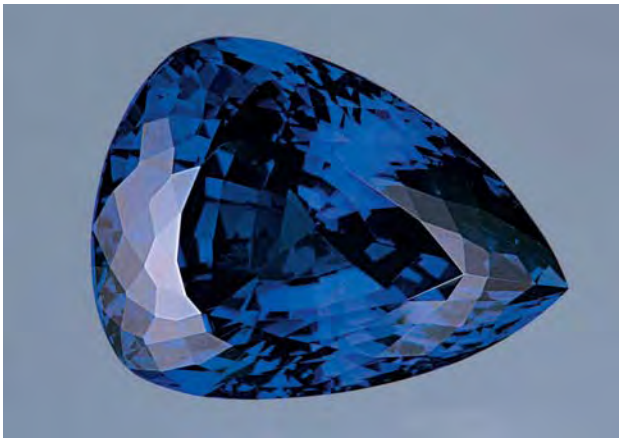

Figure 34. This customized processing plant has been converted by AFGEM from a former graphite plant to extract tanzanite. This photo, taken from the dense media separation area, shows a network of conveyor belts that eventually routes material to the sort house (far right), where it is hand-picked under stringent security measures. Photo by Reyno and Claire Scheepers.

systems. In the latter, the ore is placed into 10 kg sacks that are hooked to a cable which runs the full length of the tunnel. This automated cable moves the material slowly and continuously to the surface. The ore is then stored in large bins and discharged directly onto dump trucks for transport to the DMS plant (figure 34), which is situated 4 km from the mine at the source of the water supply (derived from an underground river). Once processed, the heavy fraction containing tanzanite is routed to a high-security sort house for hand picking. The tanzanite rough is either cut by in-house lapidaries or sold directly to large global customers (mostly cutters and dealers). The faceted tanzanite is heated on-site in a temperature-controlled kiln, whereas the rough is sold without being heat treated.

AFGEM Tanzania operates a continuous in-house training program whereby the locals are taught gem cutting by skilled professionals. One of the lapidary facilities (employing five cutters) is located in the processing plant, directly opposite the sort house, and a larger facility (with 15 full-time cutters) is situated at AFGEM's headquarters in Johannesburg.

Preventing stone theft remains a challenge. AFGEM Tanzania's mine employs stringent security systems and procedures in all producing areas and at shaft entrances, as well as at the plant, sort-house, and lapidary facility. An X-ray body scanning system, which will be the first of its kind in Tanzania, has been specifically developed for the mine and will be operational by early 2004.

The mine operates in compliance with an environmental impact study done in 1999. AFGEM is in the process of a multi-year environmental rehabilitation project, repairing much of the preexisting damage to the local landscape. Most of the ditches, open pits, and small tunnels dug by informal diggers have been filled in and are being replanted with indigenous flora.

AFGEM has created an ambitious grading and certification program for tanzanite. Each gemstone produced is evaluated using a proprietary grading system (according to cut, carat weight, color, and clarity) developed in conjunction with Independent Colored Stone Laboratories (Johannesburg), and is sold with a certificate of origin and authenticity issued by the Tanzanite Foundation. Although this system is currently used exclusively by AFGEM, steps are being taken to include tanzanite from all producers in this program.

Reyno and Claire Scheepers (rsc@sun.ac.za)
Gemstone Research Centre
University of Stellenbosch, South Africa

Figure 35. Fiberglass imitation cat's-eyes from China are available in many colors. Photo by A. Cossard.

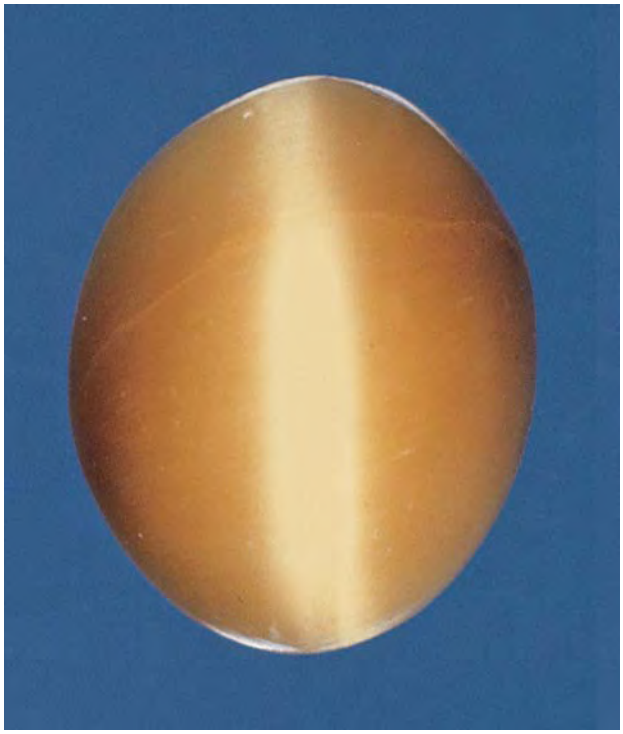

Figure 36. Some of the Chinese fiberglass cabochons provide a realistic imitation of cat's-eye chrysoberyl. Photo by A. Cossard.

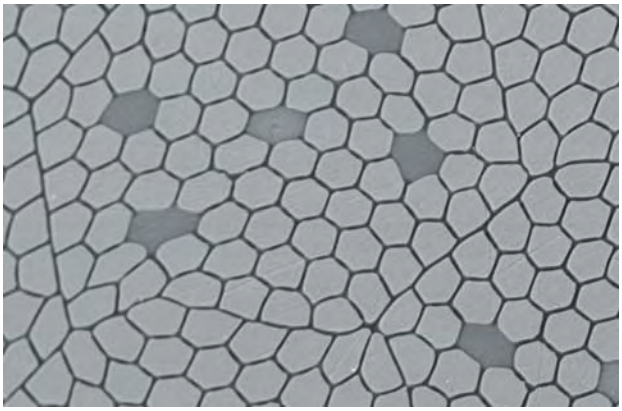

Figure 37. This scanning electron micrograph of a glass imitation cat's-eye from China clearly shows the bundled grouping of internal fibers. Colored fibers show up in this image as darker gray. The field of view is 200 µm; each individual fiber is about 10 µm across.

SYNTHETICS AND SIMULANTS

Chatoyant glass cabochons from China. Since at least the early 1990s, fiberglass imitation cat's-eyes from China have been very common in the market. They are available in many colors (figure 35), some providing good imitations of cat's-eye chrysoberyl (various shades of yellow-brown in particular; see, e.g., figure 36). Even tricolor pieces have been developed (red-white-green and green-red-blue). They can be fashioned as cabochons or beads, but they may have other forms as well (e.g., for personal seals).

This contributor recently examined 30 of these Chinese imitation cat's-eyes, in both oval cabochons (ranging from approximately 8 × 6 × 2 mm to 18 × 10 × 4 mm) and spherical beads (10 mm in diameter). The R.I. and S.G. (obtained by the hydrostatic method) values varied slightly according to color, as listed in table 1. These values are well within those commonly observed for glass gem imitations, which in this contributor's experience range from about 1.46 to 1.70 in R.I., and from 2.3 to 4.2 in S.G.

Microscopic observation revealed that this material was indeed composed of parallel glass fibers. The fibers were not always straight, but rather were often slightly bent. In some samples, fractures and black spots of an undetermined nature made these imitations look more like natural gems.

The internal arrangement of fibers was easily visible with a Jeol 5800LV scanning electron microscope (SEM; see figure 37). Individual fibers were about 10 µm across, with an approximately hexagonal cross section. An unidentified material, which looked black in the electron micrographs, appeared to cement the fibers together. The fibers were bunched in larger, roughly hexagonal units, about 120–150 µm wide, that were divided by rather straight black outlines. In each bunch, a small number of fibers (about 5 out of 90–100) were distinctly darker, and it is likely that these provided the color to the overall material. In some of the samples examined, the grouping of fibers was much less orderly, and they showed a more natural-looking cat's eye.

Qualitative microanalysis using the SEM's Princeton Gamma Tech energy-dispersive IMIX-PTS detector revealed the chemical composition of the glasses used, which are typical of "crystal"-type glass, that is, silicate glasses with Pb and K. Also detected were small amounts of Na and Ba, and traces of Al. The fibers themselves had a similar composition. However, the colored fibers were systematically poorer in Pb and richer in K than the noncolored ones, and it is possible that they contained a coloring agent as well (see below). The cementing material

TABLE 1. R.I. and S.G. values of Chinese fiberglass imitation cat's-eyes.

Color	R.I.	S.G.
Orangy red	1.52	2.65
Blue-green	1.53	2.84
"Cobalt" blue	1.56	2.99
Light blue	1.56	3.11
Violetish brown	1.57	3.12
Gray	1.57	3.14
White	1.57	3.18
Dark green	1.58	3.20
Pink	1.58	3.20

was very poor in Pb and richer in Na, Al, and K than regular fibers; all fibers had a more elevated but still modest amount of Ba.

In some cases, microanalysis revealed transition metal(s) in the color-bearing fibers. Black was associated with traces of Mn; green with Cu, Cr, and/or Fe; yellow to orange to brown with Fe; and bright blue with Co. For other colors, such as pink and red, there was no additional transition element, but rather more lead and zinc, which are not classically associated with such colors.

Raman spectroscopy, obtained on a Bruker RFS100 Fourier transform spectrometer, demonstrated the amorphous nature of the material. The spectrum consisted of essentially two broad bands at about 800 and 290 cm^{-1}. The width of the bands (at almost 200 cm^{-1}) is typical of amorphous materials such as glasses. This glass is apparently anhydrous, as no broad band was observed on the spectrum at about 3500 cm^{-1}.

The identification of these chatoyant glass cabochons is straightforward, by observing their appearance with the unaided eye (i.e., unnatural chatoyancy and unusual color in some cases) and the gemological microscope (the presence of parallel glass fibers). *EF*

New synthetic opal varieties. Kyocera Corp. of Kyoto, Japan, has been manufacturing synthetic opals since the early 1980s. They recently provided the GIA Gem Laboratory with examples of their new line of synthetic opals, which, in addition to black and white, includes "fire" and "jelly" varieties that are significantly more transparent than most other non-impregnated synthetic opals.

Figure 38. These eight cabochons (2.41–2.68 ct) are examples of the new synthetic opals being produced by Kyocera. The company has been producing the black and white synthetic material since the 1980s, but it recently introduced semitransparent varieties, including "fire" and "jelly" synthetic opals. Courtesy of Kyocera Corp.; photo by Maha Tannous.

Eight oval double cabochons (two of each type; figure 38) were provided, ranging from 2.41 to 2.68 ct. Gemological properties were collected on one sample of each variety, as follows: color—white, near-colorless, orange, and black, with all samples displaying play-of-color; diaphaneity—semitransparent (orange and near-colorless cabochons), semitransparent to translucent (white), or translucent to semitranslucent (black); optic character—singly refractive with weak to moderate anomalous double refraction; refractive index—spot readings of 1.46 to 1.47; hydrostatic specific gravity—2.22–2.27; and no reaction to the Chelsea filter. The white and near-colorless cabochons fluoresced very weak to weak chalky blue (slightly stronger to short-wave UV), the orange cabochon luminesced very weak red (also slightly stronger to short-wave UV), and the black cabochon was inert to both long- and short-wave UV; none of the samples exhibited phosphorescence. When viewed with a desk-model spectroscope, all samples had a band at 550 nm and a line at 580 nm. Three of the four exhibited a band at 500 nm, whereas the orange cabochon showed only general absorption to 500 nm. In addition, lines at 600 and 620 nm were noted for the near-colorless and black cabochons, respectively. With the microscope, all samples showed the "chicken-wire" or "snake-skin" pattern and columnar structure that are typical of most synthetic opals.

According to Kyocera, these samples were not polymer impregnated, and this was supported by FTIR spectroscopy. None of the polymer-related absorption features documented in some other synthetic opals produced by Kyocera (as described in the Summer 1995 Gem News, pp. 137–138) were found in any of the four samples. The absence of polymers was further supported by the higher S.G. values measured for these samples (2.22–2.27), as compared to those recorded for the earlier polymer-impregnated material (1.88–1.91).

Overall, the gemological properties of these synthetic opals were very close to those expected for natural opal. However, the identification of the material is not difficult due to the presence of distinctive growth features typical of many laboratory-grown opals.

Elizabeth P. Quinn

Plastic imitations of a walrus tusk and a sperm whale tooth. Recently, the SSEF Swiss Gemmological Institute received for testing two specimens that appeared to be some sort of teeth. The larger one (about 40 cm and 665 grams) strongly resembled a walrus tusk, while the smaller one (about 16 cm and 390 grams) looked like a sperm whale tooth (figure 39), complete with aging striations and accumulated dirt. Both items were carved with motifs of historical sailing vessels and whaling, with the inscriptions "Ship Sachen 1856–59" on the larger item and "The

bark Veronica" and "all in a days work" on the smaller item. They were reportedly part of a collection of several similar looking items, including elephant ivory.

By comparing the specimens with an authentic sperm whale tooth (figure 40), doubts about their identity immediately arose. The "pulp cavities" at the ends of both specimens showed no roots where they would have attached to the jawbone of a walrus or a sperm whale. Patterns such as cross-hatches, concentric lines, and dots, all of which are typical for ivory or teeth (see M. Campbell-Pedersen, *Gem and Ornamental Materials of Organic Origin*, Butterworth-Heinemann, Oxford, UK, 2003), also were not present. Even more suspicious, a broken fragment of the "walrus tusk" showed a perfect conchoidal fracture, which was interrupted by a layer of crushed material and several air bubbles (figure 41). Conchoidal fractures are typical for some homogeneous and amorphous substances like plastic, but not for organic substances, which show structured fracture planes with internal patterns.

Gemological testing quickly confirmed that both objects were plastic. Contact with a hot point produced a distinct acrid plastic smell. Testing with a hydrostatic balance revealed a specific gravity of 1.26, which is distinctly lower than the S.G. of walrus tusks and sperm whale teeth (typically 1.85).

The plastic imitations were further analyzed chemically (EDXRF), structurally (FTIR and Raman spectroscopy), and microscopically (SEM), and the results were compared with those of sperm whale teeth, ivory, and plastics. The main constituents of plastic (carbon, oxygen, and hydrogen) cannot be analyzed by EDXRF; however, these analyses did reveal information about the coloring agent of the plastic in both samples. With titanium dominant over other transition metals (Mn, Fe, Co) as well as Si, K, Ca, S, Cl, the agent is probably titanium-white, a well-known dye.

Figure 39. These specimens, resembling a walrus tusk (top, ~40 cm long) and a sperm whale tooth (bottom, ~16 cm long) proved to be plastic imitations. Photo by M. S. Krzemnicki, © SSEF.

In the authentic sperm whale tooth, Ca, P, and some Fe were found, which are the main constituents of teeth. Ca also was detected in the "walrus tusk" imitation, apparently due to the layer of crushed material mentioned above, which proved to be calcite (see below). This contributor suspects that the crushed calcite was added to the plastic to produce a density and a chemical signal somehow similar to those of natural teeth.

FTIR analyses (by Marco Nägelin, von Roll Isola, Switzerland) on the laboratory-created items were distinctly different from those of the sperm whale tooth, showing a typical polyester (unsaturated isophthalate) fingerprint with peaks at 3061, 3027, 2925, and 2853 cm^{-1}. Raman

Figure 40. Comparison with an authentic sperm whale tooth (left) raised doubts about the identity of the carved plastic imitation (right). Photo by H. A. Hänni, © SSEF.

Figure 41. A broken fragment of the plastic "walrus tusk" showed conchoidal fractures, air bubbles, and a layer of crushed calcite crystals, proving its manufactured nature. Photo by H. A. Hänni, © SSEF.

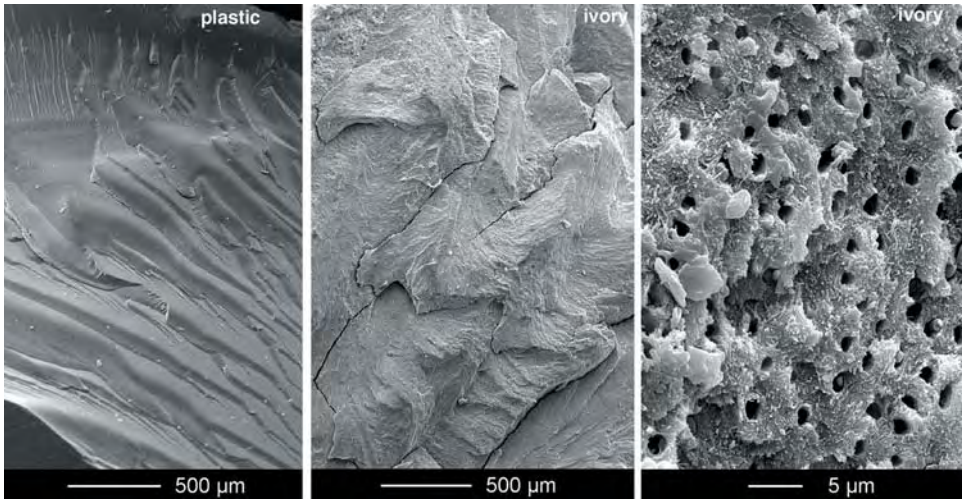

Figure 42. SEM micrographs demonstrate the obvious differences between the conchoidal fracture of the plastic "walrus tusk" (left) and the irregular splintery fracture (middle) and porous microstructure (right) in ivory (elephant tusk). Magnified 50× (left and center), 250× (right); © SEM laboratory, University of Basel, Switzerland.

spectroscopy (using an argon laser at 514 nm) was carried out on the layer of crushed material within the plastic items. These revealed peaks at 1097, 300, and 174 cm^{-1}, typical for carbonates (calcite to magnesite series). Together with the presence of Ca detected by EDXRF, this crushed material was identified as calcite. FTIR measurements on the plastic confirmed the presence of water molecules (peaks at 5284, 5250, 3471, and 3225 cm^{-1}).

SEM micrographs were taken to compare the surface structures of the plastic items with those of teeth. Figure 42 shows the fracture surfaces of the plastic "walrus tusk" (left) and ivory (center). The plastic imitations showed conchoidal fracture planes with step-like patterns, but no internal structures. In contrast, ivory (and sperm whale tooth) has a rather irregular splintery fracture. As seen under higher magnification (figure 42, right), the microstructure of ivory consists of a regular pattern of hollow channels. Similar structures are found in other types of teeth.

By careful observation and testing using standard gemological methods, the experienced gemologist will easily identify these plastic imitations, although their visual appearance can be quite convincing.

Michael S. Krzemnicki (gemlab@ssef.ch)
SSEF Swiss Gemmological Institute
Basel, Switzerland

CONFERENCE REPORTS

Antwerp Diamond Conference. The second annual Antwerp Diamond Conference was held November 3–4, 2003. The primary theme was marketing and branding of diamonds; however, many speakers also addressed the broader problems of industry finance and distribution. They agreed that the diamond industry is in the process of unprecedented change, which will forever alter the ways it does business and inevitably cause a spate of mergers and consolidations.

Maurice Tempelsman, chairman of Lazare Kaplan International, New York, told the audience of some 500 that the changes instigated since the De Beers Diamond Trading Company (DTC) abandoned its traditional custodianship of the market have increased risk throughout the diamond pipeline. Yet, the ability of the industry to deal with such risks has "not yet been tested." The DTC, he said, essentially sold off its well-capitalized, non-debt-financed diamond stockpile to its clients, many of whom financed their purchases by increasing debt as they piled up inventory. These firms have compounded their problems by making "imprudent" deals with retailers that include very long payment terms and memo purchases. Retail margins for diamond jewelry have been shrinking, he added, leading to decreased profitability.

Peter Gross, vice president of the International Diamond & Jewelry Group of ABN AMRO Bank, Antwerp, said that the industry is in an unhealthy situation, with rough diamond prices rising due to manufacturers' desire to keep their operations going, while at the same time polished diamond inventories—and the debts that finance them—have also been increasing. He explained that the industry suffers from an excess manufacturing capacity that will eventually cause some cutting operations to shut down or merge with other companies. "The quality of industry bank debt has declined in the past year," he said. "Companies must now focus more on driving sales instead of getting supplies."

Gareth Penny, DTC sales and marketing manager in London, emphasized that effective marketing and branding of diamond jewelry is the best way to break out of the discount trap that is sapping margins. In presenting the principles of branding, he showed examples of diamond jewelry advertisements featuring cluttered arrays of pieces with discount prices splashed throughout. He contrasted that with a Gucci advertisement showing a stylish woman enjoying a new handbag. "Who in the world discounts Gucci?" he asked, adding that even some U.S. mass merchandisers are starting to get the message that diamond jewelry should be advertised like a luxury product.

Paul Goris, vice president of Antwerp Diamond Bank, stressed that marketing programs require "big money," so only the largest, best-capitalized firms will be able to fund

their own branding initiatives. He expressed concern that other companies, even fairly large DTC sightholders, will draw funds from their business operations that would normally go to maintaining inventories and use them for marketing activities that may not have a swift return. He also stressed that marketing and branding initiatives must be based on solidly researched customer need and be professionally executed.

Pierre Gurdjian, a specialist for the business consulting firm McKinsey & Co., Antwerp, told the audience that major consolidations are inevitable in the diamond industry, because many firms will not be able to sustain the high costs of marketing and branding activities without taking on partners or merging with larger players. He noted that of the more than 100 new diamond cuts introduced in the past few years, only about five are truly distinctive with any consumer recognition. Branded diamond jewelry lines have even less consumer recognition, and thus for the most part their advertising campaigns "are not a sustainable platform for sales growth." At the same time, he noted that mass retailers are "trampling" their diamond suppliers, forcing diamond manufacturers to give very favorable terms while luxury companies are faced with declining margins. The skills to carry out effective branding strategies are currently lacking in the diamond industry, Mr. Gurdjian said, so diamond manufacturers must look to other fashion and retail industries to make them work

Danny Horowitz, president of IDH, an Antwerp-based rough diamond dealer, questioned whether diamonds could ever be properly branded since they are inherently a generic product. He noted that even in Japan, where consumers are the most brand-conscious, there is "branding fatigue." The branding initiatives, he added, have thus far failed to alleviate the current inventory overhang in the market. Instead, they have brought increases in industry debt that are causing liquidity problems throughout the pipeline.

Maxim Shkadov, first deputy director general of Krystall Smolensk, a diamond cutting operation in Smolensk, Russia, told the audience that his firm plans to promote Russia's tradition of well-cut diamonds as a brand, adding that its 2003 sales of polished were running 3.3% ahead of 2002's total of $250 million. He added that the domestic Russian diamond market grew 49% in the past two years, thanks in part to the country's newly wealthy, who respond strongly to the company's advertising slogan, "Measure your success in carats."

Other producers, represented by **Nigel Jones** (general manager of marketing, Rio Tinto's Diamond Product Group), **Graham Nicholls** (manager of branding operations, BHP Billiton Diamonds Inc.), and **Stephen Lussier** (executive director of marketing, DTC), presented their own diamond branding strategies. Mr. Jones, whose company owns majority shares in Australia's Argyle mine and Canada's Diavik mine, says its brand will provide assurances to consumers that its operations adhere to First World standards and include high business ethics. Mr. Nicholls noted that BHP's CanadaMark emphasizes the Canadian origin of diamonds from its Ekati mine. Mr. Lussier stressed that the diamond branding revolution "is irreversible" and essential to increasing diamond jewelry sales.

Hidetaka Kato, chairman of Kashikey Co. Ltd., Tokyo, described his company's current campaign to brand a line of brown diamond jewelry. Aimed at the casual-wear market for women's self-purchase, the program carries the tag line "free and easy" and promotes a product line that did not exist before in Japan.

Nadja Swarovski, vice president of international communications with D. Swarovski & Co., Wattens, Austria, outlined her company's strategy for introducing a brand of luxury crystal aimed at the fashion accessories market, and **Isabelle Guichet** of Van Cleef & Arpels, Paris, told how this well-established high-market jewelry house was pursuing younger buyers while keeping its signature identity.

Bernie Sensale, senior vice president of marketing with Zale Corp., Irving, Texas, said that all marketing decisions must be based on understanding consumers' decisions. He predicted that the bridal market will grow an estimated 14% over the next three years and stressed that 78% of all first-time brides in the U.S. receive a diamond engagement ring.

Former U.S. president **Bill Clinton**, in his keynote address, praised the diamond industry for its initiatives in ending the trade in conflict stones through the Kimberley Process. "The industry has put aside traditional differences for its common interests, and is working to end problems such as AIDS in Africa and conflict diamonds." He added that it is well worth the money spent to combat these problems, because they ultimately bring a more stable, peaceful world based on shared values, benefits and interests.

Russell Shor (russell.shor@gia.edu)
GIA Senior Industry Analyst

Rapaport International Diamond Conference. On October 20, 2003, the first Rapaport International Diamond Conference was held in New York City, with a standing-room-only crowd of more than 250. The conference was dominated by two controversial issues: a growing shortage of rough diamonds and the entry of synthetic diamonds into the consumer market.

Moshe Leviev, managing director of LLD, Ramat Gan, Israel, indicated that shortages of rough diamonds over 20 points, especially high-quality goods, will be a dominant factor for the next decade. He added that there will be no major new diamond mines coming on line for five to eight years at minimum, so shortages will get worse as demand rises. Mr. Leviev stressed that the De Beers DTC's Supplier of Choice initiative, which requires sightholders to fund costly marketing and advertising campaigns to increase diamond jewelry sales, will take their toll on diamond manufacturers. "The market cannot support 130

different diamond brands, so we are likely to see many companies bankrupted by high costs."

Dilip Mehta, chairman of Rosy Blue, Antwerp, noted that the industry is entering an era of fundamental change, from an excess of supply over demand, to the reverse. "We've seen how rising demand helped De Beers liquidate nearly all its buffer stocks of diamonds, and assuming that demand keeps rising, production will not be able to keep up." Mr. Mehta warned that prices for diamonds will rise significantly in coming years, beyond the point where retailers and suppliers will be able to absorb them. **S. Lynn Diamond**, executive director of the Diamond Promotion Service, New York, said that the DTC has set a growth target of 50% in worldwide diamond jewelry sales—$84 billion—by the decade's end. **Ken Gassman**, director of research, Rapaport Group, New York, added that it is apparent that most of this growth will come from price increases, not rising unit sales, because of supply shortages.

Elliott Tannenbaum, manager of Schachter-Namdar, Israel, said that the shortages in quality rough diamonds will ultimately lead to a major reorganization of the industry, with major retailers and diamond suppliers vertically integrating. "By 2010, we will see suppliers taking major stakes in retail jewelers. By 2028, we will see a situation like the oil companies, where a few major players have operations integrated from mining to retail. Retailers not attached to major suppliers may have difficulty finding supplies." **Martin Rapaport**, publisher of *Rapaport Diamond Report*, New York, stressed that future retail competition will be geared more to marketing and branding initiatives, than to price. "In short, strategy will be more important than skill."

However, **Peter Gross**, vice president of the International Diamond & Jewelry Group of ABN AMRO Bank, Antwerp, said that the future is less worrisome than the *current* industry debt and inventory situation. He maintained that an excess manufacturing supply is causing the current climb in rough prices, even as large quantities of polished are still sitting in dealers' safes. "The rising cost of rough and lengthening credit terms of U.S. retailers have contributed to a very sharp rise in industry debt during the past year." Further, he indicated that increases in the cost of rough and in the inventory of polished stock are squeezing profitability from the industry. He asserted that diamond manufacturers must rein in the ever-lengthening credit terms demanded by retailers.

Synthetic diamonds from Gemesis Corp. of Sarasota, Florida (figure 43), and Apollo Diamond Inc., Boston, Massachusetts, were the other main subject of discussion. **Ed Bridge**, president of Ben Bridge Jeweler, Seattle, said that increasing numbers of synthetics and treated gems in the market are a challenge to retailers, adding that disclosure of such goods is necessary to maintain consumer confidence. **Carter Clarke** (chairman, Gemesis) and

Figure 43. Synthetic diamonds are being set into fine-quality jewelry, as shown by this tennis bracelet set with colorless natural and yellow Gemesis created diamonds, set in 18K gold. The bracelet contains 10.62 carats of created diamonds and 3.99 carats of natural diamonds. Courtesy of Gemesis Corp.

Bryant Linares (president, Apollo) both promised "full disclosure down the line" for all their products, including laser inscriptions identifying them as lab-created diamonds. Both also stressed that their products are designed to fill a consumer desire for high-quality diamonds at affordable prices. Mr. Clarke said his products will be priced similarly to G-color, VS-clarity diamonds of comparable weight; Mr. Linares said that Apollo had not yet determined prices for their products. However, **Terry Burman**, CEO of Signet Group, London, believed that the prices consumers will pay for synthetic goods cuts off far below manufacturer expectations. "We've found little consumer interest above $500."

William E. Boyajian, president of GIA, stressed that there is a legitimate place in the industry for synthetic and treated gems, provided they are disclosed. However, he added, there are rogue treaters who refuse to disclose treatments. The consequences of non-disclosure can be major, he noted, citing the damage to the emerald market caused by new filling practices, the collapse in prices for beryllium-diffused corundum, and the "volatile" reaction of the trade to HPHT-treated diamonds.

Russell Shor

ANNOUNCEMENTS

2004 AGTA Cutting Edge Award winners. The winners of the 2004 American Gem Trade Association Spectrum and Cutting Edge Awards were announced November 17 in New York City. The competition was held October 31–November 2, 2003, and a total of 564 submissions in all categories were considered.

The winners of the Cutting Edge Awards were, by division: Classic Gemstone: Allen Kleiman, A. Kleiman & Co., Boulder, CO; All Other Faceted Gemstones: Ben Kho, Kho International Ltd., Decatur, GA; Phenomenal Gemstones: Jeffrey Bilgore, Jeffrey Bilgore LLC, New York; Faceting: John Dyer, Precious Gemstones Co., Eau Claire, WI; Carving: Dalan Hargrave, Gemstarz, Spring Branch, TX; Combination: Andrew Gulij, Gemfix, Big Bear City, CA; Pairs and Suites: Matt Casteen, Raleigh, NC; Objects of Art: Ralph Wobito, Wobito Gems Ltd., Stouffville, Ontario, Canada.

Winning entries will be displayed during the 2004 AGTA GemFair Tucson, February 4-9, 2004.

***Professional Jeweler*'s Stone of the Year.** Starting in 2004, *Professional Jeweler* will select a Stone of the Year to be featured in the magazine's January issue. The stone will be chosen according to its contemporary importance in the gem trade and will be covered in a feature article with abundant photos showing its diversity of appearance, a pricing guide, and a fashion section. The initiative is designed to create excitement about colored stones. The 2004 Stone of the Year is sapphire (figure 44).

Afghanistan/Pakistan gem tour. In August-September 2004, Gary Bowersox of GeoVision Inc., Honolulu, Hawaii, will lead a three-week tour to colored gem deposits and marketplaces in Pakistan and Afghanistan. Visit www.gems-afghan.com/guidedtours.htm.

Figure 44. Professional Jeweler*'s Stone of the Year for 2004 is sapphire. This assortment, ranging from approximately 3 to 8.59 ct, illustrates the diversity of color shown by natural-color sapphires from various sources. Courtesy of James Alger Co. Inc.; photo by Robert Weldon*/Professional Jeweler.

Conferences

PDAC 2004. The Prospectors and Developers Association of Canada convention will take place March 7–10 in Toronto. Diamonds will be featured in a session called "Diamonds: Rooting Around for Carats," and also in presentations on geophysics and legal issues. The guest program will include a jewelry-making workshop. Visit www.pdac.ca/pdac/conv.

ICNDST-9 in Tokyo. The 9th International Conference of New Diamond Science and Technology will be held at Waseda University in Tokyo, Japan, March 26–29, 2004. Among the topics covered will be growth of diamond and diamond-like materials, as well as diamond processing and characterization. Visit www2.convention.co.jp/ICNDST-9.

BASELWORLD 2004. The BASELWORLD show will be held April 15–22 in Basel, Switzerland. GIA will host GemFest Basel on April 17, 4–6 pm at the Basel Convention Center, Hall Montreal. The program will include an update from the GIA Gem Laboratory, as well as an "Update on GIA's Diamond Cut Research." The event will conclude with a panel discussion, and be followed by a reception. During the show, *Gems & Gemology* editor-in-chief Alice Keller will be available at the GIA Booth in Hall 2, Stand W23. Visit www.baselshow.com.

GAC-MAC joint annual meeting. On May 12–14, 2004, in St. Catherines, Ontario, Canada, the Geological Association of Canada and the Mineralogical Association of Canada will co-host a conference that will include special sessions titled "Kimberlites and Diamonds: New Discoveries and New Developments" and "Rare Element Geochemistry and Ore Deposits." The latter session will include a short course and field trip to visit granitic pegmatites in Ontario, Canada. Visit www.stcatharines2004.ca.

GAA conference. The 58th Annual Federal Conference and Seminar of the Gemmological Association of Australia will take place May 13–16, 2004, in Perth, Australia. Visit www.gem.org.au.

Santa Fe Symposium. On May 23–26, 2004, in Albuquerque, New Mexico, this symposium will offer technical information on jewelry manufacturing procedures. Visit www.santafesymposium.org.

20th Colloquium of African Geology. Gemstones and small-scale mining will be among the topics covered in a seminar on "Earth Resources and Sustainable Development of Africa" at this conference in Orléans, France, June 2–7, 2004. Visit http://cag20.brgm.fr.

GEORAMAN 2004. This conference will take place June 6–11, at the University of Hawaii Manoa Campus in Honolulu. Applications of Raman spectroscopy to the identification of gem materials and minerals in ancient arts and archaeology will be among the wide range of topics covered. Visit www.soest.hawaii.edu/GEORAMAN2004.

Geoscience Africa 2004. Hosted by the University of the Witwatersrand in Johannesburg, South Africa, July 12–16, this conference will feature a symposium titled "Kimberlites, Diamonds and Mantle Petrology." Field trips to the Cullinan diamond mine and alluvial diamond deposits along the Orange River will be offered. Visit www.wits.ac.za/geoscienceafrica.

International Geological Congress. The 32nd Session of the International Geological Congress will be held August 20–28, 2004, in Florence, Italy. Symposia are planned that will cover gem materials, inclusions in minerals, and mineral spectroscopy. Visit www.32igc.org/default1.htm.

Gems of Pacific continental margins. The International Association on the Genesis of Ore Deposits will host a symposium titled "Gem Deposits Associated with the Pacific Continental Margins" at the Interim IAGOD Conference on Metallogeny of the Pacific Northwest: Tectonics, Magmatism & Metallogeny of Active Continental Margins. The conference will take place September 11–19, 2004, in Vladivostok, Russia. Visit www.fegi.ru/IAGOD.

Diamond 2004. A review of the latest scientific and technological aspects of natural and synthetic diamond (as well as related materials) will take place at the 15th European Conference on Diamond, Diamond-Like Materials, Carbon Nanotubes, Nitrides & Silicon Carbide, September 12–17, in Riva del Garda, Italy. Visit www.diamond-conference.com.

ICAM 2004 in Brazil. The 2004 International Congress on Applied Mineralogy will be held in Águas de Lindóa, Brazil, September 19–22, and will include a special session on gem materials. Pre- and post-conference field trips will tour colored gemstone and diamond deposits in the Ouro Preto and Diamantina areas, as well as agate and amethyst mines in Rio Grande do Sul State. Visit www.icam2004.org.

Exhibits

Turquoise at the San Diego Museum of Man. "The Turquoise Path/El Camino Turquesa: The Story of Turquoise in the Native American Southwest" will be on display at the Museum of Man in San Diego, California, through April 2004. The exhibit examines turquoise jewelry-making techniques and showcases the unique historical, social, cultural, and economic significance of this gem material. Visit www.museumofman.org.

Jade at The Field Museum. The newly renovated "Hall of Jade" will return to permanent exhibition at The Field Museum in Chicago beginning March 12, 2004. Featuring a collection of nearly 500 jade artifacts, the display explores the gem as a cultural symbol of prosperity, power, and virtue in China for more than 8,000 years. Visit www.fieldmuseum.org.

ERRATUM

The list of 2003 *G&G* Challenge Winners in the Fall 2003 issue (p. 251) contained two errors. Veronika Riedel's name was misspelled, and Arthur Spellissy, of South Freeport, Maine, was mistakenly placed in the list of winners for Maryland. *Gems & Gemology* apologizes for the errors.

2003 MANUSCRIPT REVIEWERS

GEMS & GEMOLOGY requires that all articles undergo a peer review process in which each manuscript is evaluated by at least three experts in the field. This process is vital to the accuracy and readability of the published article, but it is also time consuming for the reviewer. Because members of our Editorial Review Board cannot have expertise in every area, we sometimes call on others in our community to share their intellect and insight. In addition to the members of our Editorial Review Board, we extend a heartfelt thanks to the following individuals who reviewed manuscripts for *G&G* in 2003:

Dr. Curt W. Beck
Mr. George Bosshart
Ms. Dona Dirlam
Mr. Richard Fassler
Ms. Cecilia Gardner
Mr. Al Gilbertson
Dr. Gaston Giuliani
Mr. John Kim
Dr. Frank C. Hawthorne
Ms. Karin Hurwit
Mr. Bert Krashes
Ms. Terri Ottaway
Mr. Russell Shor
Dr. Chris Welbourn
Mr. Benjamin Zucker

Book REVIEWS

2003

Tiffany Flora & Fauna

*By John Loring, 256 pp., two vols., illus., publ. by Harry N. Abrams, New York, 2003. US$50.00**

John Loring has done it again. *Tiffany Flora & Fauna* is a beautiful two-volume set showcasing the best of Tiffany & Co.'s jewelry and *objets d'art*. The first book features Tiffany flora. Loring notes Tiffany's unofficial motto, "Mother Nature is the best designer," and clearly she has been the inspiration for countless Tiffany pieces. In fact, Edward C. Moore, Tiffany's head designer in the late 1800s, established one of the first design schools in the U.S., where he would often have students create studies of botanical specimens in pencil and watercolor. Moore himself was strongly influenced by Asian prints, and many of his original designs featured peonies, irises, and patterns reminiscent of Japanese and Persian art. In later years, one of his students, Paulding Farnham, was highly successful in designing enameled floral jewels, particularly orchids, for Tiffany. Several of Farnham's orchid brooches are featured in the pages of this book.

Of course, the use of botanical elements was not confined to jewelry. Tiffany glass and silver also featured amazingly realistic flowers and fruits. Most notable is the Louis Comfort Tiffany–designed glass screen called "Three Seasons," which was displayed at the 1900 Paris Exposition.

The second book focuses on fauna in Tiffany designs. Tiffany & Co. jewelry has always featured animals of all kinds. Indeed, their contemporary "Nature" collection includes butterflies, salamanders, dragonflies, birds, turtles, and frogs in diamond-pavéed platinum. Especially pleasing in the fauna volume are the fanciful creatures designed by Jean Schlumberger, Donald Clafin, and Elsa Peretti.

Both volumes contain design sketches from the Tiffany archives. Loring also includes examples of Audubon paintings, Asian prints, and botanical photographs that served as inspiration for some Tiffany designers. The photos in both volumes are simply magnificent, making the books a visual delight. In these pages, it's easy to see why Tiffany & Co. has maintained its position as one of the world's most popular retailers of fine jewelry and luxury objects for more than a century.

JANA E. MIYAHIRA-SMITH
Gemological Institute of America
Carlsbad, California

Burma Ruby: A History of Mogok's Rubies from Antiquity to the Present

By S. K. Samuels, 254 pp., illus., publ. by S.K.S. Enterprises, Tucson, AZ, 2003. US$45.00

The author, a native of Burma, has used his wealth of personal experience in compiling this book. Dr. Samuels lived under the British rule of Burma and, later, its occupation by the Japanese during World War II. After the war, he earned a medical degree from the University of Rangoon and traveled around the Mogok district. In 1960, he emigrated to the U.S., and did not return to Burma (now Myanmar) until more than 20 years later.

In *Burma Ruby*, Dr. Samuels looks at the Mogok mines from the local perspective, in contrast to the occidental histories put together by the "noble enterprise" of colonialism. He tells much of this history via anecdotes and personal communications, using a variety of unique Burmese sources as well as more traditional references.

In the first chapter, "Lure of the Ruby," one of the author's major points is that many references to ruby in antiquity fail to note the actual sources of the material. He concludes that, since Sri Lankan rubies are predominantly pink, many rubies in the ancient European references might be from Mogok. Unfortunately, this deduction ignores the fact that some Sri Lankan rubies are decidedly red; he also does not take into account any of the African localities, which produce rubies of very similar look to Mogok. As one can imagine, attempting to document anecdotes covering 1,000 years of history is no easy task.

The second chapter is a concise natural history of the geography, climate, topography, and geology of Myanmar, as well as the ethnic and linguistic groups that make up the complicated land of the ruby. The next 80 pages deal with the history of Burma leading up to and through World War II, again relying on local Burmese legends and histories,

*This book is available for purchase through the GIA Bookstore, 5345 Armada Drive, Carlsbad, CA 92008. Telephone: (800) 421-7250, ext. 4200; outside the U.S. (760) 603-4200. Fax: (760) 603-4266.

prefacing them with this statement: "Not much credence can be given to such stories, but they do suggest that rubies and other precious gems were known, valued, and used by inhabitants of the country for a long time."

The following chapter, "Developing the Post-War Gem Trade," first describes the escalating political and economic problems leading up to the March 1962 military coup and beyond. It then looks at development of the Myanmar Gems Corporation and the auctions held by the Union of Myanmar Economic Holdings Limited.

In the "Stone Tract" chapter, the author discusses the Mogok area itself, covering the geography, geology, and mines. Briefly mentioned are the Mong Hsu mines, which today produce most of the world's rubies (albeit, treated). At the end of the chapter, he discusses rubies and their classification, as well as the sapphires of Burma.

Next is a section of unnumbered pages with 33 color plates. Most are original photos by the author, and all have interesting gemological themes, including pictures of the palaces, King Thibaw's ruby-encrusted slippers, and a flawless sapphire of approximately 20 ct, offered for $100,000 in 2002 by a private party. The tragedy is the poor color reproduction. Fortunately, the black-and-white photos throughout the book are of better quality.

In "Properties of Burmese Rubies and Sapphires," Dr. Samuels mixes gemology with emphasis on local customs. For instance, he mentions that the color of ruby is due to impurities such as chromium, but then goes on to discuss the term *pigeon's blood*. He is accurate in commenting that, while such terms are relics of the past, they carry a certain romanticism that is very important to gemstones.

The chapter titled "Smuggling, Heat Treatment, and Provenance of Burma Rubies" presents some amusing stories, including how the 496.5 ct SLORC ruby (named for the country's State Law and Order Restoration Committee) came to be spirited out of the country and back again. Heat treatment and provenance are discussed briefly, but not from a scientific standpoint. The chapter ends with a list of five local gem labs that do origin reports, along with addresses.

"The Gem Trade in Modern Burma" covers the economic structure of Burma, exchange-rate issues, and the country's poor economic performance of the last decade. The author also covers the annual gem emporium, but only in general terms (mostly just in table form), without any photos or depictions of specifics.

"Buying Gems in Burma" includes a short history of Rangoon, plus the ins and outs of trying to buy at the MGE auction or at Rangoon's Gems Museum. Dr. Samuels gives a rather simplistic summation of three of the C's (color, clarity, and cut), plus precautions to take when buying.

Following the author's closing remarks are various appendices, especially of interest for Burma-philes. There is also a somewhat limited bibliography. One major flaw of the book, given the breadth of issues it covers, is that it lacks an index.

All in all, while there is some interesting information here, the book would have benefited greatly from better editing and production.

WILLIAM LARSON
Pala International
Fallbrook, California

Gems from the East and West: The Doris Duke Jewelry Collection

By Janet Zapata, Ulysses Dietz, and Zette Emmons, 120 pp., illus., publ. by the Doris Duke Charitable Foundation, New York, 2003. US$27.50
www.newportrestoration.com/jewelryexhibit.html

When American Tobacco Company and Duke Power magnate James B. Duke died in 1925, he left his fortune to his only child, Doris. At the tender age of 12, she became the richest girl in America. Years after her death in 1993, the heiress remains an enigmatic figure, despite many biographies and notwithstanding a family legacy of achievement in education and charity.

Among her many passions, Doris Duke was undeniably fond of jewelry. This catalog, the Doris Duke Charitable Foundation's third publication about her collections, represents a collaborative effort by jewelry historian Janet Zapata, the Newark Museum's curator of decorative arts Ulysses Dietz, and Indian jewelry scholar Zette Emmons. Organized to reflect Duke's heritage and the evolution of her personal style, it memorializes the one-time touring exhibit of her collection and illustrates a rarefied segment of American society—a stratum populated by persons whose lives were defined by unabashed wealth and privilege.

Two essays set the stage. The first describes the Duke family; the second recounts events in Doris Duke's life that lend meaning to the collection. For example, Duke's yearlong honeymoon around the world at age 22 is described as the sentinel event that ignited a lifelong passion for Indian, Southeast Asian, and Islamic arts.

The first 110 images capture the collection's more significant pieces, which benefit from larger photographs and more extensive narrative than the 200-plus pieces that were not included in the exhibit. Period photos of the Duke family and estates mark the passage from Gilded Age gentility to the acquisitive reaches of the family's 20th century prosperity.

Heirloom cameos and carved coral demiparures of Civil War–era neoclassicism give rise to the belle époque jewelry favored by Doris's mother. Cartier's 1908 platinum festoon necklace, said to be one of the most opulent of its time in the New World (and set with diamonds provided by J. B. Duke), symbolizes the young nation's rising economic status, celebrating its emerging royalty rooted in railroads, oil, tobacco, and ore.

Doris Duke's personal jewelry is described as an "unintentional collection." Aside from her Indian and Asian pieces, no unifying theme emerges. The design houses of Cartier and Van Cleef & Arpels are well represented in Duke's earlier years, when she favored classical glamour. Later,

flamboyant pieces from Verdura and David Webb suggest the collector's greater comfort with extravagant flair and independence.

Above all, the mystical beauty of Indian and Southeast Asian jewelry held sway over Duke. Dramatic pieces from her Asian travels and acquisitions include hand ornaments as well as ruby and emerald necklaces that reveal a passion for exotica and regalia.

Sketches and diagrams enhance the book's multi-sourced photography. Archival images of the Duke estates and the few photos of the reclusive Duke wearing her jewelry add context to the compilation.

The Duke collection is scheduled to go to auction at Christie's New York in the spring of 2004. Those fortunate enough to have viewed the 2003 exhibit will savor Gilded Age and modern glamour as well as Asian treasures. The catalog also offers ample content for jewelry designers and historians, collectors, curators, appraisers, auction house associates, and admirers of Eastern arts.

MATILDE PARENTE, G.G.
Indian Wells, California

Minerals of the World

By Ole Johnsen, 439 pp., illus., publ. by Princeton University Press, Princeton, NJ, 2002. US$49.50

This good-looking field guide was written by well-known mineralogist Ole Johnsen of the University of Copenhagen. It is divided into three parts: "Mineralogy & Crystallography," "Mineral Descriptions," and "Tables." The first part covers "What is a mineral?" as well as crystal geometry, the seven crystal systems, formation and growth, and the chemical, physical, and optical properties of crystals. In the second part, minerals are listed according to their chemical families, such as carbonates, native elements, and the like; the silicates are subdivided into cyclosilicates, tectosilicates, and others. The tables in the third part cover common minerals and their properties, with one table for minerals with metallic or submetallic luster and a second for those that are nonmetallic. There is also a periodic table of the elements. The book concludes with a glossary and an index.

The softcover edition is well bound and uses good paper stock. It is bigger than most field guides, which makes it harder to pack, but you wouldn't want to ruin it in the field in any event. The inside boasts more than 600 color photos and diagrams. Most of the images show good examples of the more than 500 minerals included and are helpful in identification. The color rendition is better than in other books of similar import. The crystal and atomic diagrams are quite effective in creating an understandable visual image.

A book with the (somewhat overused) title *Minerals of the World* should give a balanced representation of all important minerals and their prime localities. This guide is unusually rich in minerals and localities for Scandinavian countries, especially Norway. However, many will appreciate their inclusion here, as they are often given scant coverage in other works. Because nearly all specimens depicted are part of the Geological Museum of the University of Copenhagen—and the author admits his bias in the preface—the selections in this book are understandable.

Some errors, mostly minor, were noted. A few involved incorrect or misspelled localities. For instance, *Stirling* was used for Sterling Hill, New Jersey, and the Sterling mine in Antwerp, New York. On page 233, the text correctly states that lazulite comes from the Yukon, but it places the Yukon in the U.S. rather than Canada. There are also errors of a technical nature, mostly gemological. The purple of amethyst quartz is not due to iron alone but to iron in unison with radiation-induced color centers. The term *fire opal* does not properly apply to opal with intense play of red or orange but rather to opal that has a red, orange, or yellow body color—with or without play of color. The orthoclase in figure 567 does not show labradorescence but rather adularescence.

There are also some notable omissions. For example, important localities for titanite (sphene, not an obsolete name as this book states)—such as Brazil, Madagascar, and Pakistan—were not included. There is no mention of Afghanistan or Pakistan as sources of tourmaline, and the species liddicoatite is somehow omitted. Afghanistan, Madagascar, and North Carolina are not mentioned as spodumene localities. There are important amber sources besides the Baltic. The Maori of New Zealand are indeed well known for their carvings of nephrite, but the author inexplicably fails to touch on far more important Chinese nephrite carvings. Of jadeite jade, one of the rarest and most valuable of all gems in its finest qualities, the author says merely that it "is a highly appreciated material for carving."

Despite these negatives, *Minerals of the World* has a tremendous amount to offer. On a mineralogical level, this is a fine introductory work, especially since it was written to show minerals and their properties that can be seen by the unaided eye or with a loupe. Those who appreciate minerals in general or want to learn more about the minerals of Norway, Greenland, and other countries in that part of the world will especially enjoy this book.

MICHAEL T. EVANS, G.G.
Gemological Institute of America
Carlsbad, California

OTHER BOOKS RECEIVED

Cultured Pearl: Charm of the Pearl. *By Shigeru Akamatsu, 179 pp., illus., publ. by Shinju Shinnbun Co., Tokyo, 2003 (in Japanese). 3,800¥. Fax: (+81) 03-3834-6493.* The author is a well-known veteran of the pearl industry, having served with K. Mikimoto & Co. for decades. In this book, he surveys the spectrum of cultured pearls, covering the history of the pearl (natural and cultured), the science of the pearl, the pearl culturing process, quality standards, and more.

STUART OVERLIN

Gemological **ABSTRACTS**

2003

COLORED STONES AND ORGANIC MATERIALS

Classification of amber based on thermal analysis. E. Ragazzi, G. Roghi, A. Giaretta, and P. Gianolla, *Thermochimica Acta*, Vol. 404, No. 1/2, 2003, pp. 43–54.

It is difficult to determine the chronological age of fossil resins by chemical analysis alone, because amber samples of the same geologic age may have experienced different chemical reactions and temperatures during their fossilization. This study was undertaken to evaluate the possibility of classifying ambers by thermal analysis techniques. Thermal analysis involves the detection of small changes in the weight of a sample as it is subjected to controlled heating. Two methods—thermogravimetric (TG) and differential thermogravimetric (DTG) analyses—were used for 13 amber samples of various ages (present day to Triassic, 225 million years ago) and eight geographic origins. Using the DTG method, all samples exhibited a main weight-loss event at about 400°C, but the exact temperature varied according to age (i.e., the temperature increased linearly with age). The results suggest that thermal analysis provides an additional way to characterize fossil resins. *JES*

Death and taxes: The case of the depletion of pearl oyster beds in sixteenth century Venezuela. A. Romero, *Conservation Biology*, Vol. 17, No. 4, 2003, pp. 1013–1023.

Commercial pearling began off the coast of what is today Venezuela when Christopher Columbus brought a number of pearls back to Spain from his third voyage to the New World in 1498. From 1508 to 1520, large numbers of Lucayan Indians from the Bahamas were taken by Spanish settlers to Cubagua, an island off the Venezuelan coast, to work as pearl divers. The Lucayans were prized for their deep-diving skills. By 1518, so

This section is designed to provide as complete a record as practical of the recent literature on gems and gemology. Articles are selected for abstracting solely at the discretion of the section editor and his reviewers, and space limitations may require that we include only those articles that we feel will be of greatest interest to our readership.

Requests for reprints of articles abstracted must be addressed to the author or publisher of the original material.

The reviewer of each article is identified by his or her initials at the end of each abstract. Guest reviewers are identified by their full names. Opinions expressed in an abstract belong to the abstracter and in no way reflect the position of Gems & Gemology *or GIA.*

many Lucayans had been forced from the Bahamas that the islands were left nearly deserted. The divers worked six per boat, dawn to dusk. In one or two weeks, each boat would typically harvest some 35,000 oysters from depths of 15–22 m.

In 1515, the Spanish government began keeping precise tax records and recording pearl production from the area. That year saw the equivalent of 100 kg of pearls harvested. Production increased greatly after 1520, when the Spanish military established a fort at Cubagua to secure the pearling area and the town of Nueva Cádiz. Harvesting of oysters increased dramatically over the next several years, peaking at 1,650 kg in 1527. Production, however, fell off just as sharply afterward. To revive it, Spanish King Charles V approved the use of dredges to work the pearl beds. By 1531, depletion of the oyster beds was well underway. Production had fallen to about one-third of the peak, causing the local administration to place severe restrictions on pearling activities. This is possibly the first attempt at conservation in modern history. Nevertheless, by 1539 the oyster beds were almost totally decimated and fewer than 50 people remained on the island; in 1543, the once-thriving colony was abandoned. Eventually, the habitat that had been dominated by the *Pinctada imbricata* pearl oyster was taken over by the stronger, non-pearl-bearing turkey-wing mussel *Arca zebra*. *RS*

Time-resolved luminescence of Cr^{3+} in topaz $Al_2SiO_4(OH,F)_2$. M. Gaft, L. Nagli, R. Reisfeld, G. Panczer, and M. Brestel, *Journal of Luminescence*, Vol. 102–103, 2003, pp. 349–356.

This article reports the study of various luminescence centers in natural topaz crystals (two colorless, four yellow, and one orange) using laser-induced time-resolved luminescence spectroscopy. With this method, various luminescence centers in minerals can be detected according to their unique decay times. In the colored samples with elevated Cr contents, the study showed evidence of Cr^{3+} and Cr-Cr pair centers. Radiation-induced centers also were discerned in a yellow sample and determined to be thermally unstable; these centers could possibly be related to Mn^{4+} and/or V^{2+} impurities. *AI*

DIAMONDS

Diamond-bearing dykes. M. Marx, *Rough Diamond Review*, No. 1, June 2003, pp. 21–24.

Diamonds are usually mined from primary kimberlite (or lamproite) pipes or from secondary deposits along rivers, beach terraces, or the sea bed. Although rare, dike deposits can also be important. Kimberlite dikes are found on all continents, but currently only four dike mines, all in South Africa, are in production. One of these is the Messina mine, where diamond-bearing kimberlite is being extracted at ~700 m below the surface. When the Snap Lake mine in Canada comes into production in a few years, dikes may produce ~1.5 to 2.0 million carats per year (~1.5% of the world's supply of diamonds).

A dike network represents the deep root zone of a volcanic event that can be associated with the formation of a diamond-bearing pipe. If a pipe is completely eroded, the underlying dikes may remain along with their diamonds and indicator minerals (e.g., pyrope, Cr-diopside). However, kimberlite dikes are difficult to find because they are typically weathered, frequently buried beneath sand or other types of cover, and have relatively small surface expressions. Although they may form linear features up to several km in length, they are also very narrow (often <1 m). Underground mining—mostly by the "shrinkage stoping" method—is more efficient than open-pit mining because dikes are narrow and near vertical, so the latter would require excessive stripping ratios. *CT*

Getting the most out of our diamonds: Namibia, De Beers and the arrival of Lev Leviev. M. Boer and R. Sherbourne, *Institute of Public Policy Research, Briefing Paper No. 20*, September 2003, 20 pp., www.ippr.org.na.

Although its diamond production is relatively small in volume (1.7 million carats in 2002), Namibia is the world's sixth largest producer by value, at $472 million in 2002. The average value of Namibian diamonds is ~$280 per carat, nearly twice that of the next highest value producer (Angola). De Beers and predecessors have controlled Namibia's diamond production for over 80 years, but new players in the diamond market may offer the country a better return on its resources. The future of Namibia's diamond production lies in the seabeds just offshore. Currently over half (55% in 2002) of the country's output is extracted offshore. The government is also trying to encourage diamond cutting to increase employment. However, labor costs are not competitive with low-wage nations like China and India.

The Namibian government and De Beers together mine and manage the vast majority of the country's diamond resources through a 50-50 corporation called Namdeb. Namdeb, however, issues no public reports, so it is difficult to ascertain whether the government is getting the most out of its diamonds. An alternative may be offered by Lev Leviev, an Israeli industrialist who has already opened a diamond-cutting operation there. He became involved in Namibia's diamonds through an interest in the financially troubled Namco Corp., which formerly operated an offshore mining concession. Namibia has done well through its partnership with De Beers, and Leviev remains a relatively new, unknown competitor. *RS*

A guide to rough diamond classifications. *Rough Diamond Review*, No. 1, June 2003, pp. 9–12.

The classification of diamond rough provides a framework for valuing and trading stones. For gem diamonds, the De

Beers Central Selling Organisation (CSO) uses several value-classifying factors: estimated yield (the weight of the polished product as a percentage of the rough weight), processing costs, and quality (i.e., size, color, and clarity factors). Traders and manufacturers have developed their own categories to describe and value rough diamonds. However, all classifications are based on four commonly recognized terms and descriptors:

- *Size:* Most smaller stones are screened and assigned to a sieve size or class, based on either the DTC (De Beers) or Antwerp (Christensen) sieve-size classification. Stones above 0.66 ct are weighed individually, as accuracy of weight is critical to valuation.
- *Quality:* Quality is judged with back-lighting. The quantity, position, nature, and severity of inclusions dictate a stone's quality. Diamond qualities are broadly grouped into one of the following classifications: Gem, Near Gem, Rejections, and Industrial (or Bort). Subcategories also have been established (i.e., first, second, third, and fourth qualities).
- *Type:* Type primarily encompasses shape, which also reflects a relationship with yield and the manufacturing processes required. The six principal types are sawables, makeables, macles, flats, chips, and clivage.
- *Color:* Color is judged by placing rough diamonds on a white surface without any back-lighting. The color of most diamonds falls in the range of colorless to yellow or colorless to brown; other color terms include *white*, *light brown*, *Cape*, and *fancy*. Each group has subcategories.

In general, all diamond deposits contain most of the quality and type categories in varying proportions, but not all color groups. Industrial diamonds are classified differently. *CT*

Indicator mineral and till geochemical dispersal patterns associated with the Ranch Lake kimberlite, Lac de Gras region, NWT, Canada. M. B. McClenaghan, B. C. Ward, I. M. Kjarsgaard, B. A. Kjarsgaard, D. E. Kerr, and L. A. Dredge, *Geochemistry: Exploration, Environment, Analysis*, Vol. 2, No. 4, 2002, pp. 299–320.

Diamond indicator minerals in glacial till collected around the large (12.4 ha; 31 acres) Ranch Lake kimberlite in the Lac de Gras region, NWT, Canada, define a spectacular dispersal train according to the length (70 km), narrow ("ribbon") shape, and abundance of indicator minerals (thousands of mineral grains in a 10 kg till sample). Cr-diopside and pyrope are the most abundant indicator minerals, while chromite is less abundant, and Mg-ilmenite is rare; most indicator minerals occur in the 0.25–0.50 mm fraction of the till. At its head, the train is 500 m wide and gradually widens to 2 km at 20 km down-ice. The lateral edges of the train are sharply defined by the presence or absence of the indicator minerals in the till. Patterns for Cr-diopside and pyrope abundances are similar, and concentrations reach their highest levels 15–20 km down-ice. The location of these high concentrations is unusual, because most studies indicate that the highest concentrations of indicator minerals in till occur immediately down-ice from the kimberlite, after which there is a gradual decrease due to dilution. The great length of the dispersal train suggests it was formed by a single ice flow event.

Not all kimberlites in the Lac de Gras region have indicator mineral dispersal trains, and of those that do, few are as well developed or as well preserved as that at Ranch Lake. Nevertheless, the use of till dispersal patterns is popular for diamond exploration in the glaciated terrains of Canada because of the effectiveness, versatility (both regional- and local-scale surveys), and relatively low cost. *AAL*

Laser processing of diamonds. J. Chapman, *Rough Diamond Review*, No. 1, June 2003, pp. 25–28.

Modern diamond factories have replaced traditional hand-fashioning of diamonds with laser systems that can perform many steps in the cutting process with precision. The capital expenditure for a laser system specifically designed to process diamonds is high (US$60,000–100,000), but there are numerous benefits, including high throughput rates, unattended operation, short training periods compared to traditional techniques, and insensitivity to crystal orientations. Most systems used for diamond processing employ a YAG laser with a beam diameter of 1–4 mm emitting at an infrared wavelength. The systems are supported by custom software for sawing, kerfing, bruting, and inscribing.

The advantages of lasers in each stage of the fashioning process are indisputable. For example, sawing with lasers can be achieved in any crystal direction, and bruting with lasers requires half the time of traditional bruting. However, there are occasional disadvantages. For example, during laser sawing diamonds may crack, especially those that are internally stressed, such as brown or pink stones. Additionally, after laser bruting, the girdle is sometimes slightly tapered and thus is unsuitable for the dops used in automatic polishing machines. In the future, the industry may adopt ultraviolet lasers, which recently have seen major developments in manufacture and reliability. UV lasers have the advantage of ablating (i.e., removing) diamond by a process of atomic disassociation rather than by thermal vaporization. This could decrease sawing weight loss to the range of 1–2%, compared to the 4–5% seen with current laser technology. *CT*

Morphology of diamond crystals from the Bingara Range, northern New South Wales, Australia. J. D. Hollis, *Australian Gemmologist*, Vol. 21, No. 9, 2003, pp. 350–359.

The crystal morphology of 300 small (average 0.13 ct) euhedral diamonds selected from over 8,700 crystals from

Mesozoic gravels at the Monte Christo prospect, Bingara, New South Wales, reflects progressive chemical corrosion of primary forms. Etching and resorption features, which in some cases result from a loss of more than 50% of the original size of the diamonds, were acquired during complex formational and eruption events. Many of the forms (illustrated in numerous line drawings) are those typical of kimberlitic and lamproitic diamonds worldwide, but some unusual features also are described. Some give evidence of their probable eruption histories in an unorthodox mobile-belt setting, far removed from cratons. *RAH*

The pressures and temperatures of formation of diamond based on thermobarometry of chromian diopside inclusions. P. Nimis, *Canadian Mineralogist*, Vol. 40, 2002, pp. 871–884.

Mineral inclusions in diamond have been used to estimate the pressure and temperature conditions of diamond formation in the earth's mantle. In most instances, this estimate requires that data be obtained from at least two syngenetic mineral phases in equilibrium. Finding diamonds with appropriate inclusion pairs is difficult, and there are additional challenges in collecting and interpreting the compositional data. In this article, the author uses a thermobarometry method that relies on just one inclusion phase (chromian diopside, a clinopyroxene), and he presents an analysis of published electron-microprobe data for more than 100 clinopyroxene inclusions in diamonds from worldwide occurrences. The results of this analysis appear to be consistent with estimates of mantle temperatures and pressures determined by other methods.

Use of this clinopyroxene thermobarometer may also have implications for diamond exploration strategies, since mantle-derived pyroxene recovered as an indicator mineral can be analyzed to see if there is evidence of a thermal or metasomatic event that occurred in the mantle which would have led to a resorption of diamond (thus indicating an unlikely target for diamond potential). *JES*

Sierra Leone diamond sector financial constraints study. Prepared by Management Systems International under U.S. Agency for International Development Cooperative Agreement 636-A-003-00003, June 2003, 52 pp., www.peacediamonds.org (click on "Links and Publications").

Harnessing Sierra Leone's diamond wealth to benefit its citizens has been an elusive goal for three-quarters of a century. The country's diamond deposits, generally rich in larger, high-quality goods, are found in easily looted alluvial pockets spread across a wide swath of the nation. What is more problematic, nearly all the nation's commerce—especially diamonds—has been controlled by a coterie of Lebanese traders. And, tragically, the rebel group RUF used diamonds to help fund a brutal civil war that ended in 2002. Last year, an estimated US$300–320 million in diamonds were extracted from Sierra Leone, with 85–90% of that total either smuggled out or "legally" exported at grossly understated values to avoid taxes.

The U.S. Agency for International Development and the U.K. Department for International Development, in cooperation with the government of Sierra Leone, nongovernmental organizations, and local officials, are trying to overhaul the country's diamond production to finally accomplish more equitable distribution of its diamond wealth. This study, conducted by Chaim Even-Zohar (Tacy Ltd. Consultants, Ramat Gan, Israel), offers a set of solutions on how to tackle the massive hemorrhaging of diamonds and cash from Sierra Leone.

Problems:

1. The diamond areas are still unregulated. An estimated 300,000 diggers have returned to the alluvial fields, thwarting any efforts at control.
2. Many of these diggers are debt-bonded to local dealers and exporters, who acquire these diamonds for a fraction of their sales value.
3. Virtually all diamond business is conducted in cash, and money laundering occurs on a massive scale.
4. The small groups of exporters and dealers who control an estimated 80% of the trade all sell to affiliates in Antwerp, Switzerland, Dubai, or other markets. These groups also squeeze out competition and keep local prices artificially low, resulting in huge profits from sales in diamond centers.
5. The government is ill-equipped to deal with managing its diamond resources, and its banking system remains in a shambles.

Recommendations:

1. Invite major players (De Beers, Rio Tinto, etc.) to serve as marketing alternates to the local cartels that control most exports. This would promote competition and help protect small miners. Local cartels could not intimidate large multinationals.
2. Reform finance and credit systems to bring in capital and end the debt-bondage system that has existed for years. These reforms must be backed by large banks to ensure compliance and resist local pressures to maintain the status quo.
3. Establish paper trails on cash transactions to reduce the potential for money laundering.
4. Train locals in diamond valuation.

The report also reviews the history of Sierra Leone diamond production. *RS*

The significance of mineral inclusions in large diamonds from Yakutia, Russia. L. A. Taylor, M. Anand, P. Promprated, C. Floss, and N. V. Sobolev, *American Mineralogist*, Vol. 88, No. 5–6, 2003, pp. 912–920.

It is generally accepted that mineral inclusions in diamonds are syngenetic (i.e., formed contemporaneously and

under the same conditions of temperature and pressure, and from the same genesis) with their diamond hosts. On the basis of this premise, these inclusions are considered pristine, as they have presumably been isolated since their encapsulation. Among the several applications of this concept is the assumption that the inclusions and their host diamonds are identical in age.

However, this article seriously questions the syngenetic relationship between diamonds and these inclusions, based on the interpretation of inclusion chemical data obtained with electron and ion microprobes. The inclusions used in this study, primarily garnets of harzburgitic paragenesis, were obtained from large (10–200 ct) diamonds from three kimberlites (Udachnaya, Mir, and Aikhal) in Yakutia. The most striking chemical feature of the garnet composition is the distribution pattern of their rare-earth elements, which is sinusoidal. These patterns are obtained from all harzburgitic garnets worldwide, both within and independent of diamonds, and are indicative of a complex origin for the garnets, including partial melting and metasomatic enrichment. Such events are believed to have occurred *prior* to their encapsulation in diamond. This result is taken as proof that basically all harzburgitic garnet inclusions are nonsyngenetic with their diamond hosts. If confirmed, these results may have significant ramifications for current concepts relative to conditions and age of diamond formation. *AAL*

X-ray diamond recovery techniques. A. Clegg, *Rough Diamond Review*, No. 1, June 2003, pp. 14–17.

Diamond has physical and chemical properties that permit several potentially successful recovery techniques. These properties include a hardness of 10, a non-magnetic and hydrophobic nature (i.e., will not be wetted by water and will stick to grease), and a reasonably high specific gravity (3.52). Historically, this enabled recovery based on the use of grease tables and belts, and heavy-media separation. However, these methods were not suited to the arctic climates of the former Soviet Union where, starting in 1958, X-ray sorting machines were developed based on the fact that most diamonds will fluoresce when exposed to X-rays. Thus, when crushed rock or gravel containing diamonds passes through an X-ray beam, the diamonds can be detected by their fluorescence and subsequently recovered.

The first Soviet X-ray sorters were extremely crude and hazardous by today's standards (e.g., operators would hand pick any fluorescing particle off a belt and be exposed to the high-energy X-rays). Later automated processes improved not only in safety but also in security. Currently, the diamonds are separated from ore by a puff of compressed air (activated by a light-sensitive photomultiplier tube) that blows the diamond into a collection chamber. Modern diamond X-ray sorters are tailored for the type of ore being processed (e.g., small-sized stones, large tonnages, wet or dry ore), with recovery of over 98% of the diamonds. *CT*

GEM LOCALITIES

CO_2–H_2S–COS–S_8–AlO(OH)-bearing fluid inclusions in ruby from marble-hosted deposits in Luc Yen area, North Vietnam. G. Giuliani, J. Dubessy, D. Banks, H. Q. Vinh, T. Lhomme, J. Pironon, V. Garnier, P. T. Trinh, P. V. Long, D. Ohnenstetter, and D. Schwarz, *Chemical Geology*, Vol. 194, No. 1–3, 2003, pp. 167–185.

Gem-quality rubies have been mined in the Luc Yen area of Vietnam since 1987. They are found in primary deposits hosted by Cambrian-age metasediments, or in associated placer deposits. In the former, ruby occurs in marble lenses interlayered with amphibolites within garnet-mica schists and gneisses. Typical associated minerals include phlogopite, dravite, graphite, pyrite, margarite, and calcite. These and other minerals can occur as inclusions in the rubies.

Twenty-five representative rubies were selected for fluid-inclusion analysis using microthermometry, Raman and infrared spectroscopy, and chemical analysis techniques. Primary and secondary fluid inclusions provided evidence of CO_2–H_2S–COS–S_8–AlO(OH)-bearing fluids containing daughter minerals such as native sulfur and diaspore, but little water. The ruby is inferred to have grown from a CO_2-rich and water-poor fluid that was at equilibrium with Na-Ca-Cl salts (in the form of evaporitic minerals). Aluminum was transported in this fluid at high temperatures and pressures (thought to be on the order of 500–600°C and 3–5 kbar) to form the ruby. There is no evidence that corundum mineralization involved the magmatic rocks exposed in the area. Ruby crystallized within the marble, which acted as a closed system.

JES

Geology of an amber locality in the Hukawng Valley, northern Myanmar. R. D. Cruickshank and K. Ko, *Journal of Asian Earth Sciences*, Vol. 21, No. 5, 2003, pp. 441–455.

Amber ("burmite") from the Hukawng Valley in northern Myanmar has been known since at least the 1st century AD. It is currently being produced from Noije Bum, a hill located about 20 km southwest of the town of Tanai. This hill was first documented as a locality for amber in 1836, and it has remained the principal source in the country since that time. The two authors visited the site in April 2001. Based on geologic and fossil evidence, the rocks hosting the amber are Cretaceous in age (as opposed to a Tertiary age inferred by geologists who visited the locality between 1892 and 1930). The amber is found along one horizon (about 1 m thick) in a series of steeply dipping clastic sedimentary rocks. The deposit is being worked from an open pit by a small group of miners using manual methods.

The amber occurs as small discoid-shaped clasts ranging up to several centimeters in diameter. The clasts are

oriented parallel to the bedding of the host rocks. There is little evidence that the shape of the amber clasts has been modified due to transport from another location. The amber is typically reddish brown, with various shades of yellow, orange, and red also occurring. These colors range from light to dark, and the material can vary from transparent to opaque. Insect fossils are found in the amber, but most are microscopic in size. The amber is thought to have been deposited along with fine clastic sediments along the floors and banks of tidal channels in a nearshore marine environment. *JES*

Genesis and gemmology of sapphires from the Nezametnoye deposit, Primorye region, Russia. A. Khanchuk, B. Zalishchak, V. Pakhomova, E. Odarichenko, and V. Sapin, *Australian Gemmologist*, Vol. 21, No. 9, 2003, pp. 369–375.

Research into inclusions in sapphires from a placer deposit at Nezametnoye in the Russian Far East is reported, together with a study on the heavy accessory minerals in the underlying gold-bearing granite porphyries. Other minerals found with the sapphires include zircon and spinel. This is the only deposit of gem-quality corundum, spinel, and zircon presently known in Russia.

The sapphire inclusions were identified as columbite, albite, zircon, Zn-bearing hercynite, rutile, and glass. Based on the compositions of these inclusions and on the unusual occurrence of corundum as an accessory in the granite porphyries, it is concluded that the placer sapphires originated from rare-metal pegmatites, greisens, and metasomatic rocks associated with the widespread Mesozoic granitic bodies in the area. *RAH*

Horse-tail inclusions in demantoid garnet from Val Malenco, Italy. P. W. O. Hoskin, R. H. Grapes, H. Catchpole, and J. Klaudius, *Journal of Gemmology*, Vol. 28, No. 6, 2003, pp. 333–336.

Gem-quality demantoid garnets from the Malenco Valley, northern Italy, may contain fibrous hair-like inclusions. These inclusions were assumed to be byssolite (tremolite-actinolite) asbestos by analogy with Russian demantoids. However, X-ray powder diffraction analysis of the matrix material in which the garnets are found, as well as electron-microprobe analysis of the inclusions themselves, showed that both the matrix material and the fibrous inclusions are chrysotile (asbestiform serpentine).

Optical examination of the chrysotile inclusions in transmitted light revealed that they have a light green to brown color. Although the authors confirmed the presence of chromium (0.03–0.84 wt.% Cr_2O_3) in their garnets—the primary cause of color in demantoid—they found no correlation between the intensity of the green color and Cr_2O_3 abundance. Instead, they believe that the color variations are related to the relative abundance of the green-brown chrysotile inclusions. *WMM*

Iron-rich chrysoberyl from Kalanga Hill, Muyombe District, north-eastern Zambia. V. Žáček and S. Vrána, *Neues Jahrbuch für Mineralogie Monatshefte*, No. 12, 2002, pp. 529–540.

Abundant chrysoberyl has been found in a granitic pegmatite dike near the Zambia/Malawi border at the base of Kalanga Hill (6 km northeast of Muyombe). The pegmatite has sharp contacts against the granulite host rock. The dike has a roughly N-S strike, and is at least 30 m long and 30–50 cm wide. It is symmetrically zoned and consists mainly of quartz, feldspar, muscovite, and beryl. Accessory minerals include rutile, ixiolite, samarskite, microlite, and zircon.

Chrysoberyl is found in the intermediate zones, or adjacent to the quartz core, of the pegmatite. It forms either translucent yellow-green to green euhedral crystals up to 3 cm long, or slightly larger intergrown aggregates. Some crystals exhibit typical pseudohexagonal twinning. Electron-microprobe analyses show that the chrysoberyl has high iron concentrations (3.16–6.25 wt.% Fe_2O_3). Values are given for the unit-cell parameters and the measured density (3.72 g/cm^3), but typical gemological properties (e.g., R.I.) are lacking. Data are presented to compare the chemical composition of this material with that of samples from other sources. At this locality, the authors propose that the chrysoberyl formed by reactions involving feldspar and beryl, or muscovite and beryl. *JES*

A new chrome chalcedony occurrence from Western Australia. M. J. Willing and S. M. Stocklmayer, *Journal of Gemmology*, Vol. 28, No. 5, 2003, pp. 265–279.

Chrome chalcedony, an ornamental rock first discovered in 1955 in Zimbabwe (where it is known commercially as *mtorolite*), has been found in the Newman area of Western Australia. The color, attributed to chromium (~0.24 wt.% Cr_2O_3), is a fairly uniform deep green (grading to brown when traversed by later quartz veinlets), but a banded texture and variations in the green color can be seen with transmitted light. This translucent material differs from chrysoprase in two ways: (1) Ni is the chromophore in the latter; and (2) chrysoprase occurs as late-stage fracture fillings, whereas this chrome chalcedony occurs as masses representing the silicification of serpentine.

The chemical composition is predominantly SiO_2 (95.01 wt.%), with minor amounts of Al, Fe, Mg, Cr, and H_2O and traces of Mn and Ni (e.g., 0.01 wt.% NiO). Quartz and traces of talc and mogánite (a metastable silica polymorph) were identified in the chrome chalcedony by X-ray diffraction methods. The microcrystalline groundmass is composed (90%) of individual silica grains about 0.02 mm in diameter; localized rosettes and micro-fans of radiating chalcedony about 0.5 mm in diameter also occur. Some opaque magnetite grains with the margins altered to hematite occur as inclusions. Gemological properties are within the range characteristic of chalcedony: R.I. = 1.539,

S.G. = 2.57, H = ~7, intense red under the Chelsea filter, and inert to long- and short-wave UV radiation. The UV-Vis, NIR, and Raman spectroscopic characteristics of this material are documented. *KSM*

Origin of a dolomite-related jade deposit at Chuncheon, Korea. T-F. Yui and S-T. Kwon, *Economic Geology*, Vol. 97, No. 3, 2002, pp. 593–601.

Nephrite jade deposits may be divided into those associated with serpentinites and those associated with dolomitic rocks. Although most occurrences are hosted by serpentinites, the more significant deposits in terms of ore tonnage occur in the latter. The Chuncheon deposit, located in the north-central portion of the Republic of Korea, represents one of the largest deposits of nephrite jade in the world, with estimated reserves of 300,000 tonnes of ore, one-quarter of which is considered to be gem-quality. This study was undertaken to better understand the conditions of formation of nephrite in dolomitic rocks.

At the Chuncheon location, nephrite occurs in Precambrian dolomitic marble and amphibolite schist that were intruded by a late Triassic-age granite. The nephrite is found in lenses up to 1 m thick and several meters in length along the contact between the marble and the schist. It displays a waxy luster and ranges from greenish gray to yellowish green. The nephrite, along with chlorite and several calcium silicate minerals (i.e., diopside, grossular, tremolite), are products of the hydrothermal alteration of the dolomitic marble.

The authors present oxygen and carbon stable-isotope data for samples of dolomite and silicate minerals from the deposit and associated country rocks. Based on these data and field observations, they suggest that the nephrite formed as the result of a metasomatic reaction involving fluid circulation at the contact between the marble and the schist. Formation of the deposit postdated late Triassic regional metamorphism of the area. The fluid involved in the metasomatism was of meteoric origin, and its regional circulation may have been induced by the intrusion of the nearby granite. The authors compare the geology and genesis of this deposit with that of the serpentinite-related Fengtien nephrite occurrence in Taiwan. *JES*

Pink sapphire from southern Kerala, S. India: Implications on India-Madagascar correlation within Gondwana assembly. M. Santosh, R. Katori, S. Yoshikura, S. Higashi, and A. K. Salim, *Gondwana Research*, Vol. 5, No. 4, 2002, pp. 894–901.

Southern Kerala and the adjacent state of Tamil Nadu are historically important regions for gem production in southern India. A wide variety of gems—including beryl, chrysoberyl, corundum, garnet, quartz, spinel, topaz, and zircon—are found in primary deposits (mainly in pegmatites emplaced in granulite facies metamorphic rocks), or in associated alluvial deposits. Pink sapphire is found at Melankode near Balaramapuram, and at Rose Mala near Tenmala. Electron-microprobe data indicate that the pink sapphire is nearly pure Al_2O_3 (98.43–99.48 wt.%). Cr_2O_3 and FeO are each present in amounts up to 0.12 wt.%. Abundant CO_2-rich fluid inclusions occur in the sapphires.

The estimated temperatures of formation of the Melankode pegmatite are in the 650–750°C range. The crystallization age of the pegmatite (based on U-Pb and Pb-Pb dating of gem zircons) has been calculated by others to be about 513 million years (My), whereas granulite-facies metamorphism in the same region is dated at about 540 My. Thus, pegmatite emplacement postdated the main period of granulite metamorphism. Both the pegmatite formation and regional metamorphism occurred during the Pan-African Orogeny (a geologic event beginning about 600 My that led to the assembly of the Gondwana supercontinent).

Pink sapphires from these two Indian deposits are similar to material from a number of localities in southern Madagascar (Betroka, Ilakaka, Andranondambo), as well as from the Ratnapura district in Sri Lanka. These occurrences are cited by the authors as additional evidence for the juxtaposition of southern Madagascar, Sri Lanka, and southern India when these areas were brought together as part of Gondwana. Gem deposits in all three areas are within or closely proximal to a regional shear zone that extended at the time across Madagascar, southern India, and Sri Lanka, and terminated in Antarctica. *JES*

Pressure, temperature and fluid conditions during emerald precipitation, southeastern Yukon, Canada: Fluid inclusion and stable isotope evidence. D. Marshall, L. Groat, G. Giuliani, D. Murphy, D. Mattey, T. S. Ercit, M. A. Wise, W. Wengzynowski, and W. D. Eaton, *Chemical Geology*, Vol. 194, No. 1–3, 2003, pp. 187–199.

In 1998, emeralds were discovered at the Crown showing, located 7 km north of Fire Lake in southeastern Yukon. At this site, emerald mineralization occurs within muscovite-tourmaline alteration zones (up to 1.5 m thick) adjacent to quartz-tourmaline veins that crosscut metavolcanic rocks of Devonian-Mississippian age. Eight distinct emerald zones within a few hundred square meters have been mapped on the property. The emerald crystals reach 4 cm in length; they are of good color with up to 7,816 ppm chromium. They contain abundant fluid inclusions, mostly along healed fractures, and some mineral inclusions (including tourmaline, calcite, quartz, zircon, scheelite, and sulfide minerals).

Analysis of the primary fluid inclusions (and using stable-isotope data) suggests that emerald precipitation took place from H_2O–CO_2–CH_4 (± N_2, H_2S)-bearing saline brines at temperatures of 365–498°C and pressures of 700–2,250 bars (corresponding to burial depths of 2 to 7 km). Emerald deposits are generally formed when geologic

conditions bring together Cr and Be. At this site, Cr is thought to have originated locally from mafic and ultramafic rocks during hydrothermal alteration, while Be is most likely derived from a nearby (within 600 m) granite intrusion of Cretaceous age. *JES*

Some lesser known Australian opals. G. Browne, *Gemmologie: Zeitschrift der Deutschen Gemmologischen Gesellschaft*, Vol. 51, No. 2–3, 2002, pp. 97–106.

Australia produces a range of lesser-known opals, of minor economic significance, that display properties and features of interest to gemologists and collectors. A selection of six such opals is described in this article. (1) Opal "pineapples" are found rarely, and only in the White Cliffs opal field, western New South Wales (NSW). They are pineapple-shaped opal pseudomorphs after an unidentified precursor that consisted of radiating clusters of monoclinic crystals. (2) Volcanic opal with play-of-color occurs as cavity fillings in amygdaloidal basalts, or as nodules in associated soils, near Tintenbar, northeastern NSW; this opal tends to craze. (3) Opal with and without play-of-color occurs as veinlets in metamorphic rocks near Coolgardie, Western Australia (WA). Although mined on a small scale in the 1960s, very little is known about this deposit or its opal. (4) Matrix opal, "cream" to gray in color, is found at Andamooka, South Australia, where it impregnates and partly replaces limestone cobbles and boulders. (5) Opal-infiltrated "thunder eggs" occur in the Upper Tweed River valley, northeastern NSW. In addition to play-of-color opal, the thunder eggs may be filled with common opal and chalcedony. (6) Facetable common opal of note occurs in two localities: "Sun" opal from Minyon Falls, NSW, is transparent and yellow to "amber" in color; the best specimens of yellowish green to brown "siliciophite" (opalized chrysotile asbestos) are found at Lionel, WA. *MWF*

Spectroscopic studies of spessartine from Brazilian pegmatites. S. G. Eeckhout, C. Castañeda, A. C. M. Ferreira, A. C. S. Sabioni, E. de Grave, and D. C. L. Vasconcelos, *American Mineralogist*, Vol. 87, No. 10, 2002, pp. 1297–1306.

Mössbauer and FTIR spectra were acquired for spessartine-almandine garnets collected from three granitic pegmatites in Brazil to provide further information on garnet crystal chemistry. The garnets were sampled from the complex zoned Alto Mirador dike near Acarí in Rio Grande do Norte, and simple zoned dikes at two localities in Minas Gerais—Escondido near Conselheiro Pena, and Poaiá near São José da Safira. The garnets from these two kinds of pegmatites displayed different chemical compositions in terms of Fe, Mg, and Ca contents. For the Alto Mirador samples, both Fe^{2+} and Fe^{3+} were found to be present. A comparable Fe^{2+}/Fe^{3+} ratio for all the samples from this pegmatite implies they formed under similar conditions. In contrast, no Fe^{3+} was detected in the garnets collected from the two simple pegmatites. These chemical differences were attributed to different magmas that produced the pegmatites.

Although absorptions due to molecular H_2O were not present in the infrared spectra of any of the garnet samples, several features due to hydroxyl (OH) were detected. The authors concluded that hydrogen incorporation in these garnets resulted from the substitution of $(O_4H_4)^{4-}$ for $(SiO_4)^{4-}$. *JES*

INSTRUMENTS AND TECHNIQUES

Cathodoluminescence of diamonds. W. Taylor, *Rough Diamond Review*, No. 1, June 2003, pp. 38–42.

Diamond emits visible light of various wavelengths when bombarded with a beam of electrons; this is known as cathodoluminescence (CL). CL is of practical importance in the study of both natural and synthetic diamonds, as it provides insight into their growth history and reveals radiation damage, lattice deformations, and impurity distributions. The two basic types of instrumentation used for viewing CL are the luminoscope (an attachment for an optical microscope) and the electron microscope. A spectrophotometer may be added to record spectra as a function of wavelength. Such spectral information is essential for determining the optical centers responsible for CL emissions. Photoluminescence (PL) spectroscopy using a Raman microspectrometer can provide equivalent information. CL imagery and CL or PL spectroscopy have been used to document more than 100 luminescence bands and optical centers in diamond. At present, satisfactory explanations exist for only a handful of those detected; these include explanations for CL emissions associated with synthetic growth, radiation damage, nitrogen-related optical centers, and platelets. *CT*

A compilation of infrared absorption spectra of some specific gemstones as an aid to their identification. S. Fernandes, M. Khan, and G. Choudhary, *Australian Gemmologist*, Vol. 21, No. 9, 2003, pp. 361–367.

A compilation is presented of infrared absorption spectra for specific gemstones, all of which appear similar in color but otherwise display distinct properties. Using the transmission mode of an FTIR spectrometer, the authors recorded spectra for some 25 samples of each gem species examined, bearing in mind the variation in properties to be expected in anisotropic gem minerals with orientation. The aim is to provide "fingerprint" absorption patterns that allow gemstones of a similar color to be distinguished from one another (and, in some cases, natural stones from synthetics). Tables are presented with the characteristic IR spectra for blue, green, yellow, red, and colorless stones. No attempt is made to specify the causes for the various absorption bands. *RAH*

Identification of B jade by Raman spectroscopy. E. Zu, D. Chen, and P. Zhang, *Spectroscopy and Spectral Analysis*, Vol. 23, No. 1, 2003, pp. 64–66 [in Chinese with English abstract].

Infrared absorption spectroscopy is one of the most widely used methods for identifying polymer-impregnated jadeite (B-jade). However, with this technique it is difficult to locate the exact areas within a stone that contain the impregnated materials. These authors used Raman spectroscopy to overcome this deficiency inherent in the IR technique.

Four types of filling materials (paraffin wax, paraffin oil, AB [acrylate-epoxy] glue, and epoxy resins) in bleached and polymer-impregnated jadeites were identified using Raman spectroscopy. Their characteristic peaks were located in two ranges: 1700–1100 cm^{-1} and 3100–2800 cm^{-1}. The four strongest peaks of both the AB glue and epoxy resins are related to phenyl. The 1609 and 1116 cm^{-1} peaks are assigned to the C-C stretching mode, while the peaks at 3069 and 1189 cm^{-1} are attributed to the C-H in-plane bending mode and C-H stretching mode, respectively. Paraffin wax and paraffin oils displayed strong peaks at 2882 and 3848 cm^{-1}, respectively. *TL*

JEWELRY HISTORY

Mineralogy and alteration of Chinese archaic jade artifacts. H.-H. Tsien and J.-N. Fang, *Western Pacific Earth Sciences*, Vol. 2, No. 3, 2002, pp. 239–250.

Archaic tremolite jade artifacts unearthed from various cultural sites in China show very different sedimentary structures and textures. On jade artifacts that suffered alteration due to weathering, powder X-ray diffraction patterns of whitened zones and unaltered regions are identical, suggesting that the alteration did not change the mineral composition. However, scanning electron microscopy shows that in unaltered areas the microstructure is compact and formed of platy crystals, whereas the whitened areas are porous and formed of acicular crystals. The authors attribute the alteration to degradation or aggrading crystallization in wet or humid conditions. *RAH*

JEWELRY RETAILING

He turned web site in the rough into online jewel. B. Acohido, *USA Today*, October 20, 2003, p. 5B.

This article profiles Mark Vadon, founder and CEO of Blue Nile, the Internet diamond and jewelry retailer. In 1999, Vadon was a consumer products consultant at Bain & Co. when he visited a retail jeweler to buy a diamond engagement ring. He wanted information about diamonds, but the retailer advised him to buy a diamond that "spoke" to him. After checking for diamond information on the Internet, he forged a deal with a small outfit then known as internetdiamonds.com. At the height of the "dot.com" boom, he raised $57 million to transform the small company into Blue Nile.

His marketing strategy: aim at men, keep profit margins low, and provide lots of information "to make the consumer comfortable." He now claims an inventory of 30,000 certified diamonds and offers a choice of 70 engagement ring settings. Blue Nile, still privately held, passed its fifth profitable quarter in August 2003, and will record an estimated $125 million in sales for the year, a 74% increase over 2002. *RS*

SYNTHETICS AND SIMULANTS

Natural versus hydrothermal synthetic Russian red beryl: Chemical composition and spectroscopic measurements. M. Fumagalli, L. Prosperi, A. Pavese, and S. Bordiga, *Journal of Gemmology*, Vol. 28, No. 5, 2003, pp. 291–301.

Six hydrothermal synthetic red beryls produced in Russia were compared to two natural specimens from Utah to determine the most reliable chemical-physical parameters to distinguish them. The results of standard gemological testing on all eight samples indicated that R.I., S.G., and fluorescence are not diagnostic. However, magnification revealed that inhomogeneous growth structures, described as "angular" or "chevron-like," only occurred in the synthetic samples and therefore are diagnostic. The synthetics also had much stronger pleochroism.

Chemical analysis was also useful for separating synthetic from natural red beryl. The former will likely contain Co, whereas the latter will contain characteristic (and generally higher) amounts of K, Na, Mn, Cs, and Zn. Infrared spectroscopy revealed a significant presence of water in synthetic red beryl. Raman spectroscopy showed additional peaks above 2000 cm^{-1} in the synthetics compared to the natural specimens, as well as a broad hump over the interval 3500–1500 cm^{-1} that is attributed to significant fluorescence of synthetic red beryl to the 1064 nm laser. *WMM*

A note on sky-blue glass with needle-like inclusions. J. M. Duroc-Danner, *Journal of Gemmology*, Vol. 28, No. 5, 2003, pp. 280–282.

A convincing glass imitation is described that weighed 2.44 ct and was "sky" blue. The sample had a vitreous luster, with R.I. = 1.593 and S.G. = 3.28. The absorption spectrum showed a band at 400–420 nm, with three fine lines at 640, 660, and 670 nm. It fluoresced a strong chalky greenish yellow to short-wave and a moderate orange to long-wave UV radiation. Except for the blue color, these properties are similar to those of ekanite (which is typically green). Further testing revealed no radioactivity; ekanite is typically strongly radioactive.

The sample contained numerous needle-like inclu-

sions intersecting in different planes and a few pinpoint inclusions. Careful examination revealed that the needles were most probably hollow canals similar to those used in fiber optics; this characteristic could easily be mistaken as natural on quick inspection.

The physical and optical properties are consistent with those of leaded glass, which was confirmed by EDXRF analysis (Si, Pb, K, and Ca were the main constituents). It was concluded that this glass simulant with its needle-like inclusions was deliberately cut to fool a potential buyer into thinking that it was a natural gem. *CT*

TREATMENTS

Behavior of Brazilian Imperial topaz at high temperature. A. C. S. Sabioni, G. M. da Costa, J. M. Dereppe, C. Moreaux, and C. M. Ferreira, *Journal of Gemmology*, Vol. 28, No. 5, 2003, pp. 283–290.

The effect of heat treatment on the structure and composition of orange Imperial topaz from the Capão mine, Ouro Preto, Brazil, is reported. To insure consistency, the studied samples were taken from a single large crystal. The samples were subjected to a range of temperatures (0–1,400°C) for varying lengths of time (1–23 hours). Variations in structure were detected by X-ray diffraction, and the abundances of H and F were measured by nuclear magnetic resonance.

The results showed that the samples were structurally and chemically stable below 1,000°C, although optical properties did change; on heating, the orange color changed to pink at approximately 600°C and then became colorless at 900°C due to destruction of the color centers. Above 1,100°C, the topaz began to change both chemically, by losing H, F (and some Si), and structurally. At approximately 1,300°C, it was completely transformed to opaque white mullite ($Al_6Si_2O_{13}$). *WMM*

MISCELLANEOUS

The billionaire who cracked De Beers. P. Berman and L. Goldman, *Forbes*, September 15, 2003, pp. 109–116.

Lev Leviev is a Russian émigré living in Israel who has built the world's largest diamond business outside of the De Beers Diamond Trading Company (DTC). In recent years, he has challenged De Beers's exclusive marketing deals in Russia and Angola, and shaken the traditional structure of the diamond business.

Leviev was born in Tashkent, Uzbekistan, to a family that defied the communist ban on religion by following the Chabad-Lubavitch movement of Judaism. His family emigrated to Israel in 1971. Six years later, Leviev opened his own cutting factory and, avoiding the speculative boom in diamonds that gripped the market shortly thereafter, managed to weather the crisis of 1981–82 in good shape. Leviev became a DTC sightholder in 1987, and two years later was invited by Russia's state-run diamond operation to set up diamond-cutting operations.

Leviev kept his connections to Russia's diamond hierarchy and cultivated relationships with top government officials including Mikhail Gorbachev, Boris Yeltsin, and Vladimir Putin. By 1995, Leviev had managed to secure supplies of rough from Gokhran, the country's diamond stockpile. This resulted in De Beers ending his sight. Leviev was believed to be the major conduit through which the Russian government sold off much of its stockpile (estimated to be as much as $12 billion) in the mid-1990s. Leviev also moved into civil-war-torn Angola after De Beers stopped buying there because the government could not certify the legitimate origins of its diamonds, and then moved on to offshore mining operations in Namibia. After building his diamond business internationally, Leviev has since entered real estate development, and has engaged in numerous philanthropic activities in his native country and Israel. *RS*

Birefringence vs. double refraction divergence. R. Cartier, *Journal of Gemmology*, Vol. 28, No. 4, 2002, pp. 223–226.

The author discusses a terminology problem often encountered in gemology, but not always recognized: use of the phrase "double refraction" (or "DR") when the concept of birefringence is actually what is intended. The latter is a property of a medium that has two simultaneous differing optical densities that result in two distinct refractive indices (i.e., different velocities for light traveling in the medium). As a quantifiable property, it has come to mean the numerical difference between two measured refractive index readings for the same wavelength of light. In contrast, refraction is the behavior of light when it goes from one medium into another and changes its direction of travel. This change in direction is not only dependent on the refractive index value(s), but also on the angle of incidence of the light.

The author presents a summary table for uniaxial and biaxial materials for normal-incident light traveling parallel, perpendicular, or at some intermediate angle to the optic axis (or axes), and indicates when both the birefringence and what he terms the "double refraction divergence" are negligible, intermediate, or maximum. He proposes that the contraction "BI" be used for birefringence, and "DD" be used for double refraction divergence. He also recommends that the use of "DR" for double refraction be discontinued, because for too long it has been confused with birefringence. *JES*

Doubling of images in gemstones. D. B. Sturman and M. E. Back, *Journal of Gemmology*, Vol. 28, No. 4, 2002, pp. 210–222.

Doubling of images (e.g., facet junctions) is a phenomenon that is seen in some anisotropic gemstones and can down-

grade their appearance. This article presents an analysis of this doubling effect for both uniaxial and biaxial gem minerals, for instances when light exiting the gemstone is parallel, perpendicular, or at some intermediate angle to the mineral's optic axis (or axes). Maximum doubling occurs when the exiting light travels at an angle of about 45° to the optic axis (as a result of this light being split into two component rays with different refractive indices, vibration directions, and directions of travel). The visual extent of doubling increases with the angular separation of the two component rays and thus the size of the gemstone. Diagrams are presented which allow the maximum possible separation of images to be determined for particular minerals, and for the effect of the angle between the optic axis and a line perpendicular to the table facet. The mathematical basis of these diagrams is presented in two appendices. *JES*

"Hot money" and daring consumption in a northern Malagasy sapphire-mining town. A. Walsh, *American Ethnologist*, Vol. 30, No. 2, 2003, pp. 290–305.

Sapphire deposits were found near the town of Ambondromifehy in northern Madagascar in 1996. Within two years, the sleepy village of 400 was transformed into a boom town of about 14,000. Lured by the prospect of easy money from sapphire digging, many young men flocked to the town, causing the boom-town plague of crime, disease, and inflated living costs. What separates Ambondromifehy from some other boom towns is that miners tend to work for themselves instead of for companies or claim holders.

Some three-fourths of the town's inhabitants are miners, who dig pits in the soil and scour cave bottoms (where sediments were trapped) for sapphires. Since the deposits have no adequate water source, the miners must carry their diggings in sacks to an area near the town for sieving. More-experienced miners often help newcomers with details such as where to dig, how to negotiate prices, and how to avoid the local police. This is in keeping with Malagasy hospitality traditions. Miners also rely on diviners to reveal digging sites, and avoid certain "medicines" that might repel sapphires.

Because few miners consider making Ambondromifehy their permanent home, the town remains a jumble of makeshift buildings. Miners who don't spend their money on flashy consumables send it back to their families, leaving no local investment in wells, houses, or cattle. *RS*

Jurisdiction over offshore diamond mining. L. E. Moller. *Journal of Energy & Natural Resources Law*, Vol. 21, No. 2, 2003, pp. 168–185.

This article reviews the various laws under which the government of Namibia controls the mining of diamonds off its coast. While the government exerts full mineral rights over deposits within its territorial waters, a potential problem may arise with mining vessels that are registered under some other national flag, especially South Africa, where most of the mining ships are registered. In addition, Article 73 of the UN Convention, which allows states to exercise jurisdiction over fishing vessels in their waters, does not specifically cover mining and exploration ships. However, other Articles of the UN Convention (56, 77, 80, and 81) grant Namibia the sovereign right to all exploration activities, jurisdiction over resources within its territorial waters, and the sole right to authorize exploration and mining within those waters. Finally, there is no agreed-upon maritime boundary between Namibia and South Africa.

Namibia's Minerals Act and Diamond Act allow its courts to try any offense committed in its territorial waters, but the country does not have adequate law enforcement and monitoring facilities to check diamond-mining vessels.

The study recommends that the government cooperate more closely with South Africa for mutual assistance in monitoring mining activities and that it thoroughly review its law enforcement activities to safeguard its national interests, in view of its UN-sanctioned rights. *RS*

Safeguarding rough diamonds. R. Corfield, *Rough Diamond Review*, No. 1, June 2003, pp. 32, 35–37.

Theft and trafficking in stolen diamonds is known as Illicit Diamond Buying (I.D.B.), and it occurs almost anywhere diamonds are mined or processed. The United Nations estimates 15% of the rough (non-conflict) diamond trade is I.D.B. The extent of theft at the mining stage is difficult to establish, because there is no way to determine what quantity of diamonds *should* have been recovered. Thefts also occur at all stages of diamond processing and may involve individuals ranging from plant maintenance workers to polishers and sorters. Many sophisticated methods have been used to steal diamonds; these include using carrier pigeons and hiding the rough in self-inflicted wounds. Collusive thefts are the most serious in terms of losses; these can involve people from security guards to those in senior level and accounting positions, and can involve changing records and altering production data.

The approach to security by diamond producers must be multidisciplinary, and must involve senior management to implement a proactive and technically focused program that recognizes unusual employee behavior and temptation. Practical solutions include automation, which provides less human contact at the mining and processing stages, and reliable audits of all phases of plant operations. Exchanging information with other mine producers, and legislation that favors security measures, can also be helpful in curbing thefts. *Ron Stumman*